The condensin ATPase: towards a mechanistic view of chromosome condensation

Rahul Rajan Thadani*

A thesis submitted for the degree of
Doctor of Philosophy

UCL

September 2014

*Supervisor: Dr. Frank Uhlmann. Thesis committee: Dr. Martin Singleton, Dr. Takashi Toda. Address: Chromosome Segregation Laboratory, Cancer Research UK London Research Institute, 44 Lincoln's Inn Fields, London WC2A 3LY.

Declaration

I, Rahul Rajan Thadani, confirm that the work presented in this thesis is my own. Where information has been derived from other sources, I confirm that this has been indicated in the thesis.

_____

Abstract

The central aim of cell division is the accurate transmission of replicated genetic material to daughter cells. To enable this segregation, centimetre-long DNA molecules must be organised into condensed micrometre-sized chromosomes. This critical but poorly understood process is principally effected by the chromosomal condensin complex. Condensin is a multisubunit protein complex, comprising a core dimer of ATPases of the structural maintenance of chromosomes (SMC) family. However, the role of the condensin ATPase in chromosome condensation has remained unclear.

Using specific structure-based point mutations, along with quantitative measurements of chromosome condensation, and novel conditional alleles of condensin in the eukaryotic model budding yeast *Saccharomyces cerevisiae*, I show that the ATPase activity of condensin is crucial for its function. Mutations in the ATPase domain alter the dynamic DNA binding properties of condensin, and compromise its ability to form compact mitotic chromosomes. Taken together, these results shed light on critical events in the assembly and faithful segregation of mitotic chromosomes.

Contents

List of Figures

List of Tables

Glossary

ANOVA analysis of variance. 72

ATP adenosine triphosphate. 18, 31–35, 100, 102, 104, 108

BiFC bimolecular fluorescence complementation. 113

CDK cyclin-dependent kinase. 25, 28, 30, 52, 55, 57, 115

CK2 casein kinase II. 31

CPC chromosomal passenger complex. 28–30

CPF cleavage and polyadenylation factor. 31

DAPI 4',6-diamidino-2-phenylindole. 48–50, 59, 100, 102, 104, 106, 107, 111

DMSO dimethyl sulphoxide. 63, 96

DNA deoxyribonucleic acid. 7, 15, 16, 26–28, 31–35, 38, 39, 41–43, 55, 56, 59, 98, 100, 104, 108

EGTA ethylene glycol tetraacetic acid. 16

FCCS fluorescence cross-correlation spectroscopy. 25

FCS fluorescence correlation spectroscopy. 25

FEAR cdc-fourteen early anaphase release. 30

FFT fast fourier transform. 49, 59

FISH fluorescence in situ hybridisation. 69, 74

FKBP12 FK506 binding protein. 62

FRAP fluorescence recovery after photobleaching. 25, 26, 113, 115

FRB FKBP12 rapamycin binding. 62, 63

FRET fluorescence resonance energy transfer. 25, 33, 113

GFP green fluorescent protein. 26

HRP horseradish peroxidase. 57, 65

IAA indole-3-acetic acid. 37, 64, 65, 67, 70, 71, 76, 77, 79, 86, 97, 100

IQR interquartile range. 73, 74, 80, 83, 89, 107, 110

MEN mitotic exit network. 30

NEBD nuclear envelope breakdown. 16, 23, 25, 26

NPC nuclear pores complex. 25, 26

ORF open reading frame. 38, 39, 41, 43

PBS phosphate buffered saline. 45

PCR polymerase chain reaction. 36, 38, 39, 41, 42

PLK1 polo-like kinase 1. 28

PP2A protein phosphatase 2A. 27, 31

PSF point spread function. 49, 50

rDNA ribosomal DNA. 26, 27, 30, 69–80, 84, 85, 87–90, 102, 111

RFB replication fork barrier. 27

RNA ribonucleic acid. 27, 31

rSAP recombinant shrimp alkaline phosphatase. 41–43

SCF Skp1, Cullin and F-box. 64

SIM structured illumination microscopy. 69, 70, 79

SMC structural maintenance of chromosomes. 3, 16–18, 20, 24, 27, 28, 32, 34, 35, 43, 61, 64, 68, 91, 108, 112, 113

TFIIIC transcription factor IIIC. 27

tRNA transfer RNA. 27, 28

Valap vaseline lanolin paraffin. 48, 49

Acknowledgements

I am grateful to my supervisor, Dr. Frank Uhlmann, for his continual guidance and support throughout the course of this project, to my thesis committee, Dr. Martin Singleton and Dr. Takashi Toda, for valuable discussions, to fellow members of the Chromosome Segregation Laboratory for uncontrived generosity with their time and reagents, to staff of the Core Facilities at the London Research Institute for technical assistance, and to Tomas and my family for their unwavering encouragement and patience.

I would also like to acknowledge all sources of funding that made this work possible, including Cancer Research UK, Boehringer Ingelheim Fonds, University College London, and the European Research Council.

'There is grandeur in this view of life, with its several powers, having been originally breathed into a few forms or into one; and that, whilst this planet has gone cycling on according to the fixed law of gravity, from so simple a beginning endless forms most beautiful and most wonderful have been, and are being, evolved.'

Charles Darwin
On the Origin of Species (1859)

1 Introduction

The large scale reorganisation of interphase chromatin into mitotic chromosomes is one of the most striking morphological events of the cell cycle. Cells entering mitosis must compact centimetre-long DNA molecules, within the confines of micrometre-sized nuclei, into the stable thread-like structures that give mitosis its name (from the Greek *mitos*, meaning thread). This process of chromosome condensation enables DNA molecules to withstand the considerable forces generated during segregation, and thus underlies the accurate transmission of replicated genetic material to daughter cells, and ultimately, at a molecular level, the fidelity of the propagation of the blueprint of life.

1.1 Chromosome condensation: a historical perspective

The origins of chromosome biology date to the late nineteenth century, when Walther Flemming first observed mitotic chromosomes as 'stainable bodies' (*chromosomen*) in developing salamander embryos (Flemming, 1882; Paweletz, 2001), and Theodor Boveri, working with eggs of the parasitic nematode *Ascaris megalocephala*, posited the theory of chromosome identity — that chromosomes did not form *de novo* during each mitosis but were formed from material that persisted through interphase (Boveri, 1888):

> *… die chromatischen Elemente selbständige Individuen sind, die diese Selbständigkeit auch im ruhenden Kern bewahren.* // '… the chromatin elements are individual entitites that retain their independence in the resting nucleus.'

Yet remarkably, more than a century after the seminal discoveries of Flemming and Boveri, mechanistic explanations of the process of chromosome condensation remain elusive.

N.B. This introduction is based, in part, on the following self-authored review: Thadani R, Uhlmann F, Heeger S (2012), Condensin, chromatin crossbarring and chromosome condensation, *Curr Biol* **22**(23): R1012.

Indications of a mitosis-specific condensation factor in cells began to emerge in the 1970s, when classical cell fusion experiments demonstrated that chromosome condensation could be rapidly induced in interphase HeLa cells in a dose-dependent manner by fusing them to mitotic ones (Johnson and Rao, 1970). In a cell-free system derived from *Xenopus* eggs, interphase nuclei could be driven to undergo nuclear envelope breakdown (NEBD), chromosome condensation and spindle formation when incubated with mitotic extracts treated with the calcium chelator EGTA (Lohka and Maller, 1985). These processes were shown to be biochemically separable, with NEBD being enzymatically driven, and chromosome condensation involving both binding proteins and enzymatic activities including topoisomerase II (Newport and Spann, 1987).

Subsequent studies led to the identification of Smc2 and Smc4[†], core components of the condensin complex, as ATPases essential for chromosome condensation and segregation. In budding yeast, temperature-sensitive mutations in the *SMC2* gene led to chromosome decondensation in metaphase-arrested cells and segregation failure during anaphase (Strunnikov et al., 1995). Similarly, fission yeast temperature-sensitive *smc2/cut14* and *smc4/cut3* mutants failed to contract chromosome arms during DNA segregation, leading to a cut chromosome phenotype (Saka et al., 1994). In *Xenopus* egg extracts (Hirano and Mitchison, 1994), Smc2/XCAP-E and Smc4/XCAP-C were found to be required for the formation and structural maintenance of chromosomes assembled *in vitro*; in chicken cells (Saitoh et al., 1994), Smc2 was isolated as a significant structural component of mitotic chromosomes.

1.2 The condensin complex

Accumulating lines of evidence over two decades indicate that the chromosomal condensin complex is the principal effector of condensation (Hirano et al., 1997; Freeman et al., 2000). Condensin is a large, evolutionarily conserved multisubunit protein assembly that is found, with a broadly similar architecture, throughout the domains of life, including bacteria, archaea and eukarya (Figure 1.1). Along with cohesin and Smc5/6, it is one of three complexes built from dimers of SMC proteins, members of the structural maintenance of chromosomes family of ATPases, that are intimately involved in diverse aspects of higher order chromosome organisation. Indeed, condensin has been ascribed roles apart from chromosome

[†]The budding yeast names for condensin subunits are used throughout this thesis, along with the species-specific name where relevant. See Table 1.1 for a detailed listing.

condensation in several cellular processes such as interphase genome organisation, gene dosage compensation, metazoan development and meiosis (Haeusler et al., 2008; Jans et al., 2009; Gosling et al., 2007; Hagstrom et al., 2002). Conversely, the related SMC complexes might also contribute to chromosome condensation (Guacci et al., 1997). However, this introduction focuses on the role of condensin in mitotic chromosome condensation, which is of immediate relevance to the following work.

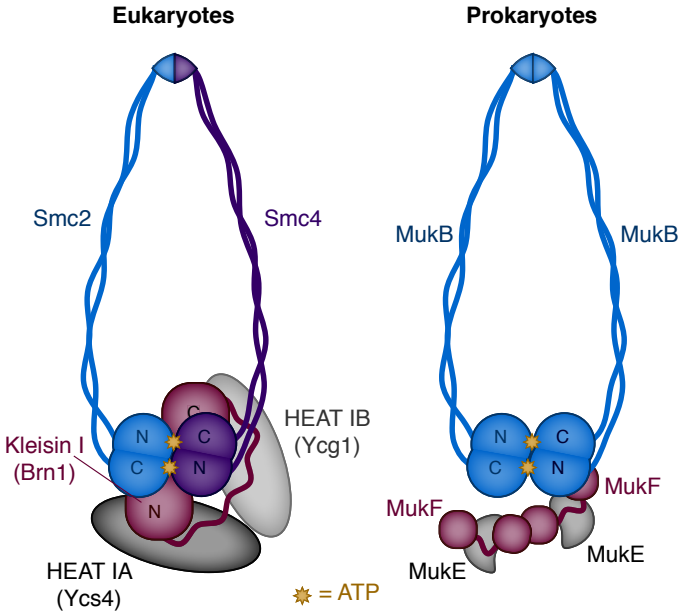

Figure 1.1 Molecular architecture of condensin. Subunit composition of eukaryotic (*left*) and bacterial (*right*) condensins. Condensins are composed of a core dimer of SMC or SMC-like ATPases with a dimerisation hinge at one end and catalytic head domain at the other. The core dimers are closed into rings by kleisins, which are monomeric in eukaryotes and dimeric in prokaryotes. One or more additional regulatory subunits interact with the kleisin and/or SMC core. *Reproduced with permission from Thadani et al. (2012)*.

1.2.1 Condensin architecture

Eukaryotic condensin

Eukaryotic condensin is a large pentameric complex of ~630 kilodaltons, comprising a core catalytic Smc2-Smc4 heterodimer. Smc2 and Smc4 each contain two terminal globular parts linked by long coiled coils to a central globular segment, a characteristic architecture of all SMC proteins. Each SMC protein folds back on itself through antiparallel coiled-coil arm interactions. This forms an SMC dimerisation hinge domain from the central part at one end, and an ATPase

head domain from association of the terminal globular parts at the other (Figure 1.1). The catalytic head domain features canonical adenosine triphosphate (ATP)-binding cassette motifs: the N-terminal 'Walker A' motif, and C-terminal 'Walker B' and 'C/signature' motifs. The N-terminal globular part of one SMC subunit engages in trans with a C-terminal part from the other to form a bipartite ATP binding pocket.

Three accessory subunits bind to the SMC heterodimer and regulate its activity. Kleisin I/Brn1, a member of the kleisin family (Schleiffer et al., 2003), interacts at its N-terminus with Smc2, and at its C-terminus with Smc4 to form a topologically closed ring (Hirano et al., 1997; Bhat et al., 1996; Cuylen et al., 2011). HEAT IA/Ycs4 (Biggins et al., 2001; Bhalla et al., 2002) and HEAT IB/Ycg1 (Ouspenski et al., 2000) contain HEAT repeats, and interact with the N- and C-terminal halves of Kleisin I/Brn1, respectively, and weakly with each other (Onn et al., 2007). All three accessory subunits of condensin are required for its functional association with chromatin (Lavoie et al., 2002; Piazza et al., 2014). It is noteworthy that while integrity of the ring-like structure of condensin is necessary for its function (Cuylen et al., 2011), details of its mechanistic significance remain to be determined. This is in contrast to the case of cohesin, where it has been unambiguously shown that the complex topologically encircles sister chromatids until separase-driven cleavage of the kleisin Scc1 at anaphase onset enables them to segregate (Uhlmann et al., 1999; Haering et al., 2008).

Most eukaryotes possess two isoforms of condensin, termed condensin I and II. These are built from identical core heterodimers of Smc2 and Smc4 but differing accessory subunits (Table 1.1), which may modulate the differential localisation patterns, dynamics, and functions of two condensins. Condensin I is termed the canonical condensin due to its phylogenetic ubiquity (Figure 1.2) and relative cellular abundance, although the ratio of condensin I and II varies substantially in different organisms, ranging from 1:1 in HeLa cells and 5:1 in *Xenopus* egg extracts (Ono et al., 2003) to 10:1 in chicken DT40 cells (Ohta et al., 2010; Green et al., 2012). The presence of condensin I and II in diverse eukaryotic taxa suggests that their last common ancestor possessed both condensin isoforms (Hirano, 2012). This implies that condensin II was independently lost from the genomes of organisms such as fungi and ciliates that possess only a single known isoform of condensin.

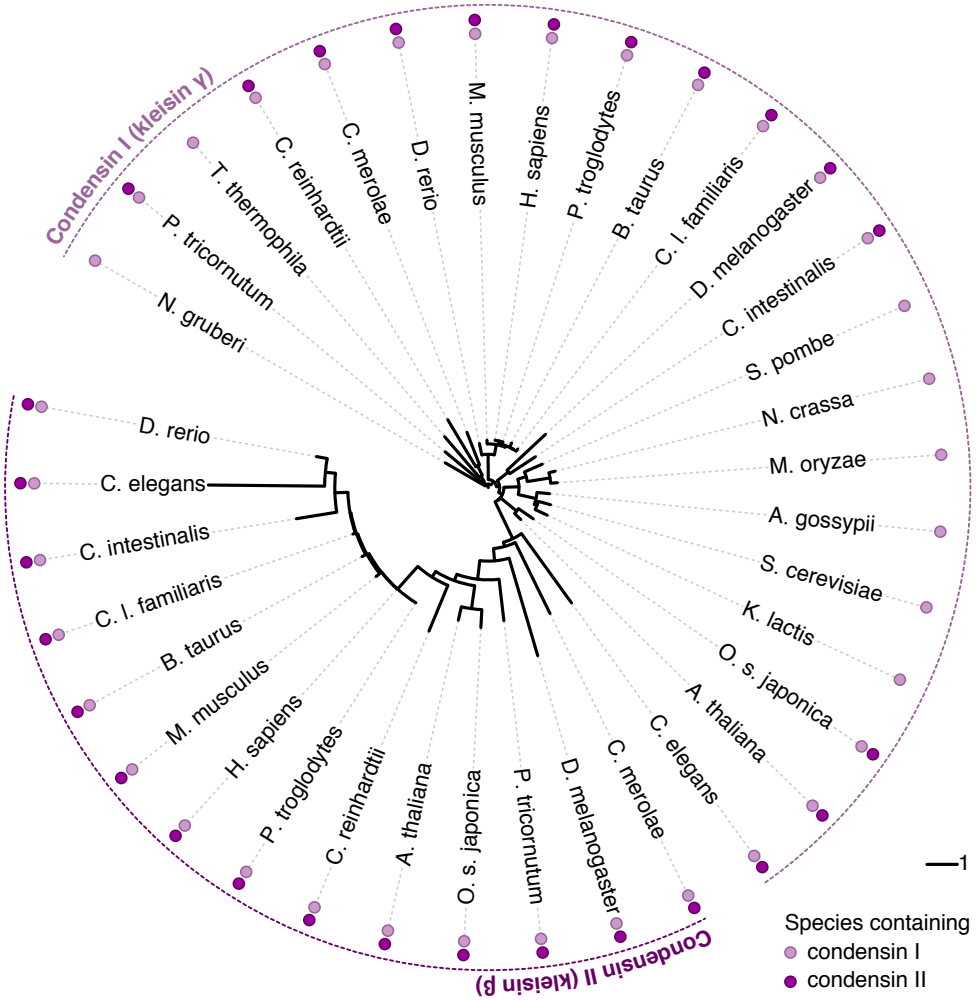

Figure 1.2 Phylogenetic analysis of condensin kleisin subunits. Phylogram representing the evolutionary relationships among eukaryotic kleisin subunits. A maximum likelihood unrooted tree was constructed in PHYLIP (Felsenstein, 1981) from a ClustalW multiple alignment (Larkin et al., 2007) and rendered radially using iTOL (Letunic and Bork, 2011). The excavate *Naegleria gruberi* was used as an outgroup (*top left*), from which taxa fan out clockwise in order of increasing branch lengths. Note that kleisins from species with a single known condensin isoform, such as fungi and the ciliate *Tetrahymena thermophila*, cluster with the condensin I sequences. The scale bar represents one unit of evolutionary distance along branches, as computed by the Jones-Taylor-Thornton method (Jones et al., 1992). *Reproduced with permission from Thadani et al. (2012)*.

Table 1.1 Condensin subunits in various species

Subunits	*S. cerevisiae*	*S. pombe*	*C. elegans*	others
Core (condensin I & II)				
SMC2	Smc2	Cut14	MIX-1	CAP-E
SMC4	Smc4	Cut3	SMC-4	CAP-C
Condensin I–specific				
Kleisin I (γ)	Brn1	Cnd2	DPY-26	CAP-H
HEAT IA	Ycs4	Cnd1	DPY-28	CAP-D2
HEAT IB	Ycg1	Cnd3	CAPG-1	CAP-G
Condensin II–specific				
Kleisin II (β)	–	–	KLE-2	CAP-H2
HEAT IIA	–	–	HCP-6	CAP-D3
HEAT IIB	–	–	CAPG-2	CAP-G2

Prokaryotic condensin

Three SMC-related complexes are known to occur in prokaryotes, SMC-ScpAB, MukBEF and MksBEF, with the two former complexes being the best characterised. SMC-ScpAB is widespread in bacteria and archaea (Britton et al., 1998; Mascarenhas et al., 2002; Soppa et al., 2002), and MukBEF is present in γ proteobacteria such as *E. coli* (Niki et al., 1991; Yamazoe et al., 1999). These two complexes are divergent at the sequence level but share a common architecture. Although the SMC-related complexes, SMC-ScpAB and MukBEF, are not strictly phylogenetically closer to eukaryotic condensin than to other eukaryotic SMC complexes (Figure 1.3), they are referred to as prokaryotic condensins due to their condensin-like null phenotypes, which include decondensed nucleoids, chromosome segregation failure, anucleate cell formation and temperature-sensitive growth (Britton et al., 1998; Mascarenhas et al., 2002; Soppa et al., 2002; Niki et al., 1991; Yamazoe et al., 1999).

SMC-ScpAB is composed of a catalytic SMC homodimer, the kleisin ScpA and accessory protein ScpB, both of which are likely binary in the complex. Similarly, MukBEF comprises an SMC-like core MukB homodimer, while the kleisin MukF and accessory protein MukE again form a dimeric frame that interacts with the MukB heads (Figure 1.1; Fennell-Fezzie et al., 2005; Woo et al., 2009). The most recently identified prokaryotic SMC-related complex, MksBEF, occurs in diverse bacterial genomes (Petrushenko et al., 2011). MksBEF is often present alongside SMC-ScpAB, MukBEF, or even other MksBEFs, suggesting that prokaryotic

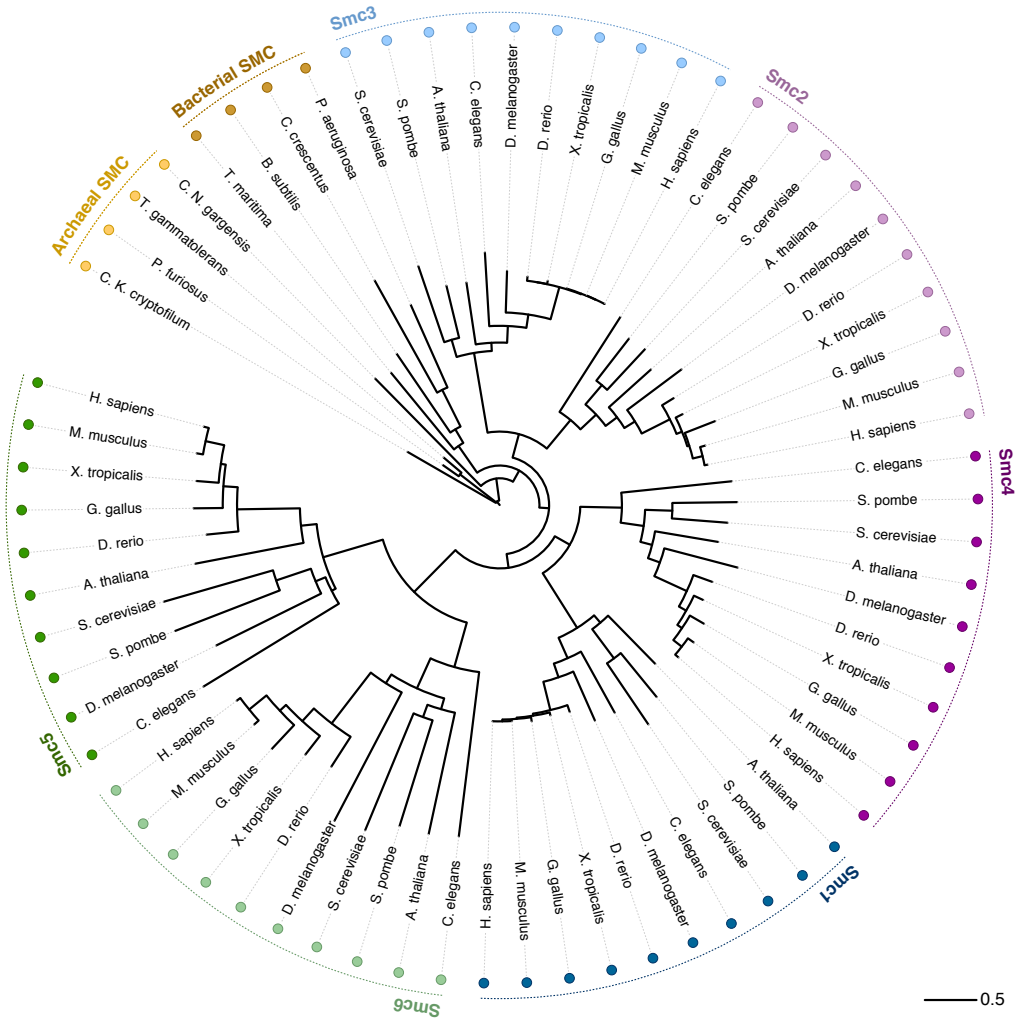

Figure 1.3 Phylogenetic analysis of SMC proteins. Phylogram representing the evolutionary relationships among prokaryotic and eukaryotic SMC proteins. A maximum likelihood unrooted tree was constructed in PHYLIP (Felsenstein, 1981) from a ClustalW multiple alignment (Larkin et al., 2007) and rendered radially using iTOL (Letunic and Bork, 2011). The archaeaon *Candidatus Korarchaeum cryptofilum* was used as an outgroup (*top left*), from which taxa fan out clockwise in order of increasing branch lengths. Note that the prokaryotic SMC proteins are not phylogentically closer to Smc2 or Smc4, than to the other eukaryotic SMC proteins. The scale bar represents 0.5 units of evolutionary distance along branches, as computed by the Jones-Taylor-Thornton method (Jones et al., 1992).

genome organisation may be more complex than previously appreciated. This also means that the possibility of as yet undiscovered molecular drivers of chromosome condensation in the larger, incompletely annotated, genomes of eukaryotes cannot be excluded *a priori*.

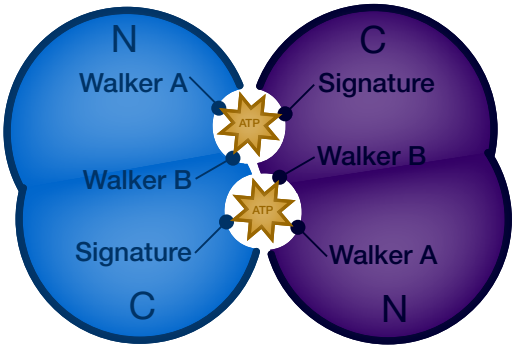

Figure 1.4 Schematic representation of the SMC catalytic domain. The SMC catalytic domain comprises two bipartite ATPase active sites, each of which contains Walker A/B motifs from one SMC subunit and a signature motif from the other SMC subunit.

1.2.2 Structure of the SMC catalytic domain

The SMC catalytic domain comprises two bipartite ATPase active sites, each of which contains Walker A/B motifs from one SMC subunit and a signature motif from the other SMC subunit (Figure 1.4). A crystal structure of the archaeal SMC catalytic heads from *P. furiosus* (Lammens et al., 2004) indicates that ATP molecules mediate SMC head dimerisation, in a reaction that involves binding of α and β phosphates to the Walker A motif of one SMC subunit, and the γ phosphate to the signature motif of the opposing subunit; the likely nucleophile for ATP hydrolysis is a water molecule activated by hydrogen bonds to the Walker B motif. This allows identification of mutants deficient in particular aspects of the SMC ATPase cycle: the Walker A mutation K39A disrupts ATP binding, the signature mutant S1070R disrupts SMC head engagement, and the Walker B mutant E1098Q strongly reduces ATP hydrolysis. In addition, an R59A mutation in a conserved arginine finger reaching into the nucleotide binding pocket, and which shows substantial conformational changes on ATP binding, abolishes DNA stimulation of SMC ATPase activity.

1.2.3 Differential contributions of condensin I and II to chromosome structure

Condensin I and II exhibit distinct spatial staining patterns on chromosome axes, as well as differing temporal localisation patterns through the cell cycle (Ono et al., 2003, 2004), suggesting that they may have non-redundant roles in chromosome organisation. For instance, in HeLa cells, condensin I is excluded from the nucleus in interphase and binds to chromatin only on NEBD in prometaphase. In contrast, condensin II is essentially nuclear in interphase, is stabilised on chromatin in early prophase, and remains associated with chromosomes throughout mitosis (Ono et al., 2004; Hirota et al., 2004; Gerlich et al., 2006). The differential contributions of the two condensin complexes to chromosome condensation are as yet poorly understood. In *Xenopus* egg extracts, the phenotypes following immunodepletion of condensin I– or II–specific subunits indicate that condensin I plays the major role in condensation (Ono et al., 2003). By contrast, in HeLa cells, the siRNA-mediated knockdown of either condensin by RNAi results in only minor abnormalities in chromosome morphology (Ono et al., 2003; Hirota et al., 2004), with condensin I depletion producing swollen chromosomes, and condensin II depletion leading to somewhat longer and curled chromosomes. The varying severity of condensation phenotypes subsequent to condensin depletion in these two systems could be ascribed either to effect of dosage, given the differing ratios of the two condensin isoforms, or to incomplete silencing by RNAi. Consistent with the observed aberrant chromosome morphologies in HeLa cells, further studies in chicken DT40 cells (Green et al., 2012) and *Xenopus* egg extracts (Shintomi and Hirano, 2011) implicate condensin II in the early mitotic axial shortening of chromosome arms, and condensin I in their later lateral compaction. More work is needed to determine how two very similar complexes are able to bind to distinct chromosomal regions, and whether it is their differential localisation or intrinsic activity that is responsible for their separable contributions to condensation.

1.2.4 Cell-cycle regulation of chromosome condensation

Numerous aspects of condensin biology are subject to control by the cell cycle machinery, making possible a multi-layered regulation of its function. Condensin activity may be regulated at the level of holocomplex formation, subcellular localisation, chromosomal loading, or chromatin binding dynamics, one or more of which are likely altered by post-translational modifications (Figure 1.5).

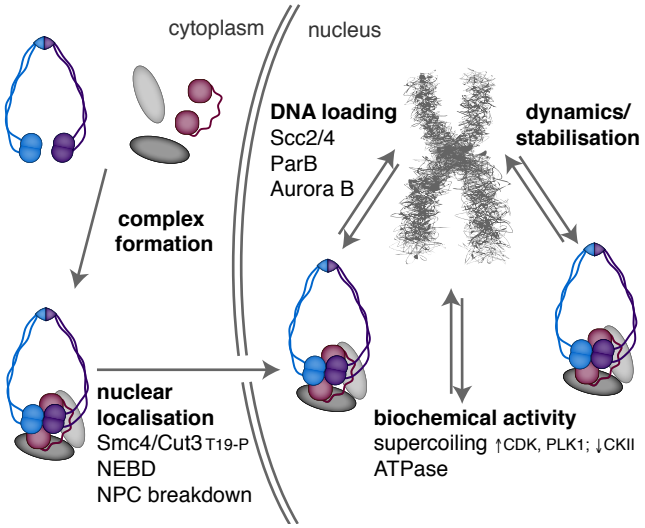

Figure 1.5 Regulation of condensin activity. Condensin can be regulated at several different levels: complex formation, nuclear import, chromosomal localisation, binding dynamics, and ATPase activity. This regulation is likely performed by posttranslational modifications, which can modulate the biochemical activities of the complex. *Reproduced with permission from Thadani et al. (2012).*

Holocomplex formation

In the test tube, condensin is often found in two major forms corresponding to the Smc2-Smc4 heterodimer and the holocomplex, as seen in early immunoaffinity purifications from *Xenopus* egg extracts (Hirano et al., 1997), as well as reconstitutions of recombinant human condensin (Onn et al., 2007). In addition, yeast Smc2 and Smc4 can form a stable heterodimer in cell extracts (Stray and Lindsley, 2003). *In vitro* studies have ascribed differing activities to the SMC/MukB dimer and the holocomplex (Hirano et al., 1997; Petrushenko et al., 2006b). However, it should be noted that the uncomplexed SMC dimer has not been directly observed *in vivo*. Interestingly, the reported role of condensin in disassembly of the *Drosophila* nurse cell polytene chromosomes depends on a timely upregulation of only Kleisin II/CAP-H2 (Hartl et al., 2008), indicating there may be a role for a limiting subunit in the regulation of complex assembly. Similarly, HEAT IA/CAP-D2 is a rate-limiting factor for the assembly of functional condensin I complexes in *Xenopus* oocytes (Watrin et al., 2003). This is reminiscent of cohesin, where levels of the kleisin Scc1 vary through the cell cycle, and determine the chromosomal association of the complex (Uhlmann and Nasmyth, 1998). Applying this principle more broadly, one could also ascribe the changing shapes of mitotic chromosomes in a developmental context to varying expression levels of condensin I and II–specific subunits (Shintomi and Hirano, 2011).

Investigations of chromatin binding dynamics of individual condensin subunits, for instance by fluorescence recovery after photobleaching (FRAP) assays, or of complex assembly by fluorescence correlation spectroscopy (FCS), fluorescence cross-correlation spectroscopy (FCCS) or fluorescence resonance energy transfer (FRET) approaches, would prove instructive in further elucidating regulation at the level of condensin holocomplex formation.

Subcellular localisation

In bacteria and archaea that lack a nuclear envelope, condensin is free to interact with chromatin at any time, limited only by the possible regulation of complex formation and DNA loading reactions. In eukaryotes, however, the nuclear envelope offers a potential barrier to chromatin access and consequently a possible mode of regulation. In organisms with a closed mitosis like the budding and fission yeasts, condensin has to be imported into the nucleus at or before chromatin compaction in mitosis. Intriguingly, in the budding yeast *S. cerevisiae*, condensin localises to the nucleus throughout the cell cycle, a behaviour reminiscent of condensin II of higher eukaryotes, despite the complex being a homologue of condensin I at the sequence level (Figure 1.2). On the other hand, condensin in the fission yeast *S. pombe* is predominantly cytoplasmic in interphase and nuclear during mitosis, an enrichment that requires the cyclin-dependent kinase (CDK)–dependent phosphorylation of the T19 site in Smc4/Cut3 (Sutani et al., 1999). In higher eukaryotes with an open mitosis, NEBD at mitotic onset ensures that the chromatin association of condensin is not hindered. In *D. melanogaster* (Oliveira et al., 2007), *C. elegans* (Collette et al., 2011), zebrafish (Seipold et al., 2009) and HeLa (Seipold et al., 2009; Hirota et al., 2004; Gerlich et al., 2006) cells, condensin I is cytoplasmic in interphase and nuclear in mitosis, while condensin II is nuclear throughout the cell cycle, at least in HeLa cells. An interesting but as yet unresolved question is how this differential subcellular localisation of condensin I and II is achieved, either by modifications to their regulatory subunits or recognition by additional factors. Intriguingly, in *Drosophila* embryos, Kleisin I/Barren associates with chromatin several minutes before NEBD (Oliveira et al., 2007). In addition, HeLa cells depleted of condensin II still initiate chromosome compaction just before NEBD (Gerlich et al., 2006). These observations suggest that chromosome compaction in these organisms may be functionally coupled to disassembly of nuclear pore complexes (NPCs) rather than the nuclear membrane (Gerlich et al., 2006; Lénárt et al., 2003). This is probably also the case in *C. elegans*, where NEBD is completed

only in anaphase but chromosome condensation is initiated in prophase, accompanied by NPC breakdown (Collette et al., 2011).

Dynamic binding to DNA

Chromosome condensation is a dynamic process, and condensin is required not only to assemble chromosomes, but also maintain them in a condensed state throughout mitosis. Immunodepletion of condensin from mitotic chromosomes assembled in *Xenopus* egg extracts results in their rapid decondensation (Hirano and Mitchison, 1994). In mitotic yeast cells, the inactivation of condensin leads to dramatic defects in ribosomal DNA (rDNA) compaction (Lavoie et al., 2002), and decondenses chromosome arms to G1-like levels (D'Ambrosio et al., 2008b).

Interestingly, while condensin exchanges dynamically from chromosomes, condensin I and II exhibit different dynamic behaviour through the cell cycle. FRAP experiments on green fluorescent protein (GFP)–tagged kleisin subunits in HeLa cells have shown that condensin I, which is excluded from the nucleus in interphase and binds to chromatin on NEBD, dynamically exchanges from chromosomes throughout mitosis. In contrast, condensin II, which is nuclear throughout the cell cycle, is stabilised on chromatin at the onset of condensation in prophase (Gerlich et al., 2006). What brings about this change in kinetic turnover, whether it is related to cell cycle–dependent posttranslational modifications, and what the consequences are on the chromosome condensation status, are important questions that remain largely unexplored. Curiously, the budding yeast condensin is bound to chromatin even in interphase, and its levels and distribution along chromosome arms remain largely unaltered through the cell cycle (D'Ambrosio et al., 2008b; Wang et al., 2005); the dynamic behaviour of this complex as a function of the cell cycle has not yet been investigated.

Condensin loading

A critical but poorly understood aspect of condensin function is its loading onto chromosomes. The two—not mutually exclusive—possibilities are that condensin directly recognises DNA sequence elements or chromatin features, or that additional recruiting factors are responsible for loading condensin onto chromatin. There is evidence for both possibilities, though considerably more for the latter.

The *Xenopus* (Kimura and Hirano, 2000) and budding yeast (Stray and Lind-

sley, 2003) Smc2-Smc4 heterodimer can directly bind to DNA *in vitro*, albeit with considerably lower affinity than holocomplexes. In addition, the budding yeast HEAT repeat subunits HEAT IA/Ycs4 and HEAT IB/Ycg1 form a double-stranded DNA binding domain, and upon binding DNA, stimulate the SMC ATPase (Piazza et al., 2014); condensin complexes lacking one of the HEAT repeat subunits also fail to associate with chromosomes in yeast and human cells. However it remains to be seen whether there is a role for direct DNA binding by the condensin SMC or HEAT repeat subunits *in vivo*.

In bacteria, the DNA-binding protein ParB recruits SMC to centromere-like parS sequences that cluster near the origin of replication (Sullivan et al., 2009; Minnen et al., 2011). In budding yeast, the cohesin loader Scc2-Scc4 promotes functional association of condensin with chromosomes, and may in turn be recruited at least in part by transcription factor IIIC (D'Ambrosio et al., 2008b). In the same model organism, replication fork barrier (RFB) sites at the 3′ end of rDNA genes serve as *cis* elements for condensin recruitment, in a manner dependent on the RFB-binding protein Fob1, the topoisomerase I–interacting protein Tof2 and the monopolin subunits Csm1 and Lrs4 (Johzuka and Horiuchi, 2009; Johzuka et al., 2006). In addition, the fission yeast homologues of these monopolin subunits, Pcs1 and Mde4 act as recruitment factors for condensin enrichment at the kinetochore (Tada et al., 2011). In the case of condensin II, protein phosphatase 2A (PP2A) acts in a noncatalytic fashion to recruit the complex to frog and human mitotic chromatin (Takemoto et al., 2009).

It should be emphasised that budding and fission yeast remain the only eukaryotes in which condensin binding sites have been comprehensively characterised (D'Ambrosio et al., 2008b; Wang et al., 2005; Schmidt et al., 2009). These studies show condensin to be enriched at centromeres, an enrichment that becomes particularly striking in mitosis compared to interphase. The molecular events governing this centromeric enrichment of condensin remain unclear. Condensin underlies, in part, the stiff elastic properties of centromeres during spindle attachment (Ono et al., 2004; Gerlich et al., 2006; Ribeiro et al., 2009; Stephens et al., 2011). Along chromosome arms, condensin is found at transcription factor IIIC (TFIIIC)–bound RNA polymerase III-transcribed genes, notably transfer RNA (tRNA) genes, as well as a subset of other strongly transcribed genes, including ribosomal protein genes. A TFIIIC binding element is sufficient to recruit condensin to previously unoccupied sites in *S. cerevisiae* (D'Ambrosio et al., 2008b), suggesting that condensin binding along chromosomes is determined by certain *cis*-acting elements. What exactly is recognised by condensin, as well as

the Scc2-Scc4 loading complex that is found at the same sites, remains to be elucidated. A chromosomal binding map of the *B. subtilis* SMC complex has also been obtained, and shows striking similarities to yeast condensin, with an enrichment at the bacterial centromere-like partitioning locus as well as tRNA, ribosomal protein and other strongly expressed genes (Gruber and Errington, 2009). Little is as yet known about chromosomal condensin binding patterns in higher eukaryotes, an area of great interest for forthcoming studies.

Post-translational modifications

CDK and PLK1 Early work using *Xenopus* egg extracts showed that mitotic CDK-dependent phosphorylation stimulates the ATPase and supercoiling activities of condensin I (Kimura et al., 1998, 1999). Subsequent studies using budding yeast condensin have established that CDK-mediated phosphorylation of Smc4 primes the complex for hyperphosphorylation of its three regulatory subunits by the Polo-like kinase PLK1/Cdc5. This hyperphosphorylation then further stimulates the DNA supercoiling activity of condensin (St-Pierre et al., 2009). Similarly, in HeLa cells, CDK phosphorylates the T1415 residue of HEAT IIA/hCAPD3, priming the complex for hyperphosphorylation by PLK1, and ensuring the fidelity of chromosome assembly (Abe et al., 2011). Taken together, these observations establish CDK and PLK1 as major molecular cell cycle regulators of condensin function. Large-scale phosphoproteomic studies (Nousiainen et al., 2006; Hegemann et al., 2011; Pagliuca et al., 2011; Kao et al., 2014) have described numerous additional cell cycle–regulated condensin phosphorylation events (some of which Bazile et al. (2010) summarise), the role of which remains to be explored.

Mps1 Mps1 is associated, in several eukaryotes, with various aspects of mitotic progression, including the mitotic checkpoint, chromosome segregation and cytokinesis (Liu and Winey, 2012). The kinase regulates early prophase condensation in HeLa cells by phosphorylating Kleisin II/CAP-H2, at S492; a failure of this phosophorylation event or depletion of Mps1 disrupts proper condensin II localisation to chromatin (Kagami et al., 2014).

Aurora B The chromosomal passenger complex (CPC) Aurora B kinase is implicated in chromosome condensation in a number of species. In the fission yeast *S.*

pombe, the CPC member Cut17/Bir1 is essential for proper localisation of the Aurora B–like kinase Ark1, condensin recruitment and chromosome condensation (Morishita et al., 2001). In this system, Aurora B kinase activity is required for the mitotic association of condensin with chromatin, but not its nuclear localisation (Petersen and Hagan, 2003; Nakazawa et al., 2008). In *Drosophila* Schneider cells, RNAi against Aurora B is associated with a loss of chromatin-bound Kleisin I/Barren, leading to incomplete chromosome condensation, abnormal segregation, a failure of cytokinesis and polyploidy (Giet and Glover, 2001). In budding yeast, the anaphase condensation of rDNA arrays requires Aurora B/Ipl1 (Lavoie et al., 2004). Similarly, the *C. elegans* Smc2/MIX1 fails to be recruited to chromatin after Aurora B RNAi (Kaitna et al., 2002), and chromosome condensation is consequently delayed (Maddox et al., 2006). In HeLa cells, RNAi, as well as treatment with the Aurora B inhibitor hesparadin, lead to a loss of chromatin association of condensin I but not condensin II (Lipp et al., 2007). Maximal anaphase chromosome compaction in rat kidney cells also depends on Aurora B (Mora-Bermúdez et al., 2007), and condensin I association with chromatin is reduced after depletion of Aurora B from *Xenopus* egg extracts (Takemoto et al., 2007).

Two common themes emerge from these studies on the role of Aurora B in chromosome condensation. First, the depletion of Aurora B impairs the association of condensin I with chromatin, an observation consistent in *S. pombe* (Petersen and Hagan, 2003; Nakazawa et al., 2008), *Drosophila* (Giet and Glover, 2001) and HeLa (Lipp et al., 2007) cells, as well as *Xenopus* egg extracts (Takemoto et al., 2007). Second, the maximal chromosome compaction that occurs in anaphase requires Aurora B (Lavoie et al., 2004; Mora-Bermúdez et al., 2007) and presumably its kinase activity (Petersen and Hagan, 2003; Nakazawa et al., 2008). However a direct link between Aurora B kinase and condensin remained elusive until *in vitro* experiments established that Aurora B/Ipl1 directly phosphorylates the budding yeast condensin accessory subunits Kleisin I/Brn1, HEAT IA/Ycs4 and HEAT IB/Ycg1 in mitosis (St-Pierre et al., 2009). Mass spectrometry studies have since identified three Aurora B consensus sites in fission yeast Kleisin I/Cnd2: S5, S41 and S52, of which S52 phosphorylation depends on Aurora B kinase *in vivo*; substitutions of the three serine residues to nonphosphorylatable alanines lead to chromosome missegregation (Nakazawa et al., 2011). These observations have been confirmed and extended to mammals. A series of *in vitro* and *in vivo* experiments show that mitotic phosphorylation of the condensin I kleisin subunit triggers its interaction with the basic N-terminal tail of histones

H2A and H2A.Z, which is required for chromatin association of the complex (Tada et al., 2011). The conservation of phosphorylation-dependent condensin interactions with histone H2A variants between fission yeast and mammals, and the general requirement of Aurora B kinase for chromosome condensation in various species, suggests this may be a fundamental mechanism common to all eukaryotes.

In *S. pombe*, the histone variant H2A.Z additionally requires N-terminal acetylation to maintain condensin association with chromatin, and hence anaphase chromosome condensation (Kim et al., 2009). Furthermore, Aurora B may also have a condensin-independent role in chromatin hypercondensation, via phosphorylation of histone H3 at S10, leading to a cascade of histone modifications that free the histone H4 tail to interact with the surface of neighbouring nucleosomes, promoting fibre condensation (Wilkins et al., 2014).

Cdc14 In addition to the kinases CDK, Polo and Aurora B, the phosphatase Cdc14 also plays a role in chromosome condensation in budding yeast. Cdc14 is sequestered in the nucleolus until it is activated in anaphase by the cdc-fourteen early anaphase release (FEAR) pathway and the mitotic exit network (MEN) (Queralt and Uhlmann, 2008). In early anaphase, Cdc14 is essential for anaphase-specific condensation and segregation of the rDNA locus, activities that in turn require condensin and Aurora B (Sullivan et al., 2004). Cdc14 promotes condensin association with rDNA, which correlates with the sumoylation of HEAT IA/Ycs4 and phosphorylation of HEAT IB/Ycg1 (D'Amours et al., 2004). The Cdc14 target(s) that promote rDNA condensation and segregation are not known. One possibility is that the Cdc14-dependent dephosphorylation of the CPC component Sli15 and the resultant anaphase-specific relocalisation of Aurora B to the spindle midzone play a role (Pereira and Schiebel, 2003). Aurora B at the spindle midzone has been proposed to promote hypercondensation of trailing chromosome arms (Tada et al., 2011; Neurohr et al., 2011). Potential roles of sumoylation or direct dephosphorylation of condensin subunits by Cdc14 remain to be explored, as is the role of Cdc14 in anaphase condensation in other species. In contrast to its early anaphase role in compaction, Cdc14 promotes chromosome decondensation subsequently in late anaphase. At this stage, CDK inhibition and Cdc14 activity impair the association of Brn1 with chromatin (Varela et al., 2009). These results are consistent with the possibility that condensin dephosphorylation by Cdc14 promotes chromosome decondensation at mitotic exit. Since phosphorylation generally appears to stimulate the biochemical activity of

the condensin complex, such as DNA binding and supercoiling, its dephosphorylation may reverse these effects to permit chromosome decondensation as cells return to interphase. Consistent with this idea, the phosphatase PP2A, which plays a role in mitotic exit in higher eukaryotes, has been implicated in the dephosphorylation of HEAT IIA/CAP-D3 (Yeong et al., 2003).

CPF In fission yeast, the 3′ end RNA processing factor Swd2.2, a component of the cleavage and polyadenylation factor (CPF), acts as a negative regulator of condensin-mediated chromosome condensation (Vanoosthuyse et al., 2014). This function is independent of Aurora B-dependent phosphorylation of Kleisin I/Cnd2 (Tada et al., 2011) or H2A.Z acetylation (Kim et al., 2009), and may instead occur by impairing the association of condensin with chromatin.

CK2 A casein kinase II (CK2)–mediated interphase-enriched phosphorylation of condensin I in human cell cultures is the only known phosphorylation that negatively regulates the supercoiling activity of condensin (Takemoto et al., 2006).

1.2.5 Towards a mechanistic understanding of chromosome condensation

Biochemical characterisation of condensin has uncovered a number of activities of the complex, including the ability to topologically encircle DNA, supercoil DNA and hydrolyse ATP. It is likely that models of mitosis-specific chromosome condensation by condensin will incorporate some or all of these activities, each of which could be modulated by post-translational modifications. Notably, postulating the topological entrapment of two chromatin strands within a single circular condensin complex provides a succinct explanation of how condensin might mediate long-range chromosomal interactions (Cuylen et al., 2011, 2013; Thadani et al., 2012). Alternatively, a handcuff-like assembly of two tethered condensin rings, as is sometimes proposed in the case of cohesin (Zhang et al., 2008), might bridge distant DNA regions (Figure 1.6).

Multimerisation

Evidence for the formation of multimeric condensin assemblies stems largely from *in vitro* studies of bacterial condensins. In electron micrographs, purified *E.*

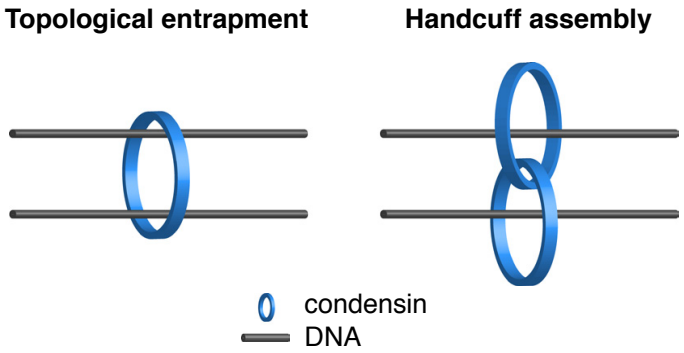

Figure 1.6 Proposed modes of condensin binding to chromatin. *Left*: A ring-shaped condensin complex topologically captures more than one strand of chromatin in a sequential manner to bring about condensation. *Bottom*: A ring-shaped condensin complex binds to a single strand of chromatin. The condensation reaction then involves dimerisation of more than one condensin complex in a handcuff-like assembly, or even their multimerisation. These models are not mutually exclusive, and it is easy to imagine the multimerisation of condensin rings that entrap more than one strand of chromatin. *Adapted from Thadani et al. (2012)*.

coli MukBEF has been seen as an oligomer, forming extended fibres and rosette-like configurations. In contrast, the MukB homodimer is rarely multimeric, suggesting that intermolecular MukE or MukF interactions mediate oligomerisation (Matoba et al., 2005). Protein volume measurements via atomic force microscopy show that *B. subtilis* SMC complexes form higher-order structures in the presence of ScpA and ScpB, further indicating that the accessory subunits may have a role in the organisation of SMC oligomers (Fuentes-Perez et al., 2012). There are several indications that DNA compaction *in vitro* can proceed by the concerted action of several condensin complexes. Direct force measurements in single molecule experiments demonstrate that MukBEF compacts DNA into stable, repetitive structures in a highly cooperative manner (Cui et al., 2008; Petrushenko et al., 2010). Similar cooperative behaviour of condensin I was observed during the ATP-dependent compaction of single nanomanipulated DNA fibres (Strick et al., 2004). In contrast to these *in vitro* compaction reactions in the presence of excess amounts of condensin, the number of condensin complexes *in vivo* is relatively small. Thus, although MukB is found in clusters in living cells (Ohsumi et al., 2001), the applicability of these results to the DNA condensation reaction at physiological concentrations of condensin remains undetermined. In both yeast and humans, chromosome condensation is achieved by one condensin complex per 5-10 kb of DNA (Wang et al., 2005; MacCallum et al., 2002). Whether and how interactions between more than one condensin complex contribute to chromosome condensation *in vivo* is as yet unknown. Fu-

ture experiments using superresolution microscopy and FRET approaches will help to investigate this possibility.

DNA supercoiling and topological selectivity

Eukaryotic and bacterial condensins have both been shown to possess the intrinsic ability to directly supercoil DNA *in vitro*, albeit with differing directionalities. Condensin purified from *Xenopus* egg extracts (Hirano et al., 1997; Kimura et al., 1998) and yeast cells (St-Pierre et al., 2009) is able to introduce positive supercoils in circular plasmid DNA in the presence of topoisomerase I and ATP. The *Xenopus* condensin preparation also produces chiral knots in DNA in the presence of topoisomerase II, leading to the idea that condensin reconfigures DNA by the introduction of a global positive writhe (Kimura et al., 1999). Like its eukaryotic counterparts, the *E. coli* MukB introduces right-handed knots into DNA in the presence of phage topoisomerase II; the net supercoiling stabilised by MukB, however, is negative (Petrushenko et al., 2006a). An interaction of condensin with type II topoisomerases has been demonstrated in *Drosophila* and *E. coli* (Bhat et al., 1996; Hayama and Marians, 2010; Li et al., 2010). However, this interaction has been implicated in the role of condensin in the decatenation of sister chromatids to facilitate chromosome segregation (Bhat et al., 1996; D'Ambrosio et al., 2008a). Any presumed role for topoisomerase II in chromosome condensation remains controversial. While supercoiling and the introduction of a writhe thus remain striking *in vitro* effects of condensin on DNA, their relevance to chromosome condensation *in vivo* in the face of abundant DNA topoisomerases that are adapted to relieve topological stress, remains uncertain.

Condensin from *Xenopus* egg extracts preferentially binds cruciform DNA molecules over unstructured linear duplexes, and longer DNA molecules over shorter ones, in electromobility shift assays (Kimura and Hirano, 1997). While such binding preferences to complex DNA structures *in vitro* remain difficult to interpret, they may point to an interesting feature of condensin. In the case of *E. coli* MukB, single molecule recordings show the protein to stabilise interactions between two strands of DNA, with a marked preference for right-handed DNA crossings (Petrushenko et al., 2010). These observations suggest that condensin does not simply capture randomly colliding DNA molecules but may recognise their topology. Such a topology distinction could contribute to a possible mechanism for distinguishing interactions within a chromatid from those between sister chromatids.

ATPase activity

SMC proteins lack sequence or structural similarity to conventional motor proteins (van den Ent et al., 1999; Lammens et al., 2004) and are thus unlikely to use the energy of ATP hydrolysis to move along chromosomes or physically reel in DNA. Instead the SMC ATPase cycle drives a series of conformational changes at the molecular level that likely influence the chromosomal association of the condensin complex. ATP binding to the SMC head domains leads to their engagement, while ATP hydrolysis allows the heads to move apart (Lammens et al., 2004). Despite some initial qualitative studies in chicken DT40 cells (Hudson et al., 2008), how precisely the catalytic cycle of ATP-dependent head engagement and disengagement is coupled to condensin's interaction with chromatin, and whether this contributes to chromosome condensation, has remained unclear.

The SMC-kleisin interaction is a candidate for regulation by the ATPase cycle. A striking ATP-dependent conformational change has been observed in structural studies of the E. coli MukBEF complex, where ATP binding–mediated engagement of the two MukB heads leads to the detachment of the dimeric MukF kleisin frame from one of the MukB heads (Woo et al., 2009). This conformational change requires a transient loss of kleisin interaction with one of the MukB heads and thus might be coupled to topological DNA entry or exit from the MukB ring. In the case of cohesin, the C-terminal winged-helix domain of the kleisin Scc1 stimulates the ATPase activity of the Smc1-Smc3 heterodimer by promoting ATP binding to the Smc1 head (Arumugam et al., 2006). In addition, the reported stimulation of condensin SMC ATPase activity upon DNA binding by its HEAT repeat subunits may play a role (Piazza et al., 2014). Little is yet known about the consequences of ATP hydrolysis for condensin function *in vivo*, though in case of cohesin it has been established that ATP hydrolysis is required for chromosome association of the complex (Arumugam et al., 2003; Weitzer et al., 2003), as well as its relocation from chromosomal loci occupied by the Scc2-Scc4 loading complex (Hu et al., 2011).

A recent model for cohesin proposes two distinct entry and exit gates for DNA. In this model, DNA enters the ring through the Smc1-Smc3 hinge dimerisation interface, and exits via opening of the Smc3-kleisin interaction (Chan et al., 2012). How conformational changes at the ATPase heads could be translated to the hinge domain some 50 nm away to allow DNA entry remains to be investigated. Such a long range interaction has been demonstrated between the two parts of

the cohesin complex (McIntyre et al., 2007). In the case of condensin, a head-hinge interaction is apparent in atomic force microscopic images of the fission yeast complex (Yoshimura et al., 2002). The archaeal SMC hinge has also been implicated in its binding to DNA. Notably an enzymatic crosstalk between DNA binding close to the hinge and ATP hydrolysis by the ATPase heads domains has been observed (Griese and Hopfner, 2011; Hirano and Hirano, 2006). At the same time, the hinges of the prokaryotic SMC and MukB proteins show substantial structural differences (Griese and Hopfner, 2011; Ku et al., 2010). The impact of ATP binding and hydrolysis on SMC complexes therefore remains an important area of study that should shed light on their ability to dynamically associate with and condense chromosomes, and is the subject of the present study.

1.3 Objectives

The aim of this project is to determine whether and how the ATPase activity of condensin affects chromosome condensation, which remains a poorly understood aspect of condensin function. Using specific structure-based point mutations, along with quantitative measurements of chromosome condensation, and novel conditional alleles of condensin in the eukaryotic model budding yeast *Saccharomyces cerevisiae*, I show that the ATPase activity of condensin is crucial for its function. Mutations in the ATPase domain alter the dynamic chromatin binding properties of condensin, and compromise its ability to form compact mitotic chromosomes. Taken together, these results shed light on critical events in the assembly and faithful segregation of mitotic chromosomes.

2 Materials and Methods

2.1 Yeast strains, growth and media

The genotypes of all budding yeast strains used in this work are specified in the List of Strains on page 130. Genes were tagged at their C-termini by transformation (Section 2.5) with one-step PCR-based gene targeting amplicons (McElver and Weber, 1992). Oligonucleotides for generating these amplicons typically had ~50 bp of homology to sequences flanking the target gene stop codon, and ~20 bp of homology to the template vector containing the tag and selection marker. Table 2.1 contains a list of all oligonucleotides and template vectors used to generate strains for this study.

Unless otherwise stated, all strains were grown at 25°C. Liquid cultures were grown with agitation at 220 rpm. Cell growth in liquid cultures was assessed by absorbance measurements on an Ultrospec 2000 UV/visible spectrophotometer (Amersham Pharmacia Biotech) at 600 nm; 1 OD unit corresponded to ~1.5 x 10^7 cells/ml.

Growth media were obtained according to standard specifications: YP ('yeast peptone' – 1.1% w/v yeast extract, 2.2% w/v bacto-peptone and 0.0055% w/v adenine-HCl) supplemented with 2% w/v D-(+)-glucose (YPD), 2% w/v D-(+)-raffinose (YPRaff) or 2% D-(+)-raffinose + galactose (YPRaffGal); YNB ('yeast nitrogen base' – 0.8% w/v yeast nitrogen base, 60 µg/ml of each of the amino acids tyrosine, uracil, tryptophan, leucine, adenine, histidine, isoleucine & phenylalanine, 3 µg/ml arginine, 4 µg/ml lysine and 5 µg/ml threonine). Solid media for plates contained 2.2% w/v agar in addition. For auxotrophic selection of transformants, YNB agar plates lacking the selective amino acid(s) were used. Alternatively, for selection based on kanamycin resistance, YPD agar plates supplemented with the kanamycin derivative geneticin G418 (200 µg/ml) were used.

2.2 Yeast cell synchronisation

For cell synchronisation in G1, cells were grown to early log phase (OD $\approx$ 0.1–0.2) before addition of the pheromone twice at 1 hour intervals. For strains of the *MAT*a mating type, 5 µg/ml α factor was used each time (1:1000 from a 5 mg/ml stock solution in methanol). For strains of the *MAT*α mating type, 0.02 µg/ml **a** factor was used each time (1:10000 from an 0.2 mg/ml stock solution in methanol; O'Reilly et al., 2012); pheromones were synthesised in-house (Peptide Synthesis Laboratory, Cancer Research UK London Research Institute). Metaphase arrests were induced by nocodazole added to growth medium at a final concentration of 4–5 µg/ml (1:500–1:400 from a 2 mg/ml stock solution in DMSO). For auxin-induced degradation, indole-3-acetic acid was used at a concentration of 1 mM (1:500 from a 0.5 M stock solution in methanol). For induction of the anchor-away technique, rapamycin was used at a concentration of 1 µg/ml (1:1000 from a 1 M stock solution in DMSO).

Table 2.1 Oligonucleotides and templates used for gene targeting

Strain	Product	Template	Oligonucleotides
RT19	*HTB2-YFP–HIS*	pCSL288	oRT11, oRT12
RT49	*SMC2-3HA–URA*	pCSL42	co132, co133
RT63	*BRN1-3Pk–LEU*	pCSL563	co311, co312
RT65	*BRN1-3Pk–LEU*	pCSL563	co311, co312
RT145	*SMC2-IAA17-9myc–KAN*	pRT40	oRT56, oRT57
RT146	*SMC2-3Pk-miniAID–KAN*	pRT21	oRT56, oRT57
RT148	*SMC4-IAA17-9myc–KAN*	pRT40	oRT58, oRT59
RT149	*SMC4-3Pk-miniAID–KAN*	pRT21	oRT58, oRT59
RT155	*BRN1-3HA–TRP*	pCSL35	co311, co312
RT159	*SMC4-3HA–TRP*	pCSL35	co134, co135
RT161	*SMC2-3Pk–TRP*	pCSL554	co132, co133
RT163	*SMC4-3Pk–TRP*	pCSL554	co134, co135
RT174	*NET1-mCitrine–HIS*	pRT22	oRT1, oRT2
RT178	*NET1-mCitrine–HIS*	pRT22	oRT1, oRT2
RT180	*NET1-mCitrine–HIS*	pRT22	oRT1, oRT2
RT184	*NET1-mCitrine–HIS*	pRT22	oRT1, oRT2
RT192	*HTB2-mCitrine–HIS*	pRT22	oRT11, oRT12
RT196	*HTB2-mCitrine–HIS*	pRT22	oRT11, oRT12
SH110	*SMC2-FRB–KAN*	pES30578	oRT49, oRT4
SH184	*SMC4-FRB–KAN*	pES30578	oRT50, oRT6

2.3 Yeast genomic DNA extraction

Genomic DNA was prepared from fresh patches of yeast growing on YPD plates. A loopful of cells were resuspended in 200 µl SCE/ME/Zymolase (1 M sorbitol; 100 mM sodium citrate, pH 7.0; 60 mM EDTA; per ml: 8 µl β-mercaptoethanol, 2 µl of 20 mg/ml zymolase T-20) and incubated at 37°C for 45 min on a shaking thermomixer. 200 µl of SDS solution (100 mM Tris-HCl, pH 9.0; 50 mM EDTA; 2% SDS) was added, and the mixture heated at 65°C for 5 min. 200 µl of 5 M potassium acetate was added at room temperature, followed by centrifugation at 14000 rpm for 10 min on a benchtop microcentrifuge. 350 µl of the supernatant was transferred to a fresh tube. 800 µl of 100% ethanol was added, followed by centrifugation at 6000 rpm for 2 min at room temperature. The ethanol was aspirated, and the pellet was rinsed with 70% ethanol, air-dried in a 37°C thermomixer for 20 min, and resuspended in 200 µl nuclease-free water. Concentration was measured on a Nanodrop ND-1000 spectrophotometer.

2.4 Cloning

2.4.1 YIplac128–P_{GAL1}–SWE1-3Pk

The *SWE1* open reading frame (ORF) was amplified by PCR using Expand High Fidelity polymerase (Roche Diagnostics), primers oRT62 and oRT63, and a K699 genomic DNA template (extracted as described in Section 2.3). The resulting 2476 bp fragment was treated with Taq polymerase (Qiagen) to create 3′ A overhangs and inserted into linearised pCR2.1 in a TopoTA cloning reaction (Invitrogen). Following sequencing, the insert was sub-cloned into pCSL520 as a BamHI, PstI fragment, generating the *LEU2*-integrable vector pRT41 (YIplac128–P_{GAL1}–SWE1-3Pk; Figure 2.1).

2.4.2 pFA6a–IAA17-9myc–kanMX

Full-length IAA17 without a stop codon was amplified by PCR as a KpnI, XmaI fragment from pMK43 (Nishimura et al., 2009) using Expand High Fidelity polymerase (Roche Diagnostics) and primers oRT87 and oRT88. 9myc was amplified from pCSL43 as an XmaI, BglII fragment using primers oRT89 and oRT90 and resolved on an acrylamide gel. The purified digested fragments were inserted

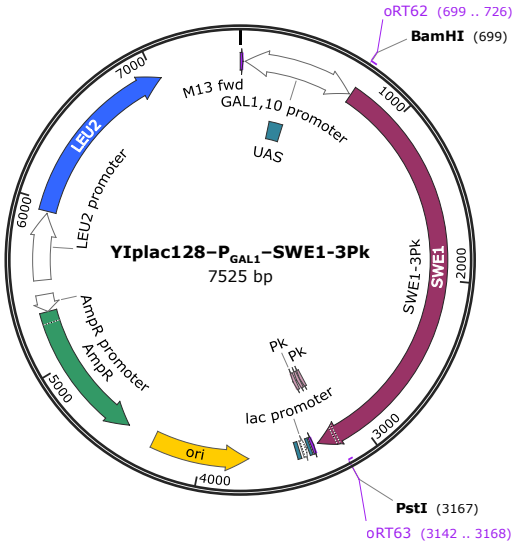

Figure 2.1 YIplac128–P_{GAL1}–SWE1-3Pk.

into KpnI, BglII–linearised pMK43, yielding the C-terminal *aid* tagging vector pRT40 (pFA6a–IAA17-9myc–kanMX; Figure 2.2).

2.4.3 pFA6a–3Pk-miniAID–kanMX

A codon-optimised (Grote et al., 2005) 3Pk tag was inserted into pMK151 (Kubota et al., 2013) with the mutagenic primers oRT136 and oRT137, using the Q5 site directed mutagenesis kit (New England Biolabs) following the manufacturer's instructions. This formed a pFA6a–3Pk-3miniAID–kanMX construct, which was subjected to further deletion mutagenesis with primers oRT176 and oRT177 using the same kit to generate the final C-terminal *aid* tagging vector pRT21 (pFA6a–3Pk-miniAID–kanMX; Figure 2.3).

2.4.4 YIplac211–P_{SMC2}–SMC2-3HA

YIplac211–P_{SMC2}–SMC2-3HA was constructed by an InFusion HD cloning reaction (Clontech) between three fragments with 15 bp overlaps: inserts P_{SMC2}–*SMC2* & 3HA and vector YIplac211. The *SMC2* ORF was amplified along with 500 bp of upstream sequence (designated P_{SMC2}) by PCR from K699 genomic DNA with primers oRT121 and oRT122, using CloneAmp high fidelity polymerase (Clontech). Similarly, a 3HA epitope tag was amplified from pCSL42 with primers oRT123 and oRT124. The vector YIplac211 (pCSL3) was prepared by overnight

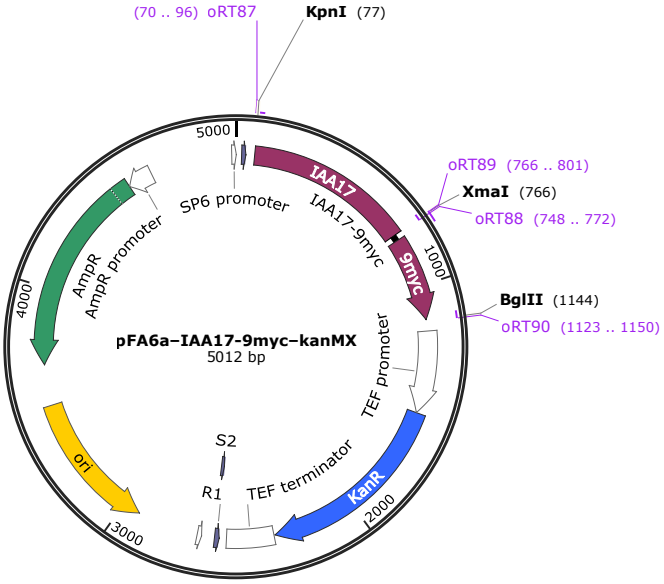

Figure 2.2 pFA6a–IAA17-9myc–kanMX.

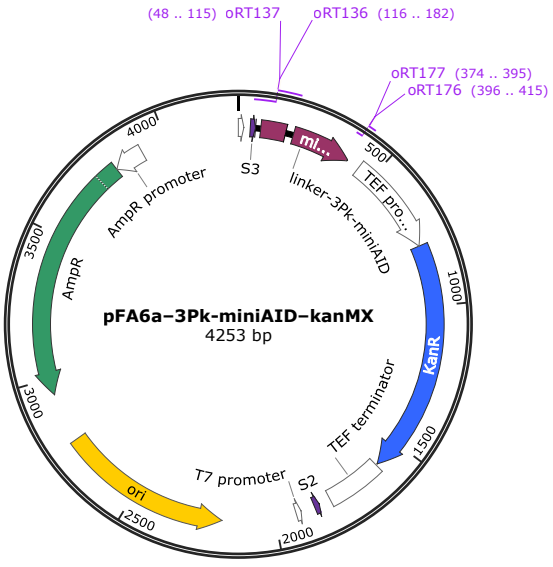

Figure 2.3 pFA6a–3Pk-miniAID–kanMX.

digestion with SphI and EcoRI, heat inactivation and treatment with rSAP (New England Biolabs). Following agarose gel purification, 100 ng of each of the three overlapping DNA fragments (P_{SMC2}–*SMC2*, 3HA and YIplac211) was used in a 10 µl Infusion HD cloning reaction as per the manufacturer's instructions (15 min, 50°C). 5 µl of the reaction mixture was transformed into one-shot TOP10F′ chemical competent *E. coli* (Invitrogen), and the cells plated on LB + ampicillin selective medium containing BluoGal for blue-white colony screening. Putative positive white clones were verified by sequencing, producing the final *URA3*-integrable vector pRT1 (YIplac211–P_{SMC2}–SMC2-3HA; Figure 2.4).

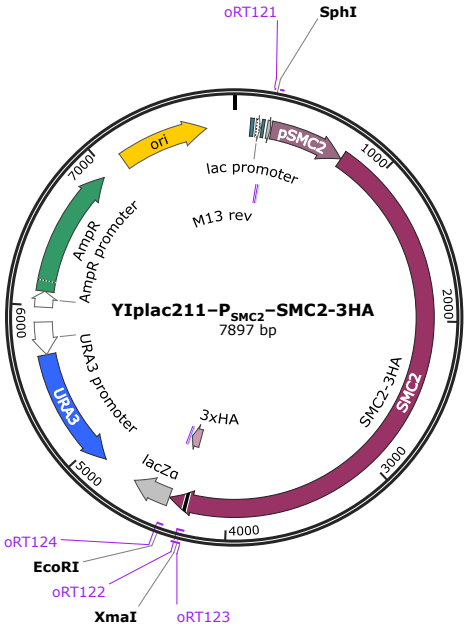

Figure 2.4 YIplac211–P_{SMC2}–SMC2-3HA.

2.4.5 YIplac204–P_{SMC4}–SMC4-3HA

YIplac204–P_{SMC4}–SMC4-3HA was constructed by a two-way InFusion HD cloning reaction (Clontech) using 15 bp overlaps between the insert P_{SMC4}–*SMC4-3HA* and vector YIplac204. The *SMC4* ORF was amplified along with 499 bp of upstream sequence (designated P_{SMC4}) by PCR from K699 genomic DNA with primers oRT125 and oRT126, using CloneAmp high fidelity polymerase (Clontech). Similarly, a 3HA epitope tag was amplified from pCSL42 with primers oRT127 and oRT124. The complete insert P_{SMC4}–*SMC4-3HA* was then prepared by a nested PCR reaction with primers oRT125 and oRT124, using gel-purified P_{SMC4}–*SMC4* and 3HA fragments as templates. The vector YIplac204 (pCSL2)

was prepared by overnight digestion with SphI and EcoRI, heat inactivation, and treatment with rSAP (New England Biolabs). Following agarose gel purification, 100 ng of each of the two overlapping DNA fragments (P_{SMC4}–*SMC4-3HA* and YIplac204) was used in a 10 µl Infusion HD cloning reaction as per the manufacturer's instructions (15 min, 50°C). 5 µl of the reaction mixture was transformed into one-shot TOP10F′ chemical competent *E. coli* (Invitrogen), and the cells plated on LB + ampicillin selective medium containing BluoGal for blue-white colony screening. Putative positive white clones were verified by sequencing, producing the final *TRP1*-integrable vector pRT8 (YIplac204–P_{SMC4}–SMC4-3HA; Figure 2.5).

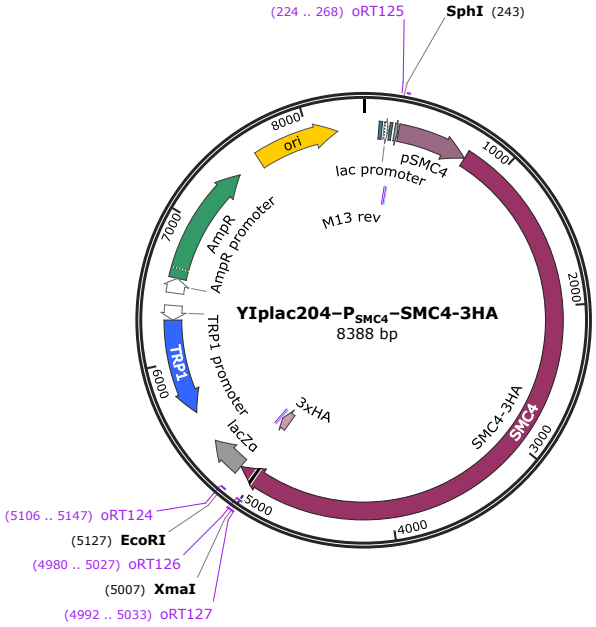

Figure 2.5 YIplac204–P_{SMC4}–SMC4-3HA.

2.4.6 ATPase mutants of *SMC2* and *SMC4*

Point mutants of *SMC2* and *SMC4* were constructed with mutagenic primers (listed in Table 2.2) on templates YIplac211–P_{SMC2}–SMC2-3HA and YIplac204–P_{SMC4}–SMC4-3HA respectively, using the Q5 site directed mutagenesis kit (New England Biolabs) following the manufacturer's instructions. Briefly, 12.5 µl PCR reactions were performed using Q5 high fidelity polymerase with 5 ng of appropriate template and 0.5 µM of each primer. Following verification by agarose gel electrophoresis, 0.5 µl of the PCR mixture was treated with the KLD (kinase, ligase & DpnI) mix provided with the kit in a 5 µl reaction, and transformed into the

supplied NEB5α high efficiency competent cells. Positive clones were identified by sequencing.

Table 2.2 Oligonucleotides used for constructing SMC ATPase mutants.

Vector		Oligonucleotides
pRT2	YIplac211–P_{SMC2}–SMC2^{K38A}-3HA	oRT105, oRT106
pRT3	YIplac211–P_{SMC2}–SMC2^{R58A}-3HA	oRT107, oRT108
pRT5	YIplac211–P_{SMC2}–SMC2^{S1085R}-3HA	oRT109, oRT110
pRT6	YIplac211–P_{SMC2}–SMC2^{E1113Q}-3HA	oRT111, oRT112
pRT9	YIplac204–P_{SMC4}–SMC4^{K191A}-3HA	oRT113, oRT114
pRT10	YIplac204–P_{SMC4}–SMC4^{R210A}-3HA	oRT115, oRT116
pRT11	YIplac204–P_{SMC4}–SMC4^{R210K}-3HA	oRT162, oRT116
pRT12	YIplac204–P_{SMC4}–SMC4^{S1324R}-3HA	oRT117, oRT118
pRT13	YIplac204–P_{SMC4}–SMC4^{E1352Q}-3HA	oRT119, oRT120
pRT14	YIplac204–P_{SMC4}–SMC4^{E1352D}-3HA	oRT163, oRT120

2.4.7 pFA6a–yEmCitrine–*Sk*HIS3

pFA6a–yEmCitrine–*Sk*HIS3 was constructed by a two-way Infusion HD cloning reaction (Clontech) using 15 bp overlaps between the insert yEmCitrine and vector pCSL879. The yEmCitrine ORF was amplified from pKT0211/pAG8734 with primers oRT138 and oRT143a using Q5 high fidelity polymerase (New England Biolabs). The vector pFA6a–HIS3MX6 (pCSL879) was prepared by overnight digestion with BglII, heat inactivation, and treatment with rSAP (New England Biolabs). Following agarose gel purification, 100 ng of each of the two overlapping DNA fragments (mCitrine and pFA6a–HIS3MX6) was used in a 10 µl Infusion HD cloning reaction as per the manufacturer's instructions (15 min, 50°C). 5 µl of the reaction mixture was transformed into one-shot TOP10F′ chemical competent *E. coli* (Invitrogen), and plated on selective LB + ampicillin medium. Putative positive clones were identified by a diagnostic digest with BglII and verified by sequencing, producing the final C-terminal tagging vector pRT22 (pFA6a–yEmCitrine–*Sk*HIS3; Figure 2.6).

2.5 Yeast transformation

Yeast cells were transformed using a variation of the high efficiency lithium acetate method (Gietz and Schiestl, 2007). 50 ml of mid log–phase cells (OD $\approx$

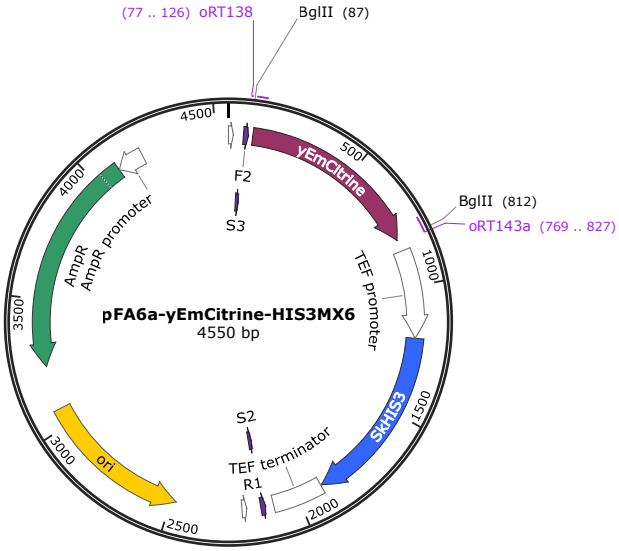

Figure 2.6 pFA6a–yEmCitrine–*Sk*HIS3.

0.5) were spun down (3000 rpm, 5 min), washed in 1 ml water, followed by 1 ml TEL (10 mM Tris-HCl, pH 7.5; 0.1 mM EDTA; 100 mM lithium acetate), and finally resuspended in 50 µl TEL. In a separate tube, upto 8 µl of DNA to be transformed (1 µg linearised vector or PCR product for integration) was added to 2 µl of 10 mg/ml salmon sperm DNA that had been boiled at 95°C for 5 min and cooled on ice for 5 min. 50 µl of the cell suspension in TEL was added to the DNA and mixed. 300 µl of TELP (TEL containing sterilised 40% PEG_{3350}) was added, the mixture vortexed for 10 sec, and incubated at 25°C for 2–4 hours. The transformation mix was then subjected to heat shock at 42°C for 15 min, spun down (4000 rpm, 2 min) and resuspended in 1 ml filter-sterilised 1 M sorbitol. 100 µl was plated as the 1/10 dilution. The rest of the mix was spun down again (4000 rpm, 2 min), resuspended in 100 µl 1 M sorbitol and plated as the 9/10 dilution. The plates were incubated at 25°C for 2–3 days, when colonies became visible. For auxotrophic selection, the appropriate selective plates were used directly (Section 2.1), whereas for kanamycin selection, YPD plates were used for overnight growth, before replica plating onto YPD + G418 plates.

2.6 Flow cytometry

For preparation of samples for flow cytometry, 1 ml of culture (OD > 0.15) was spun down, fixed in 1 ml ice-cold 70% ethanol, and incubated at 4°C overnight. Cells were pelleted and resuspended in 1 ml of 50 mM Tris-HCl, pH 7.5 contain-

ing 0.1 mg/ml RNase A (1:100 from 10 mg/ml stock, DNase free after boiling). The cells were incubated at 37°C for 2–16 hours, pelleted and resuspended in 0.4 ml of FACS buffer (200 mM Tris-HCl, pH 7.5; 211 mM NaCl; 78 mM $MgCl_2$) containing 50 µg/ml propidium iodide (1:20 from 1 mg/ml propidium iodide stock in water). Samples were sonicated for 5 seconds and stored in the dark at 4°C until analysis. For analysis, 50–100 µl of stained cells were diluted in 600 µl of 50 mM Tris-HCl, pH 7.5. Immediately after dilution, 10000 events per sample were counted on a Beckton-Dickinson FACScan with settings in linear mode (FSC threshold: 52; FSC: detector: E01, amplifier: 1.4; SSC: detector: 400, amplfier: 1; FL1, FL3 off; FL2: detector: 750, amplifier: 7). The resulting cell counts were analysed using FlowJo.

2.7 Western blotting

Chemiluminescent detection was performed using antibodies diluted in 5% non-fat milk in phosphate buffered saline (PBS), Amersham ECL Prime reagents, and an ImageQuant LAS4000 scanner. Fluorescent detection was performed using antibodies diluted in Licor blocking buffer and a Licor Odyssey scanner.

2.7.1 TCA protein extracts

5 OD units of cells (~10 ml, OD 0.5) were harvested (3000 rpm, 5 min, 4°C), resuspended in 1 ml ice-cold 20% TCA (tricholoacetic acid), centrifuged (1 min, 13000 rpm) and resuspended in 1 ml ice-cold 1 M Tris base (pH unadjusted). Cells were resuspended in 100 µl 2x SDS sample buffer (100 mM Tris-Cl, pH 6.8; 4% SDS; 0.2% bromophenol blue; 20% glycerol) with freshly added 200 mM DTT. Samples were boiled at 95°C for 2 min, 200 µl glass beads added, and boiled again at 95°C for 2 min. Cells were broken in a Yasui Kikai cooled cell breaker with two repetitions of programme 1 (2700 rpm, on 60 sec, off 60 sec, total time 420 sec) with a 5 min gap. Broken cells were again boiled at 95°C for 2 min, and the extracts transferred by centrifugal flow through needle holes (3000 rpm, 5 min) to 15 ml tubes. Extracts were transferred to fresh microcentrifuge tubes, boiled (95°C, 2 min), centrifuged (13000 rpm, 1 min) and loaded onto an SDS-PAGE gel. 5 µl of extract was typically used.

2.7.2 Primary antibodies

The following primary antibodies were used:

Clb2 Rabbit, Santa Cruz, sc9071

FKBP12 Rabbit, Novus Biologicals, NB300-508

HA Mouse 12CA5, Cell Services, Cancer Research UK
Rat 3F10, Roche, 1-867-423

Myc Mouse 9E10, Cell Services, Cancer Research UK

Pk Mouse, Serotec, MCA1360

α-tubulin Mouse TAT-1, Cell Services, Cancer Research UK

2.7.3 Secondary antibodies

The following secondary antibodies were used:

HRP–anti-mouse Sheep, Amersham, 926-32280

HRP–anti-rabbit Sheep, Amersham, NA934

IRdye800CW–anti-mouse Goat, Licor Biosystems, 926-32280

IRdye700DX–anti-rabbit Goat, Rockland, 611-130-122

2.8 Chromatin pellets

Chromatin pellets were prepared essentially as previously described (Liang and Stillman, 1997). 12.5 OD units of cells (50 ml, OD $\approx$ 0.25, 5 x 10^8 cells) were centrifuged (3000 rpm, 5 min) and resuspended in 3 ml CP1 solution (100 mM PIPES/KOH, pH 9.4; 10 mM DTT; 0.1% sodium azide) and incubated at room temperature for 10 min. The cells were then centrifuged (2000 rpm, 2 min), resuspended in 2 ml CP2 solution (50 mM potassium phosphate buffer, pH 7.4; 0.6 M Sorbitol; 10 mM DTT) and transferred to 2 ml microcentrifuge tubes. Cells were spheroplasted by addition of 4 µl 20 mg/ml zymolase T-100 and incubated in a 37°C water bath for 15 min. Spheroplastation was monitored using a spectrophotometer and halted when the OD of a 1:100 dilution of the cell suspension in water was less than 10% of the value before addition of enzyme, typically 15

min. In a cold room, cells were centrifuged (4000 rpm, 1 min), washed with 1 ml CP3 solution (1 ml 50 mM HEPES/KOH, pH 7.5; 100 mM KCl; 2.5 mM $MgCl_2$; 0.4 M sorbitol), and resuspended in 100 µl EB (50 mM HEPES/KOH pH 7.5; 100 mM KCl; 2.5 mM $MgCl_2$; 1 mM DTT; 1 mM PMSF; complete mini EDTA-free protease inhibitor cocktail). For lysis, Triton X-100 was added to a final concentration of 0.25% (1:40 from 10% stock solution), and cells were incubated on ice for 3 min with occasional vortexing. This was the whole cell extract (W). A 100 µl EBXS (EB + 0.25% Triton X-100 + 30% sucrose) cushion was prepared in a separate microcentrifuge tube. 100 µl of whole cell extract was laid on the EBX-S cushion and centrifuged (12000 rpm, 10 min). This yielded a white chromatin pellet, a clear sucrose layer, and a yellow supernatant fraction on top. Some of the supernatant (S) was saved to probe for soluble proteins. The remaining supernatant and sucrose buffer were aspirated. The chromatin pellet was resuspended in 100 µl EBX (EB + 0.25% Triton X-100), centrifuged (10000 rpm, 5 min), supernatant aspirated, and resuspended again in 100 µl EBX containing benzonase nuclease (1:1000) to yield the final chromatin pellet fraction (P). One quarter volume of 4x SDS sample buffer was added to each of the fractions before boiling (95°C, 5 min) for resolution by SDS-PAGE.

2.9 Chromosome semi-spreads

2 ml of culture was harvested (14000 rpm, 1 min), resuspended in 1 ml S1 (100 mM potassium phosphate buffer, pH 7.4; 0.5 mM $MgCl_2$; 1.2 M sorbitol), and kept on ice until all samples from the course of the experiment were harvested. For spheroplastation, cells were centrifuged (14000 rpm, 1 min) and resuspended in 200 µl S2 (S1 + per ml, 20 µl 1 M DTT and 14 µl 10 mg/ml zymolase T-100). The suspension was incubated in a 37°C water bath for 20 min. 1 ml of ice-cold S3 (0.1 M 2-(N-morpholino)ethanesulfonic acid; 1 mM EDTA; 0.5 mM $MgCl_2$; 1 M sorbitol, pH 6.4) was added. Spheroplasts was centrifuged (4000 rpm, 2 min), resuspended in 200 µl S3, and kept at 4°C until spreading, typically overnight. For spreading, 12 well multitest slides (MP Biomedicals, #6041205E) were washed with acid (1 M HCl, 60°C, 1 hour, then cooled to room temperature overnight), ethanol and polished with lens tissue. In a fume hood, the following were pipetted one after another onto each well used: 1 µl cell suspension; 2 µl fixative (4% paraformaldehyde, dissolved in water at 60–80°C; 3.4% sucrose; per ml, 1 µl 0.2 M NaOH); 4 µl 1% lipsol in water; 4 µl fixative. The drop was gently distributed onto the well using a pipette tip, avoiding contact with the glass. Slides

were dried overnight at room temperature in a fume hood. For immunostaining, slides were placed in PBS for 10 min, room temperature. 50 µl of blocking buffer (1% BSA in PBS) was pipetted onto each well, and placed in a humid chamber for 1 hour at 25°C. The blocking buffer was aspirated and 50 µl of primary antibody in blocking buffer was added to each well (e.g. rat anti-HA 3F10, 1:500), and incubated in a humid chamber for 2 hours at 25°C. The wells were rinsed 3 times with PBS before adding 50 µl secondary antibody diluted in blocking buffer (e.g. AlexaFluor 594 anti-rat, 1:1000) to each well. The slide was incubated in a darkened humid chamber for 2 hours at 25°C. Wells were again rinsed three times with PBS and then three times with water. DNA was then stained with 50 µl of a 100 µg/ml solution of DAPI in water pipetted onto each well, and incubated in the darkened humid chamber, 30 min, 25°C. Wells were rinsed 3 times with water and aspirated. Residual water was aspirated without touching the glass of the slide. 5 µl of antifade (SlowFade Diamond, Life Technologies) was pipetted onto each well. An acid washed coverslip (24 x 60 mm high precision, no. 1.5H, CellPath Ltd, SAN-2460-03A) was lowered onto the antifade mounting medium, and sealed with Valap (equal parts vaseline, lanolin & paraffin). The slide was stored in the dark at −20°C until imaging.

2.10 Immunofluorescence

For fixation, 2 ml of culture (OD > 0.2) was centrifuged and resuspended in 1 ml of ice cold IF1 (100 mM potassium phosphate buffer, pH 6.4; 0.5 mM $MgCl_2$) + 3.7% formaldehyde. Cells were fixed overnight at 4°C, centrifuged and washed once in 1 ml of cold IF1, and then in 1 ml of IF2 (100 mM potassium phosphate buffer, pH 7.4; 0.5 mM $MgCl_2$; 1.2 M sorbitol). Cells were resuspended in 200 µl of spheroplasting buffer (IF2 containing per ml, 2 µl β-mercaptoethanol + 2 µl of 20 mg/ml zymolase T-100), and incubated in a 30°C water bath for 20–40 min and monitored visually under a light microscope. The spheroplasts were centrifuged (4000 rpm, 2 min), washed in 500 µl spheroplasting buffer without additions, and resuspended in 200 µl of the same buffer. Cells were stored at 4°C until immunostaining. A 15 well multitest slide was used for staining. 5 µl of 0.1% polylysine was pipetted onto each well and the slide left in a humid chamber for 5 min. The slide was then washed under flowing distilled water briefly and dried by aspirating the remaining drops. All further incubations were carried out in a humid chamber. 5-10 µl of cell suspension was pipetted onto the wells and left to adhere for 5 min. Drops of suspension were aspirated. The slide was

plunged into methanol cooled to −20°C, left in methanol for 3 min, then transferred to acetone cooled to −20°C for 10 sec. The slide was then retrieved from the acetone and quickly warmed up on the bench top to evaporate the remaining acetone. The slide was then placed back in the humid chamber and 10 µl blocking buffer (1% BSA in PBS) was added to each well. The slide was blocked for 20–60 min in the humid chamber at 25°C. Blocking buffer was then aspirated and 5 µl of primary antibody diluted in blocking buffer added to each well (e.g. 1:1000 mouse anti–α-tubulin TAT-1, 1:1000 mouse anti-Pk) and incubated for 1 hour, 25°C. Wells were washed three times with blocking buffer. 5 µl of secondary antibody diluted in blocking buffer was added to each well (e.g. 1:1000 Alexa514–anti-mouse) and incubated in the dark for 1 hour, 25°C. Wells were rinsed again 3 times with blocking buffer. The remaining blocking buffer was aspirated, and DNA was stained with DAPI (5 µl of 0.1 µg/ml DAPI in water, 30 min, 25°C, dark). Finally, wells were rinsed 3 times with blocking buffer. The residual buffer was aspirated, 1 µl Vectashield pipetted onto each well, and the slide covered with a cover slip and sealed with Valap. Slides were stored in the dark at −20°C until imaging.

2.11 Microscopy and image analysis

For fluorescent microscopy, Menzel-Gläser superfrost slides (#AG00008032E) were washed with acid (1 M HCl, 60°C, 1 hour, then cooled to room temperature overnight), then 70% ethanol and polished with lens tissue. Zeiss High Performance coverslips no. 1.5 (D = 0.17 mm; #474030-9000-000) were similarly washed in acid and ethanol before use. Slides were sealed with Valap.

2.11.1 Conventional widefield

Conventional imagine was performed on a Deltavision Elite widefield system with broad-spectrum mercury arc illumination. Filters used for imaging were: DAPI – excitation 390/18, emission 457/50; YFP/Alexa514 – excitation 500/20, emission 535/30. Where necessary, deconvolution was applied in softWoRx using the conservative ratio method with medium noise filtering, and an experimentally determined point spread function (PSF). To improve the appearance of brightfield images, an FFT bandpass filter was applied in ImageJ (Schneider et al., 2012) with default parameters [3, 40] pixels ± 5%.

2.11.2 OMX: 3D structured illumination

Structured illumination microscopy was performed on an API OMX v3 microscope with the live filter set: DAPI – excitation 405 nm, emission 465-500 nm; YFP/AF514 – excitation 514 nm, emission 525-575 nm; mCherry/AF594 – excitation 592.5 nm, emission 602-656 nm. For images not acquired in structured illumination mode, deconvolution was applied in softWoRx using the conservative ratio method with medium noise filtering, and an experimentally determined PSF. For images acquired in structured illumination mode, default reconstruction parameters were used. For multichannel images, registration parameters for aligning the different channels were determined empirically using a 10 nm–spacing grid slide and Tetraspeck beads. Image exposure time was typically under 50 ms, and laser excitation power 1%-10%.

Genetically encoded labels

For genetically encoded fluorescent labels such as Net1-mCitrine (rDNA) and Htb2-mCitrine (histones), cells were fixed by addition of 3.6% formaldehyde directly to the liquid culture (1:10 by volume from 36% stock solution of EM grade formaldehyde, TAAB, #F003). After incubation on a roller for 10 min at room temperature, the cells were centrifuged (3000 rpm, 5 min, 4°C), washed 3 times with cold TBS (50 mM Tris, pH 8.0; 150 mM NaCl), rehydrated overnight in 1 ml TBS at 4°C, resuspended in 50-100 µl TBS, and then in a similar volume of SlowFade diamond mounting medium (Life Technologies) prior to slide preparation.

DAPI

For DAPI staining, cells were fixed similarly by addition of 3.6% formaldehyde directly to the liquid culture (1:10 by volume from 36% stock solution of EM grade formaldehyde, TAAB, #F003). After incubation on a roller for 10 min at room temperature, the cells were centrifuged (3000 rpm, 5 min, 4°C) and washed 3 times with cold PBS, pH 7.4. Cells were then permeabilised by addition of –20°C cold 70% ethanol, incubated on ice for 10 min, washed 3 times with ice cold PBS, and rehydrated overnight in 1 ml PBS at 4°C. Prior to imaging, cells were stained by addition of 0.1 µg/ml DAPI, incubated 10 min at 25°C, washed 3 times in PBS, resuspended in 50-100 µl PBS, and then in a similar volume of mounting medium (90% glycerol containing 2% n-propyl gallate) prior to slide preparation.

2.11.3 Volume quantification

For volume measurements, brightfield-guided manual cells outlines were saved as ROIs in ImageJ. Thresholds for fluorescent images and rDNA/DNA volumes were computed using the following macro:

```
// Measuring net1-mCitrine thresholded volume
// thresholds calculated from stack
setBatchMode(true);
macro "rDNAVolume" {
   workingDir = getDirectory("Select directory with images/ROIs");
   print("\\Clear");
   print(workingDir);
   fileList = getFileList(workingDir);
   for (i=0; i<fileList.length; i++) {
      if (endsWith(fileList[i], ".ROIs.zip")) {
         baseName = substring(fileList[i],0,indexOf(fileList[i],".ROIs.zip"));
         roiManager("Reset");
         roiManager("Open", workingDir+fileList[i]);
         roiManager("Show all");
         nROIs = roiManager("Count");
         for (j=0; j<nROIs; j++) {
         pixelCount = 0;
         // Open file and calculate volume
         run("Bio-Formats Windowless Importer", "open="+workingDir+baseName+"_D3D.
             dv");
         getVoxelSize(voxW, voxH, voxD, voxUnit);
         roiManager("Select", j);
         run("Clear Outside", "stack");
         setAutoThreshold("Default dark stack");
         run("Convert to Mask", "method=Default background=Dark black");
         run("Clear Results");
         run("Set Measurements...", "area min integrated stack redirect=None
             decimal=3");
         roiManager("Select", j);
         for (k=1; k<=nSlices; k++) {
            setSlice(k);
            run("Measure");
            pixelCount += getResult("RawIntDen",k-1);
         }
         pixelCount /= 255;
         print(baseName+"-"+j+1+"\t"+getResult("Area")+"\t"+pixelCount+"\t"+
             pixelCount*voxW*voxH*voxD);
         close();
         }
      }
   }
}
```

3 Results I: A Budding Yeast G2 Arrest

In contrast to well-established methods for synchronising budding yeast cells in the G1 and M phases of the cell cycle (Manukyan et al., 2011), there is no generally accepted equivalent for the G2 phase of the cell cycle. Since the chromosome condensation assays I use (detailed in the following chapters) rely on volume measurements, its was necessary to develop a robust means of arresting budding yeast cells in G2, in order to compare the condensation status of replicated interphase chromatin with mitotic chromosomes.

A pre-mitotic 'morphogenesis checkpoint' in budding yeast operates in response to perturbations of cell polarity that interfere with bud formation (Lew and Reed, 1995), such as Latranculin A–induced depolarisation of the actin cytoskeleton, and depends on the Swe1 kinase (McMillan et al., 1998). However, although called a checkpoint, the cellular response under such polarity perturbations is in the nature of a delay in cell cycle progression, rather than a stable arrest (Lew and Reed, 1995).

In the fission yeast *Schizosaccharomyces pombe*, the *cdc25-22* temperature sensitive mutant (Nurse and Thuriaux, 1980) is widely used to arrest cells in G2. Cdc25 is a phosphatase the promotes mitotic entry by removing an inhibitory Tyr15 phosphorylation on CDK1/Cdc2 (Gould and Nurse, 1989). The counteracting kinase, Wee1 (Nurse et al., 1976), is a homologue of the *S. cerevisiae* Swe1. However, in budding yeast, inhibitory phosphorylation and dephosphorylation of CDK1 are not required for cell cycle progression, and a deletion of the *S. cerevisiae* Cdc25 homologue, Mih1, only produce a minor delay in mitotic entry (Pal et al., 2008). I therefore wondered whether overexpression of the Swe1 kinase (Booher et al., 1993) instead, might arrest budding yeast cells in G2 (schematic representation, Figure 3.1).

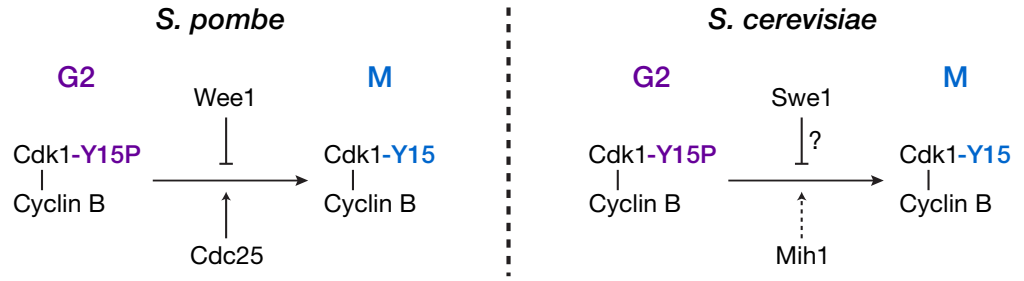

Figure 3.1 Swe1/Wee1 at mitotic entry. In *S. pombe*, the phosphatase Cdc25 promotes mitotic entry by removing an inhibitory Tyr15 phosphorylation on CDK1, which is counteracted by the kinase Wee1. In *S. cerevisiae*, the analogous phosphorylation only delays cell cycle progression and its removal is not required for mitotic entry.

3.1 Overexpression of Swe1 leads to inviability

To examine the effect of Swe1 overexpression, I introduced *SWE1* with a Pk epitope tag under galactose-inducible control of the *GAL1* promoter (cloned as described in section 2.4.1) as an additional copy at the ectopic *LEU2* locus in wild type budding yeast cells of the *MAT*a and *MAT*α mating types. These strains were grown for two days at 25°C on rich YP solid media containing glucose, raffinose, or raffinose + galactose as carbon source, corresponding to no, low or high expression of ectopic Swe1, respectively. Swe1 overexpression, induced by galactose, led to cell inviability, possibly indicative of a cell cycle arrest (Figure 3.2).

3.2 Overexpression of Swe1 leads to a G2 arrest

In order to determine whether Swe1 overexpression produced a cell cycle arrest, I assessed the results of Swe1 expression in time course experiments. In the representative experiment described below, asynchronous cultures of *MAT*a P_{GAL1}–*SWE1-3Pk* cells were grown in YPRaffinose, synchronised in the G1 phase of the cell cycle by addition of α factor, and released into medium containing galactose to induce expression of epitope-tagged Swe1 (Figure 3.3). Samples were harvested every 30 minutes for 4 hours, which provided sufficient time resolution, for parallel flow cytometry, cytology, immunofluorescence and immunoblotting analyses. For comparison, a portion of the G1-arrested culture was released into YPRaffinose medium containing the spindle poison nocodazole, which induced a metaphase arrest.

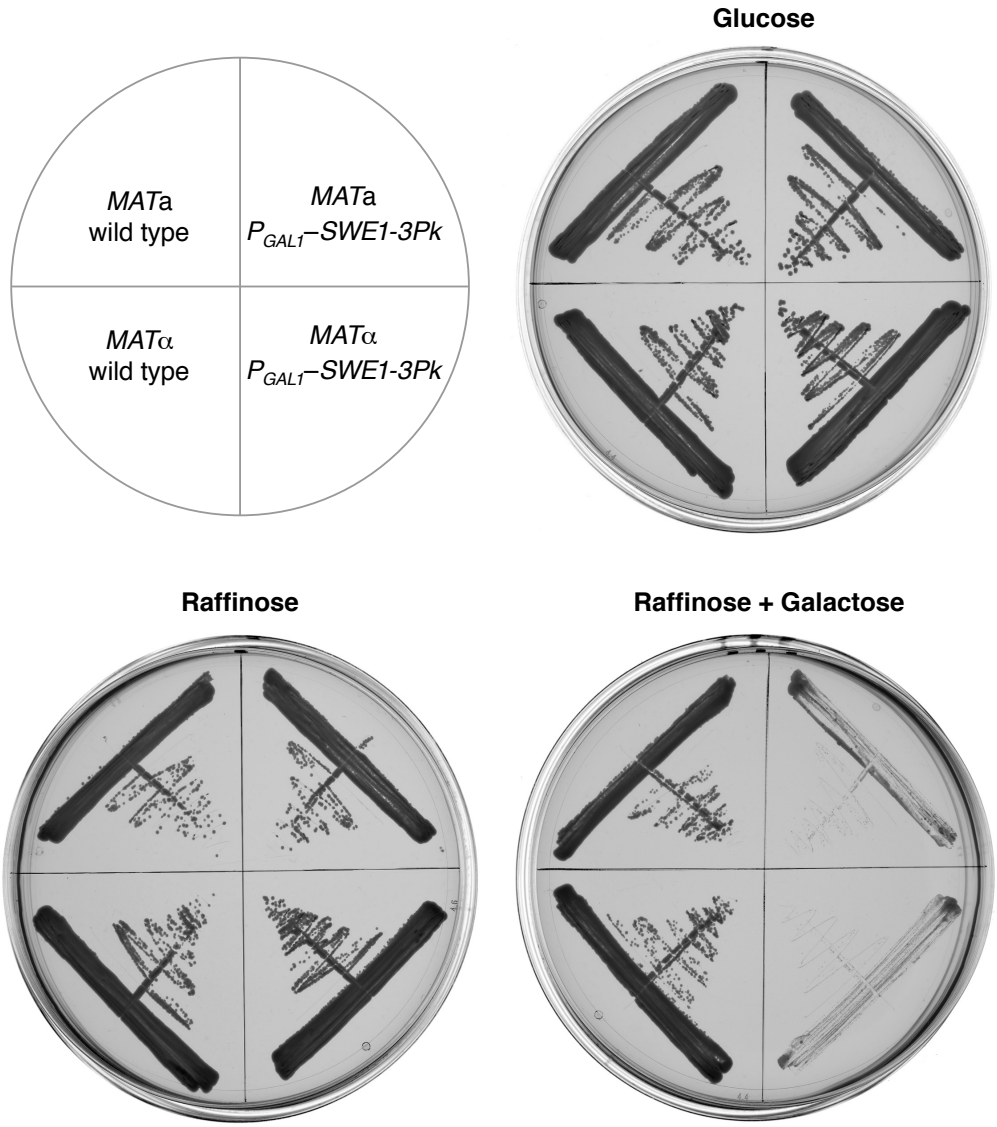

Figure 3.2 Overexpression of Swe1 leads to cell inviability. Wild type, or Swe1-overexpressing strains were grown on rich YP media containing the indicated carbon source for 2 days at 25°C. The GAL1 promoter is repressed by glucose, uninduced by raffinose and induced by galactose. *Strains, clockwise from MATa wild type: K699, RT111, RT112, K700*.

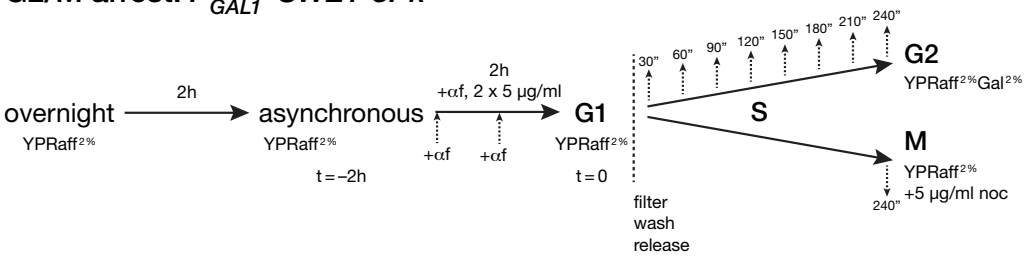

Figure 3.3 Experimental scheme. Cells were synchronised in G1 with α factor, released into a putative G2 (*raffinose + galactose*) or metaphase (*raffinose + nocodazole*) arrest, and harvested at the indicated time points for parallel analyses. *Strain: RT111.*

3.2.1 Cell cycle progression

In order to assess cell cycle progression, DNA content was measured in fixed cells by flow cytometry (as described in Section 2.6). The analysis showed that Swe1-overexpressing cells arrest with 2C, i.e., replicated, DNA content (Figure 3.4), indicating that Swe1 overexpression leads to either a G2 or mitotic arrest.

3.2.2 Cell morphology and microtubule organisation

S. cerevisiae cells exhibit characteristic morphological changes as they progress through the cell cycle (Figure 3.5). Buds emerge in early/mid S phase, and grow in a polarised/apical manner in the early budded phase through S/G2, switching to isotropic bud growth in the late budded phase in M (Farkas et al., 1974; Lew and Reed, 1993). Budding yeast cells also show distinct microtubule organisation patterns through the cell cycle, the most striking of which is the organisation of intranuclear mitotic spindles in M phase.

To distinguish between the possibilities of a G2 or mitotic arrest produced by Swe1 overexpression, I examined the morphology of cells overexpressing Swe1. Brightfield microscopy of cells fixed at 30-minute intervals (Figure 3.6) showed that buds continued to progressively elongate, supporting the notion that under these conditions, cells failed to switch from polarised growth that occurs in S/G2 to isotropic growth that is a hallmark of mitosis, a switch that is triggered by the activation of CDK1/Cdc28 by mitotic cyclins (Lew and Reed, 1993; Rancati and Li, 2007). An examination of microtubule organisation in Swe1-overexpressing cells by indirect immunofluorescence (as described in Section 2.10) showed that the cells do not form long mitotic spindles, but organise microtubules into short

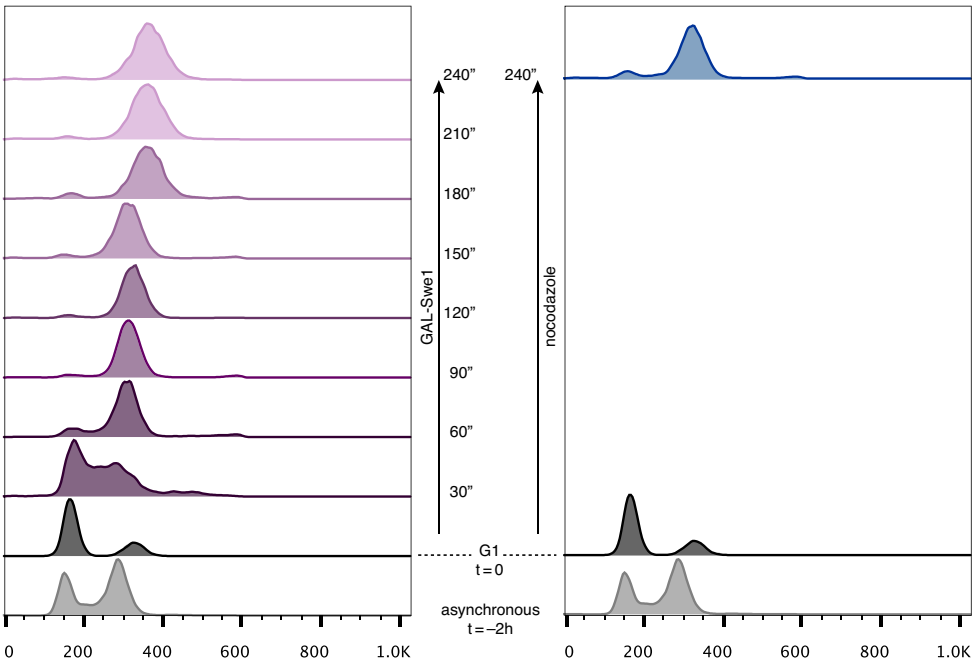

Figure 3.4 Flow cytometry. Histograms of cell count (*y axis, modal, arbitrary units*) vs. DNA content (*x axis, FL2-H*). G1-synchronised cells were released into conditions leading to Swe1 overexpression (*left*) or a nocodazole induced metaphase arrest (*right*). Cells arrest with 2C DNA content under both conditions. Swe1-overexpressing cells were harvested every 30 minutes for characterisation, whereas the commonly used nocodazole/metaphase arrest was used for comparing terminal arrest phenotypes.

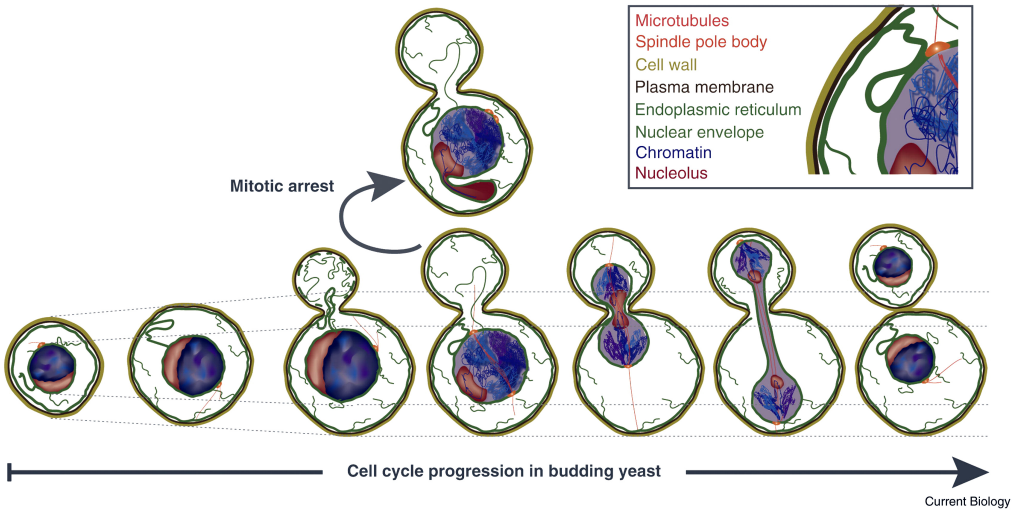

Figure 3.5 Morphological changes and microtubule organisation patterns through the budding yeast cell cycle. *Reproduced from Vjestica and Oliferenko (2012) with permission from Elsevier.*

pre-mitotic intranuclear spindles and interphase patterns in which astral microtubules often extend into the interior of the elongating buds (Figure 3.6).

3.2.3 Cyclin B levels

Clb2 is a mitotic B-type cyclin that promotes the G2/M transition by activating CDK1/Cdc28, and which shows peak levels late in the cell cycle, about ten minutes before anaphase (Surana et al., 1991; Fitch et al., 1992; Richardson et al., 1992; Mendenhall and Hodge, 1998). To probe the biochemical state of the cell cycle machinery in a GAL-Swe1 arrest, I prepared whole cell protein extracts (as described in Section 2.7.1) for western blotting. The immunoblot was probed for Swe1-3Pk (anti-Pk), Cyclin B/Clb2 (anti-Clb2) and the loading control, α-tubulin (TAT-1). Detection with horseradish peroxidase (HRP)–conjugated secondary antibodies showed that as the arrest progressed, Swe1 levels increased to an extent, driven by galactose induction; the mitotic Cyclin B/Clb2 only accumulated to levels that were far lower than in nocodazole-arrested metaphase cells.

3.3 Conclusion

Taken together, the cytological and biochemical data show that Swe1 overexpression produces a G2, rather than mitotic, arrest. Cells exhibit all the hallmarks of an inhibited G2/M transition, including a failure to switch to isotropic growth, absence of mitotic spindles, and low levels of the mitotic cyclin Clb2. Moreover, the arrest is stable for at least 4 hours, far exceeding the typical time (~2.5 hours) for which it is required in subsequent experiments. For a further characterisation of this arrest, and to distinguish the G2 and M phases of budding yeast, it would be interesting to examine endogenous levels of Swe1, as well as other mitotic markers such as Aurora B/Ipl1, Securin/Pds1 and Polo-like kinase/Plk1, in addition to Cyclin B/Clb2.

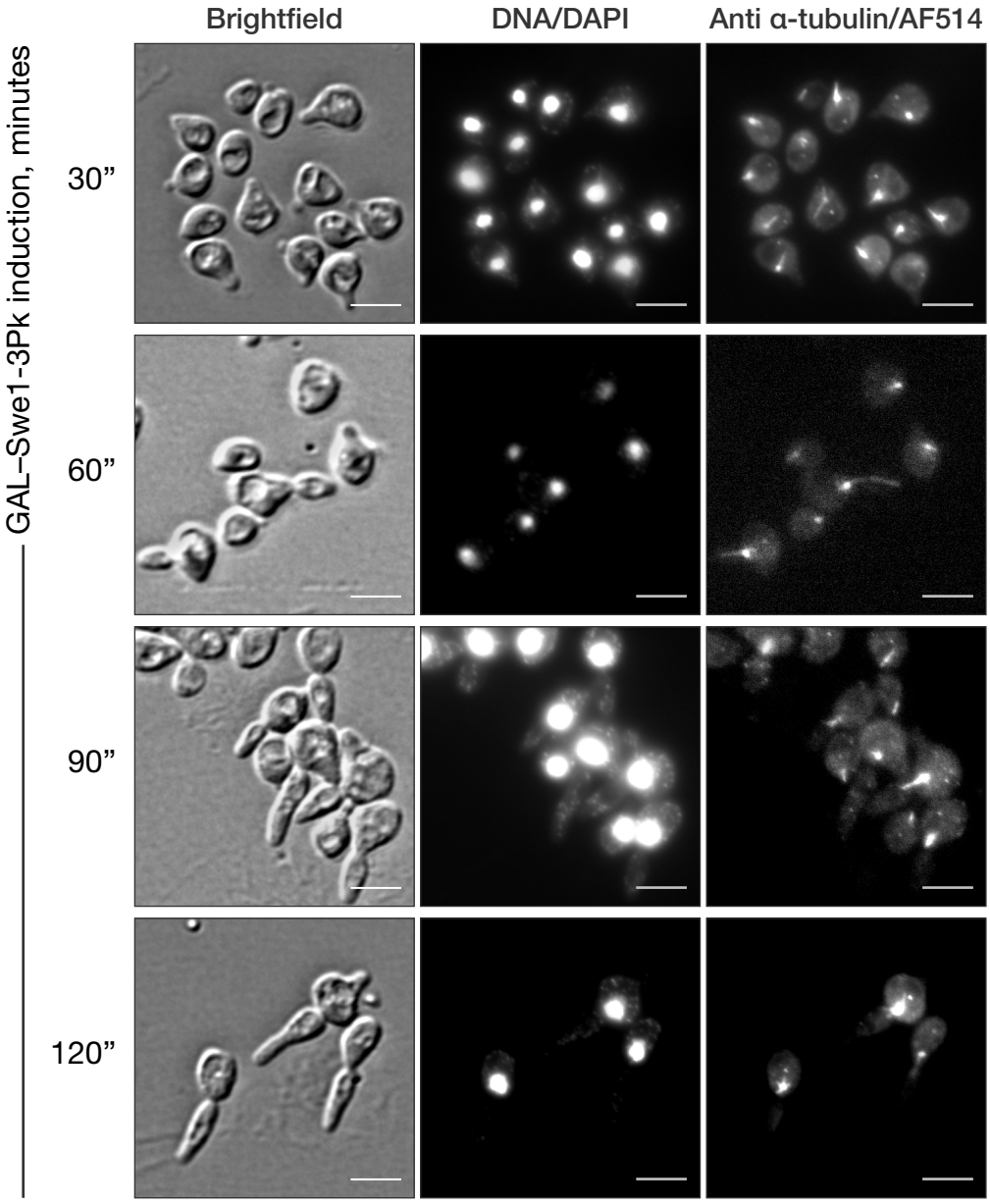

(a) Swe1 overexpression, t = 30, 60, 90, 120 min; *continued overleaf*.

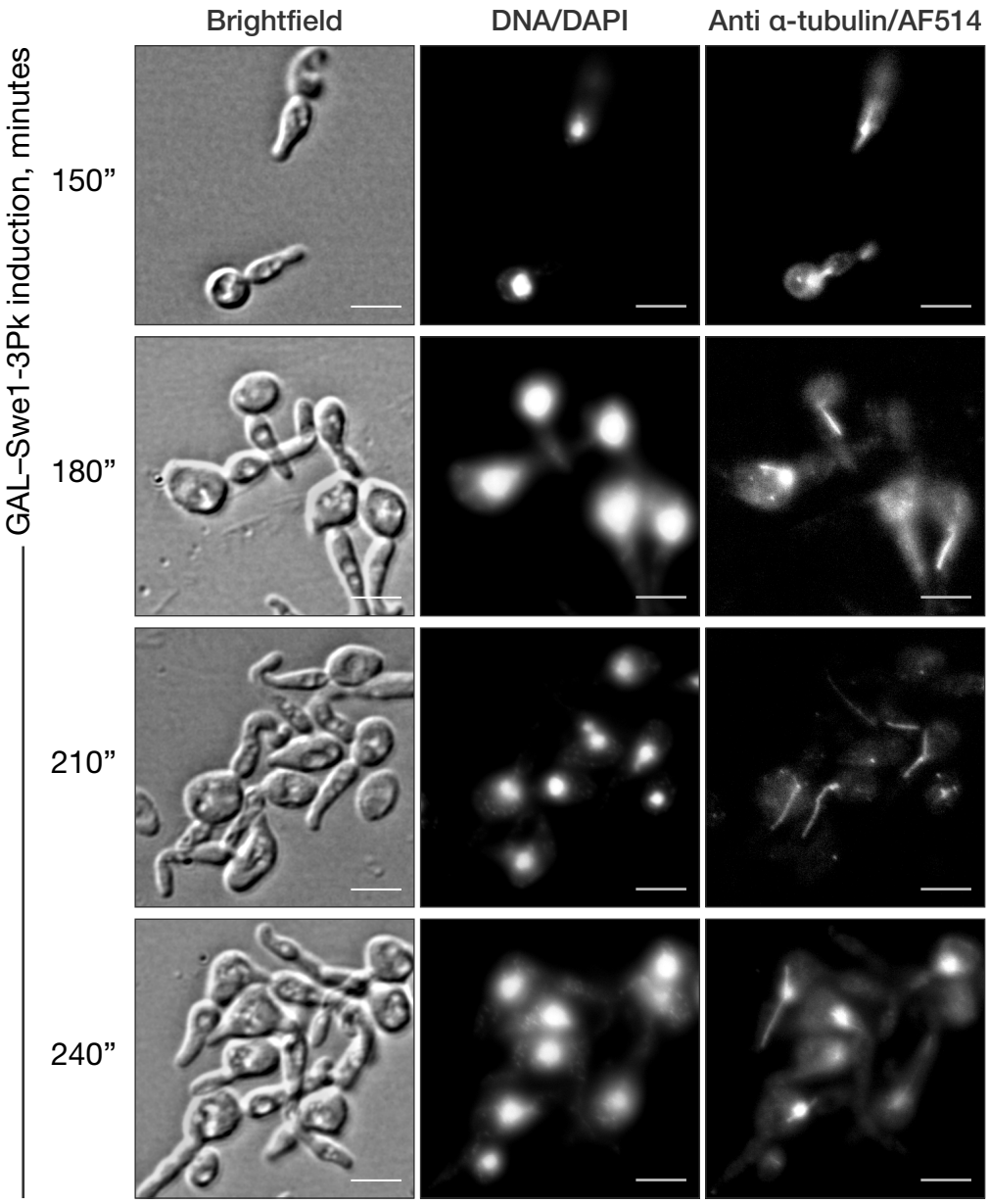

(b) Swe1 overexpression, t = 150, 180, 210, 240 min.

Figure 3.6 Swe1 overexpression: cell morphology and microtubule organisation. Swe1 overexpression results in cell growth with progressively elongating buds, indicating a failure of the switch from polarised to isotropic growth, which typically occurs at the G2/M transition. The brightfield images (*left column*) are single planes, contrast-enhanced with a bandpass FFT filter in ImageJ with default parameters (Section 2.11.1). Cells overexpressing Swe1 also do not form long mitotic spindles, but instead possess short intranuclear spindles (Winey and O'Toole, 2001) and astral microtubules that explore the interior of the elongating buds. The indirect immunofluorescence images (*centre and right columns*) are average-intensity projections of 3 planes x 0.5 μm images of fixed cells stained with the DNA-intercalating dye DAPI and mouse anti–α-tubulin/Alexa514–anti-mouse antibodies. Scale bars represent 5 μm.

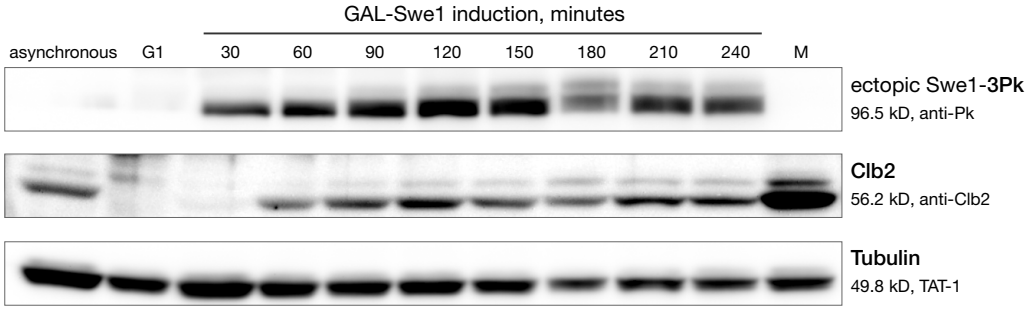

Figure 3.7 Low Cyclin B/Clb2 levels. Cells in a GAL-Swe1 arrest show far lower levels of the mitotic cyclin Clb2 than nocodazole-arrested mitotic cells (*middle row, rabbit anti-Clb2, 1:1000*). For comparison, accumulating levels of ectopic Swe1-3Pk (*top row, mouse anti-Pk, 1:5000*) and constant levels of the tubulin loading control (*bottom row, mouse anti–α-tubulin TAT-1, 1:10000*) are shown.

4 Results II: Conditional Alleles of Condensin

Since condensin is essential for cell viability, its effect on chromosome condensation in living cells can only be dissected by conditional inactivation. Although well characterised temperature-sensitive (*ts*) alleles of condensin subunits, such as *smc2-8* and *smc4-1*, have been isolated (Freeman et al., 2000), the temperature shift required for *ts* allele inactivation offers several obstacles to the accurate determination of chromosome structure. First, temperature shifts alter the diffusion and binding characteristics of nuclear proteins, and affect a number of chromosomal processes, which may alter chromosome morphology independent of any effects from condensin inactivation (Bancaud et al., 2009; Börner et al., 2004; Chan et al., 2009; Lavoie et al., 2000). Second, the accompanying heat shock produces a drastic global transcriptional response in yeast cells, which is likely to affect chromosome structure (Gasch et al., 2000; Chen et al., 2003). Finally, temperature shifts generate a high autofluorescent background in cells, which is prohibitive for sensitive fluorescence microscopy measurements (McIntyre et al., 2007). I therefore set out to generate novel conditional alleles of the condensin SMC subunits that did not require temperature shifts, evaluating initially the anchor-away technique (Haruki et al., 2008) and subsequently the auxin inducible degron (Nishimura et al., 2009), as described below.

4.1 The anchor-away technique

The anchor-away technique (Haruki et al., 2008) is a means of depleting a cellular compartment of a target protein of interest by tethering it to a suitable anchor protein in a ligand-dependent reaction. In the version of the technique used here, the target is a nuclear protein (a condensin subunit) and the anchor is an abundant protein that sweeps once through the nucleus (a ribosomal subunit protein). The target–anchor tethering is achieved by exploiting the rapamycin-dependent

heterodimerisation of FK506 binding protein (FKBP12) and the FKBP12 rapamycin binding (FRB) domain of human mTOR (Belshaw et al., 1996; Chen et al., 1995). By fusion of an FRB tag to the target, and FKBP12 to the anchor, the target can be sequestered by the anchor in the presence of rapamycin (Figure 4.1).

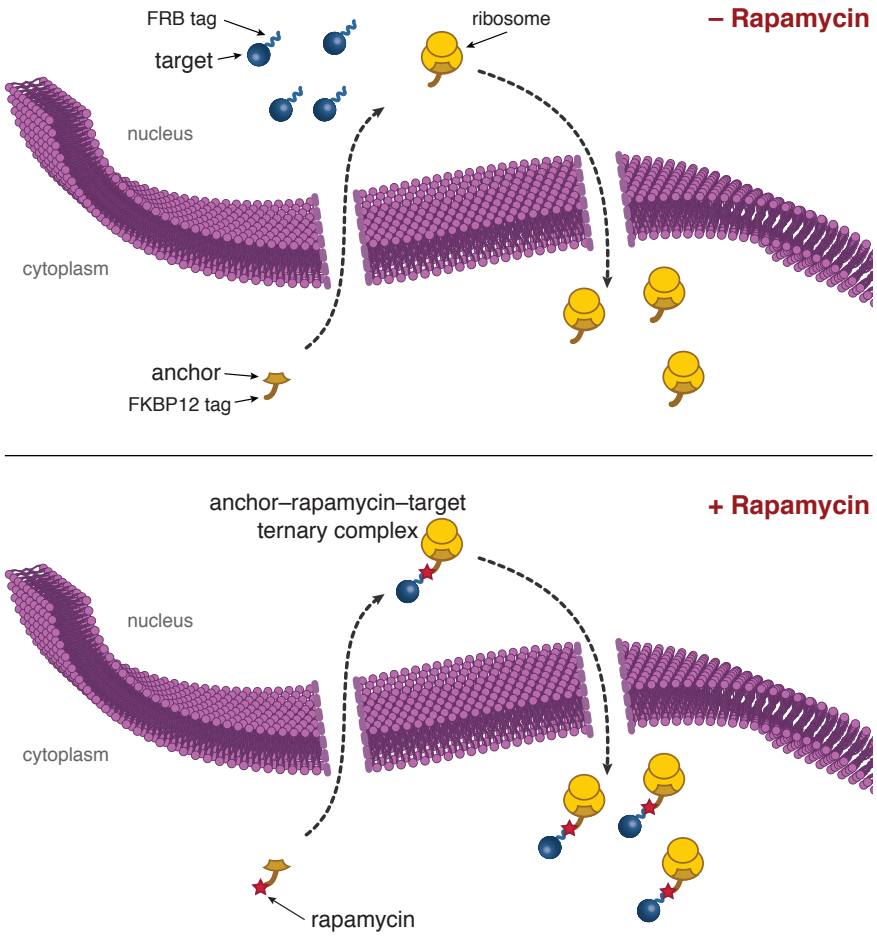

Figure 4.1 The anchor-away technique. The anchor-away technique conditionally depletes the nucleus of the target protein. In the presence of rapamycin, a complex is formed between an FKBP12-tagged anchor that sweeps once through the nucleus, and an FRB-tagged target, effectively sequestering the target protein in a ribosomal complex.

4.1.1 Condensin depletion leads to inviability

In order to deplete condensin by the anchor-away technique, C-terminal FRB tags were appended to *SMC2* or *SMC4* at their genomic loci (Section 2.1) in an anchor-away background strain. This strain contains a mutated *TOR1* (*tor1-1*) and deleted *FPR1* (*Δfpr1*) gene, conferring rapamycin resistance and eliminating competition between Fpr1 and the anchor-FKBP12 construct for binding to the

FRB domain (Haruki et al., 2008; Heitman et al., 1991). In addition, the abundant ribosomal subunit protein RPL13A is tagged with FKBP12 for use as an anchor. The strains were grown for two days at 25°C on solid rich YPD medium in the absence or presence of rapamycin; FRB-tagged *SMC2* and *SMC4* subunits conferred inviability in the presence of rapamycin, forming tight conditional alleles, termed *smc2-aa* and *smc4-aa*, respectively (Figure 4.2).

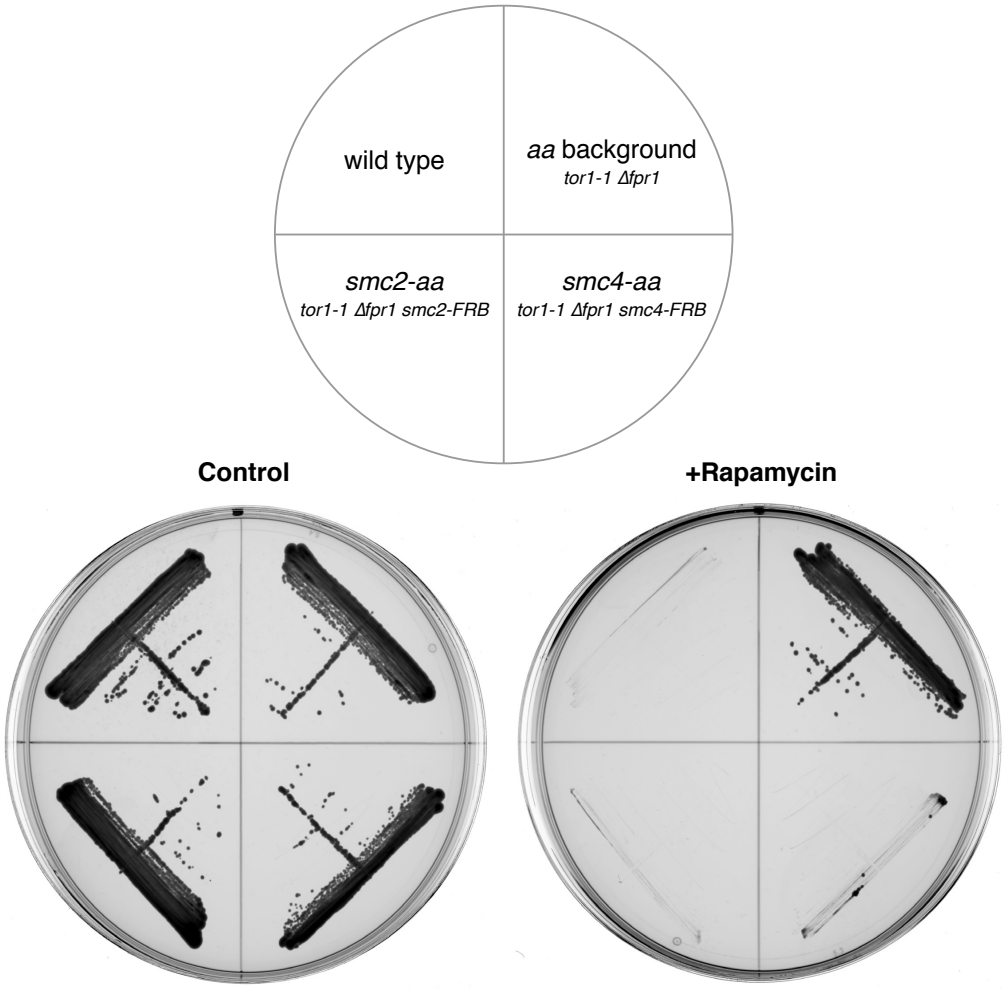

Figure 4.2 Condensin depletion leads to inviability. The indicated strains were grown for two days at 25°C on solid rich YPD medium containing either DMSO as control (*left*) or 1 µg/ml rapamycin (*right*). As rapamycin is toxic to wild type cells (*top left quadrant, each plate*), all anchor-away strains use a *tor1-1 Δfpr1* background, which confers rapamycin resistance (*top right quadrant, each plate*). Under these conditions, depletion of Smc2 (*smc2-aa*) or Smc4 (*smc4-aa*) lead to cell inviability. *Strains, clockwise from wild type: K700, CSL3793, SH184, SH110*.

4.2 The auxin-inducible degron

The auxin-inducible degron (*aid*) system is an adaptation of an auxin-dependent protein degradation pathway from plants for use in other eukaryotes (Nishimura et al., 2009). All eukaryotes possess multiple forms of the E3 ubiquitin ligase SCF (Skp1, Cullin and F-box), in which the F-box protein confers substrate specificity. However, orthologues of the F-box protein Tir1, which binds to IAA/auxin transcription repressors in the presence of auxin, are found only in plant species. Therefore ectopic expression of Tir1, along with fusion of an *aid* tag (such as the transcription repressor IAA17) to a target protein, is sufficient for transplanting the auxin-dependent degron system into non-plant cells. In place of full-length IAA17, a truncated version has been shown to be equally effective as an *aid* tag (Kubota et al., 2013; Morawska and Ulrich, 2013). At a molecular level, auxin promotes the interaction of the SCF^{Tir1} complex with the *aid*-tagged target protein. SCF^{Tir1} then recruits an E2 ubiqitin conjugating enzyme that polyubiquitylates the *aid* tag, resulting in rapid auxin-dependent degradation of the target protein, whether it is nuclear or cytoplasmic (Nishimura et al., 2009).

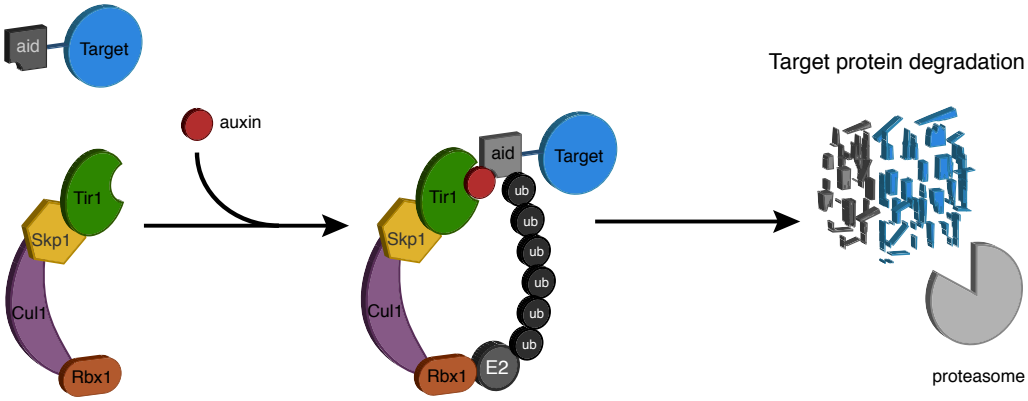

Figure 4.3 The auxin-inducible degron. The auxin-inducible degron (*aid*) is a system for rapid auxin-dependent degradation of target proteins in eukaryotic cells. On addition of auxin, the E3 ubiquitin ligase SCF^{Tir1} polyubiquitylates the *aid* tag via an E2 ubiquitin conjugating enzyme. This marks the target protein for degradation by the proteasome. *Adapted from Holland et al. (2012)*.

4.2.1 Full-length and truncated IAA17 condensin tags result in cell viability

I generated conditional auxin-repressible alleles of the condensin SMC subunits by fusing C-terminal *aid* tags to *SMC2* and *SMC4* at their genomic loci in an

aid background strain. This strain expresses high levels of epitope-tagged *Oryza sativa* Tir1, integrated at the *ADE2* locus. To facilitate immunodetection, I added epitope tags to the vectors for C-terminal *aid* tagging: a 9myc tag to full-length *Arabidopsis thaliana* IAA17 (Section 2.4.2) and a 3Pk tag to the truncated version of IAA17 called miniAID (Section 2.4.3). Since both full-length IAA17 (229 amino acids, ~25.3 kD) and miniAID (amino acids 65-132 of IAA17, ~7.5 kD) were equally effective, as seen by cell inviability on auxin-containing media (Figure 4.4), the smaller miniAID tags were chosen for further experiments to minimise impairment of protein function. For brevity, the miniAID-tagged *SMC2* and *SMC4* alleles are termed *smc2-aid* and *smc4-aid* in all subsequent work.

4.2.2 Condensin depletion by *aid* is rapid

To determine the kinetics of condensin depletion by *aid*, I performed a time-course immunoblot analysis. Asynchronous cultures of *smc2-aid* and *smc4-aid* strains were treated with 0.5 mM IAA/auxin, and whole cell protein extracts (Section 2.7.1) were prepared for Western blotting from samples taken every 30 minutes for 2 hours. The immunoblot was probed for Smc2-3Pk-miniAID and Smc4-3Pk-miniAID (mouse anti-Pk, 1:1000), with Tir1-9myc (mouse anti-myc, 1:1000) used as a loading control, followed by detection with HRP-conjugated secondary antibodies (HRP–anti-mouse, 1:5000). Quantification of normalised Smc2-3Pk-miniAID and Smc4-3Pk-miniAID levels showed that protein depletion proceeded rapidly on auxin addition, falling to below 20% of the starting value within 30 minutes, eventually becoming indistinguishable from background (Figure 4.5).

4.2.3 *Condensin-aid* is subunit-specific

To determine whether degradation was specific to the *aid*-tagged subunit of condensin, I performed a further time-course immunoblot analysis of the *smc4-aid* strain, in which the kleisin subunit Brn1 was additionally tagged with a 3HA epitope tag. An asynchronous culture of *smc4-aid BRN1-3HA* cells was treated with 0.5 mM IAA/auxin, and samples taken at 0, 5, 10, 15, 30, 60, 90 and 120 minutes after auxin addition. The immunoblot was probed for Smc4-3Pk-miniAID and Tir1-9myc as in Section 4.2.2, with the addition of anti-HA antibody (1:5000) for detection of Brn1-3HA. Quantification of normalised Smc4-3Pk-miniAID levels demonstrated the rapid degradation of the *aid*-tagged Smc4 subunit, while Brn1 levels remained unaffected (Figure 4.6).

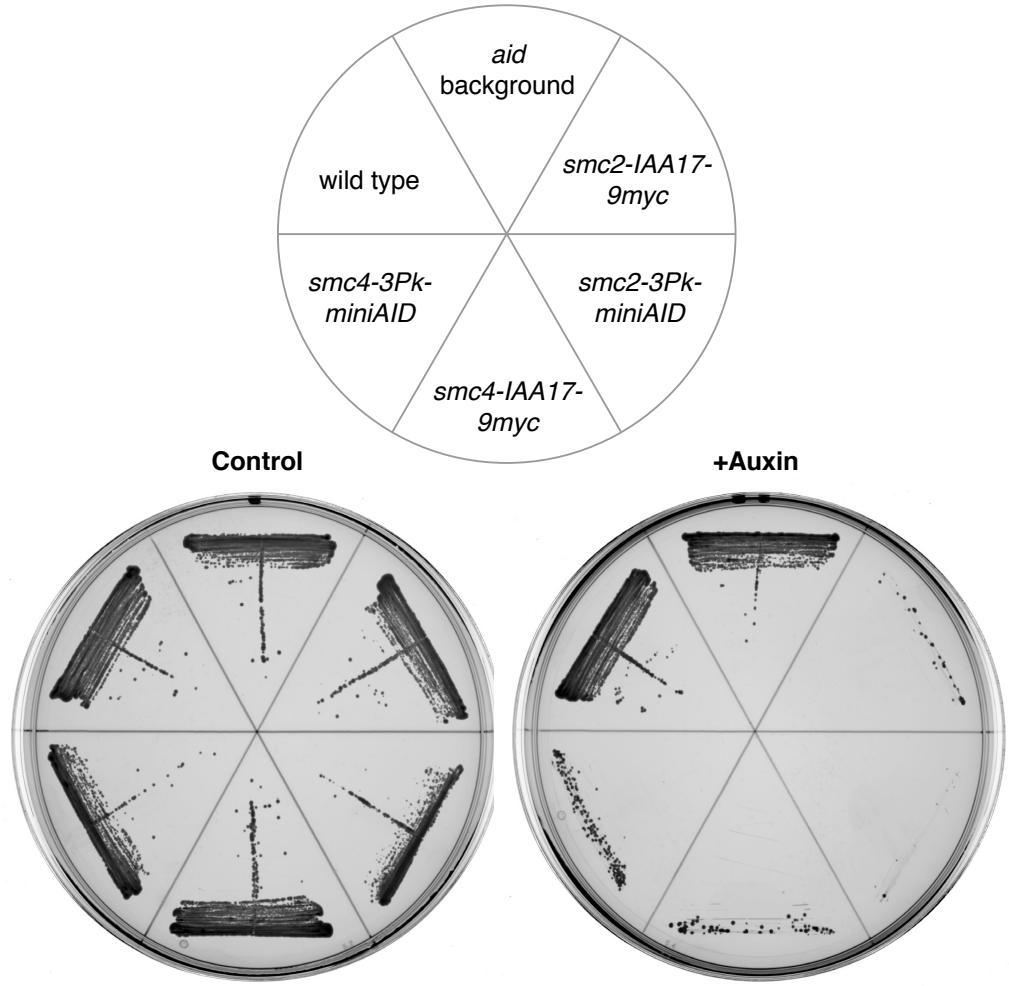

Figure 4.4 Condensin depletion by full-length or truncated *aid* tags leads to inviability. The indicated strains were grown for two days on rich solid YPD medium containing either methanol as control (*left*) or 1 mM IAA/auxin (*right*) Both the full-length IAA17 and shorter miniAID tag were equally effective, leading to auxin-dependent inviability when expressed as Smc2 or Smc4 fusions. *Strains, clockwise from wild type: K699, CSL4267, RT145, RT146, RT148, RT149*.

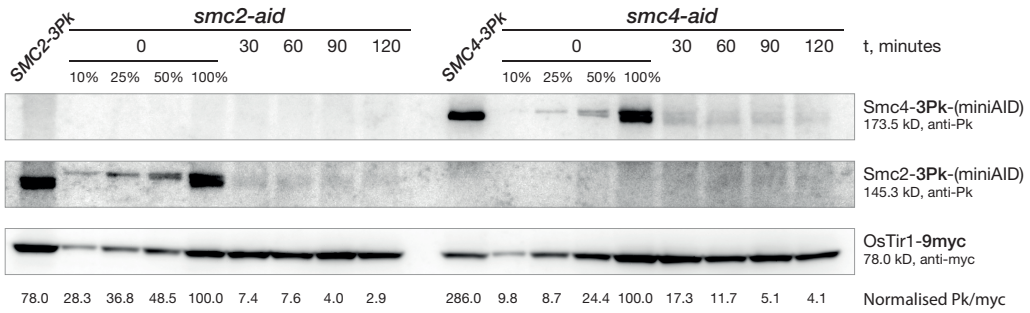

Figure 4.5 Condensin depletion by *aid* is rapid. A time-course immunoblot analysis shows rapid degradation of Smc2-3Pk-miniAID and Smc4-3Pk-miniAID. Asynchronous cultures were treated with 0.5 mM IAA/auxin, and cells harvested at the indicated times. For comparison, serial dilutions of the t = 0 time point (i.e., prior to auxin treatment) are shown, as are Smc2-3Pk and Smc4-3Pk. The bottom row shows Pk/myc levels, normalised so that the undiluted t = 0 time points are at 100.0. *Strains: RT161, RT146, RT163, RT149*.

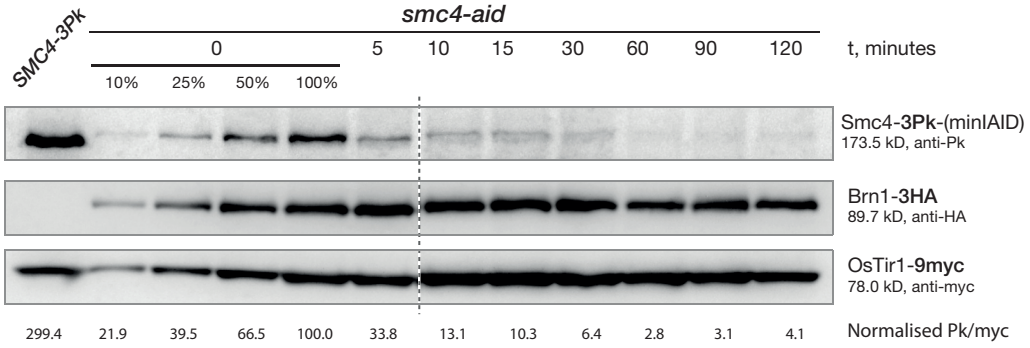

Figure 4.6 Auxin-induced degradation is specific to the *aid*-tagged condensin subunit. Asynchronous cultures of an *smc4-aid BRN1-3HA* strain were treated with 0.5 mM IAA/auxin, and samples harvested at the indicated times. For comparison, serial dilutions of the t = 0 time point (i.e., prior to auxin treatment) are shown, along with Smc4-3Pk. The bottom row shows Pk/myc levels, normalised so that the undiluted t = 0 time point is at 100.0. The vertical dotted line shows the site of image splicing; identically-exposed lanes were transposed from a single image of the entire membrane. *Strains: RT163, RT155*.

4.3 Conclusion

Both the anchor-away technique and the auxin-inducible degron are effective conditional depletion strategies for condensin SMC subunits; the *aid* alleles have the added advantage that immunoblotting provides a convenient means of verifying the extent of depletion, independent of any phenotypic assessment of its downstream effects.

5 Results III: Chromosome Condensation in Budding Yeast

The direct visualisation of budding yeast chromosomes has been challenging due to the small size of cells and chromosomes of this model organism. Consequently, the condensation status of budding yeast chromosomes in intact cells has only been assessed on subchromosomal regions by imaging of fluorescent LacI/TetR repressor fusions bound to arrays of operator sequences integrated on a single chromosome arm (Robinett et al., 1996; Vas et al., 2007). Alternatively the repetitive ribosomal DNA (rDNA) region has been visualised by fluorescence in situ hybridisation (FISH) on spread preparations of chromosomes, a relatively harsh treatment that preserves few details of chromosome structure (Freeman et al., 2000; Lavoie et al., 2000). Moreover, chromosome condensation studies in budding yeast thus far have been largely semi-quantitative, employing arbitrary phenotypic categorisation and scoring approaches, although the fluorescent dot assay has recently been improved for quantitative use in budding and fission yeast (Neurohr et al., 2011; Petrova et al., 2013). The advent of specialised superresolution structured illumination microscopy (SIM; Section 2.11.2; Gustafsson, 2000; Gustafsson et al., 2008) has made a twofold improvement in axial resolution feasible, revealing ultrastructural details of chromatin texture (Figure 5.1). Using this imaging approach, I developed novel quantitative chromosome condensation assays, employing three-dimensional microscopy of total cellular chromatin as well as the rDNA locus combined with custom-written ImageJ (Schneider et al., 2012) routines for unbiased semi-automated volume measurements.

5.1 Metaphase rDNA volume is condensin dependent

The rDNA locus *RDN1* is composed of 100–200 9.1 kB rDNA repeats spanning a ~1–2 Mb region on the right arm of budding yeast chromosome XII, which is the longest chromosome in the organism (Petes, 1979; Mortimer and Johnston,

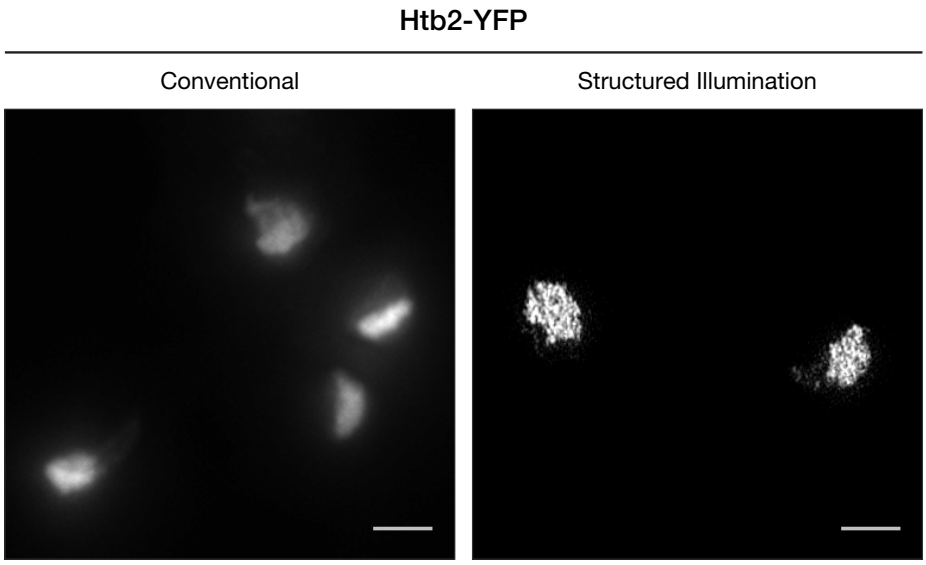

Figure 5.1 Improved chromosome visualisation with SIM. Cells expressing fluorescent-tagged histone H2B (*HTB2-YFP*) were treated with nocodazole to induce a metaphase arrest, and imaged on a conventional widefield Deltavision (*left*) or superresolution SIM OMX microscope (*right*). The latter produces images with a twofold improvement in axial resolution, making apparent some details of chromatin texture. Shown are maximum intensity projections of 41 x 0.125 µm slices, imaging a total *z* depth of of 5 µm. Scale bars represent 2 µm. *Strain: RT19*.

1986). *RDN1* has been identified as a major budding yeast condensin binding site that may be subject to additional mitotic enrichment (Freeman et al., 2000; Johzuka et al., 2006; Wang et al., 2005). To visualise the condensation status of rDNA in intact cells and determine whether this depends on condensin, I tagged the rDNA binding protein Net1 (Straight et al., 1999) with a yeast-optimised monomeric YFP variant mCitrine (Griesbeck et al., 2001; Zacharias et al., 2002; Sheff and Thorn, 2004), in *aid* background and *smc4-aid* strains. Cells of the resulting strains were grown overnight in rich YPD medium, synchronised in G1 by addition of α factor, and released into YPD containing the spindle poison nocodazole to induce a metaphase arrest, in the presence of 1 mM IAA/auxin or methanol as control (experimental scheme, Figure 5.2). Samples were harvested at pre-synchronisation, G1, M^{-auxin} and M^{+auxin} time points for quantification of rDNA volumes. Flow cytometry and immunoblotting were performed in parallel as controls to verify cell cycle arrests, and Smc4 depletion, respectively. Flow cytometry (Figure 5.3) showed the expected enrichment of 1C peaks in G1, and 2C peaks in M; condensin depletion did not affect cell cycle progression from G1 to M. The immunoblot showed the effective depletion of Smc4-3Pk-miniAID in auxin treated *smc4-aid* samples relative to mock treatment (Figure 5.4).

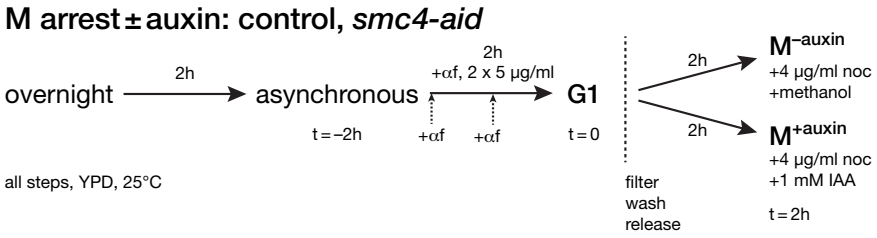

Figure 5.2 Metaphase rDNA volume, experimental scheme. Asynchronous cultures of control and *smc4-aid* strains expressing Net1-mCitrine grown in rich YPD medium were synchronised in G1 by addition of α factor and released into a nocodazole-induced metaphase arrest, in the presence or absence of IAA/auxin. *Strains: RT174 (control), RT178 (smc4-aid)*.

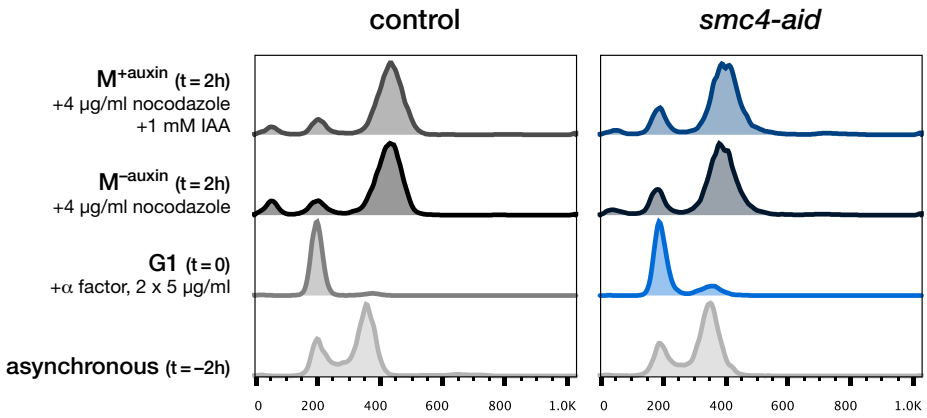

Figure 5.3 Metaphase rDNA volume, flow cytometry. DNA content of asynchronous, G1 and M ± auxin samples was analysed by flow cytometry (Section 2.6), showing the expected enrichment of 1C peaks in G1 and 2C peaks in M. Cell cycle progression was not hindered by condensin depletion between G1 and M (*top row, right panel*). *Strains: RT174 (control), RT178 (smc4-aid)*.

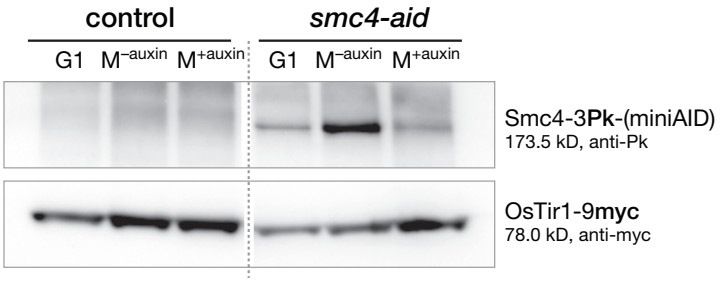

Figure 5.4 Metaphase rDNA volume, immunoblotting. Immunoblots of whole cell protein extracts (Section 2.7.1) of G1 and M ± auxin samples were probed for Smc4-3Pk-miniAID (mouse anti-Pk, 1:1000) and the loading control Tir1-9myc (mouse anti-myc, 1:1000). Detection with HRP–anti-mouse secondary antibody (1:5000) showed the expected auxin-induced degradation of Smc4-3Pk-miniAID (*top row, right lane*). The vertical dotted line shows the site of image splicing where identically-exposed lanes were transposed from a single unsaturated image; exposure varies between proteins but not between lanes/strains for a single protein. *Strains: RT174 (control), RT178 (smc4-aid)*.

5.1.1 Quantification of rDNA volume

The Net1-mCitrine–expressing cells were subjected to mild fixation (3.6% formaldehyde, 10 minutes, room temperature) and imaged in conventional mode on an Applied Precision OMX microscope using 514 nm laser excitation under conditions that minimised photobleaching (Section 2.11.2). 15 slices at 0.25 µm spacing (total depth, 3.5 µm) were acquired and deconvolved. The rDNA appeared to be organised into a characteristic loop-like metaphase morphology (Freeman et al., 2000; Lavoie et al., 2004) in control and mock-treated *smc4-aid* cells; the loops were lost upon depletion of condensin by auxin treatment in the *smc4-aid* strain (Figure 5.5).

For quantification of rDNA volumes, mother cells were manually outlined using a brighfield image of the same field. Thresholds were computed in the 514 nm channel for stacks of individual cells using the default ImageJ iterative isodata method (Ridler and Calvard, 1978). For each slice, pixels above the computed threshold were scaled to the appropriate voxel size, and summed to determine the volume occupied by the Net1-mCitrine signal in three dimensions. The resulting distributions (shown as box plots in Figure 5.6) were subjected to an ordinary one-way ANOVA, with mean values compared using Tukey's multiple comparison test. The analysis showed that the mean value of only the auxin-treated *smc4-aid* sample was significantly different from the others ($p < 0.01$), indicating that the loss of metaphase rDNA loop organisation resulting from condensin depletion corresponded to an increase in volume, reflecting decompaction.

5.1.2 Correlation between rDNA and cell volume

Since cells depleted of condensin seemed larger than equivalent control cells on average (Figure 5.5, bottom right panels), I quantified the areas of mother cells at their widest *z* position using the brightfield-guided cell outlines that were used in Section 5.1.1. Indeed, this analysis showed that in metaphase, *smc4-aid* cells treated with auxin were significantly larger than mock-treated *smc4-aid* cells, or an auxin-treated control strain (Figure 5.7). This raised the question of whether there might be a systematic correlation between rDNA volume and cell size. To examine this, I scaled the measured cell areas to approximate volumes by assuming a circular geometry for the measured cell area, and a spherical geometry for cell volume. For each sample condition, I calculated the Pearson linear correlation coefficient r between cell volume and rDNA volume using the Matlab

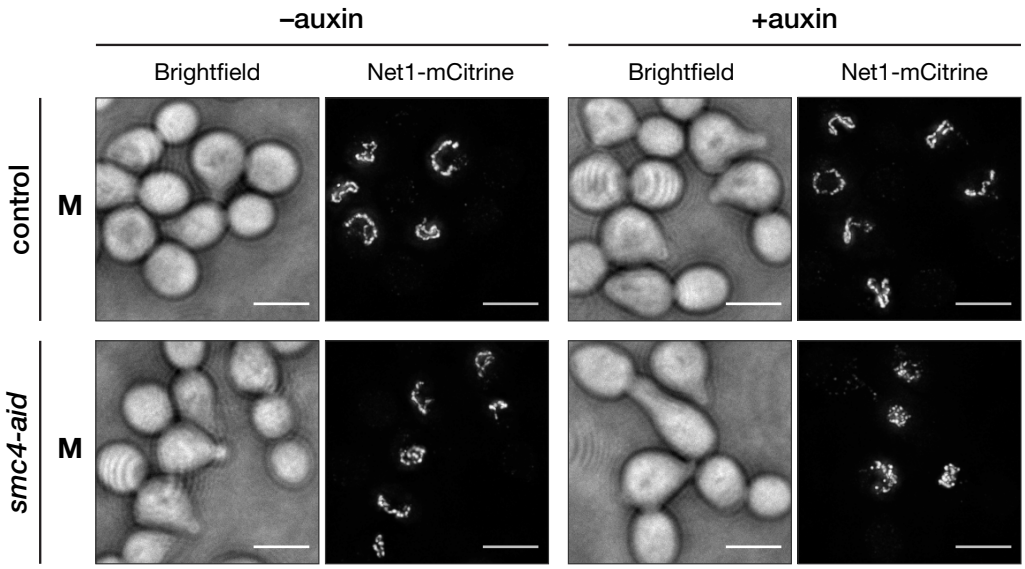

Figure 5.5 Metaphase rDNA volume, representative images. Representative brightfield and fluorescent images of Net1-mCitrine expressing strains in metaphase. Note the loss of loop organisation in the *smc4-aid* strain treated with auxin. The fluorescent images are maximum intensity projections of 15 x 0.25 µm deconvolved images of 3.5 µm *z* depth. Scale bars represent 5 µm. *Strains: RT174 (control), RT178 (smc4-aid)*.

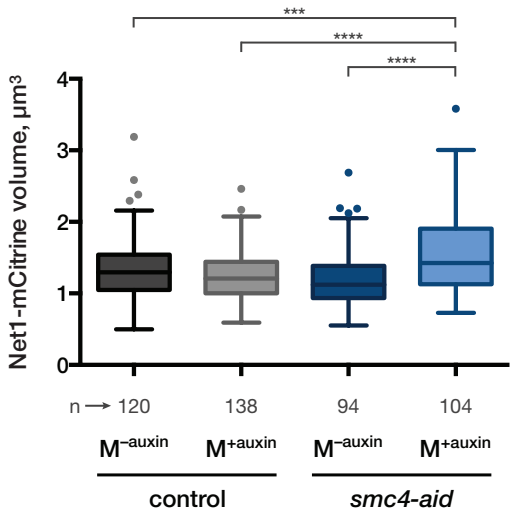

Figure 5.6 Metaphase rDNA volume, box plot. Box-and-whisker plots of the distributions of rDNA volume in metaphase arrested control and *smc4-aid* strains, with or without auxin. The boxes span the 25-75 percentiles (the IQR) of the data, centred on the median; the whiskers extend to 1.5 x IQR either side of the upper and lower quartiles, while dots denote outliers thus defined. Only the auxin-treated *smc4-aid* strain has a mean significantly different from the others ($p < 0.01$). The number of cells measured for each condition is denoted by *n*. *Strains: RT174 (control), RT178 (smc4-aid)*.

corrcoef function. In all cases, $r \approx 0.7$, corresponding to a coefficient of determination $r^2 \approx 0.5$, which can be interpreted to mean that about half the statistical variation in rDNA volume mirrors changes in cell volume.

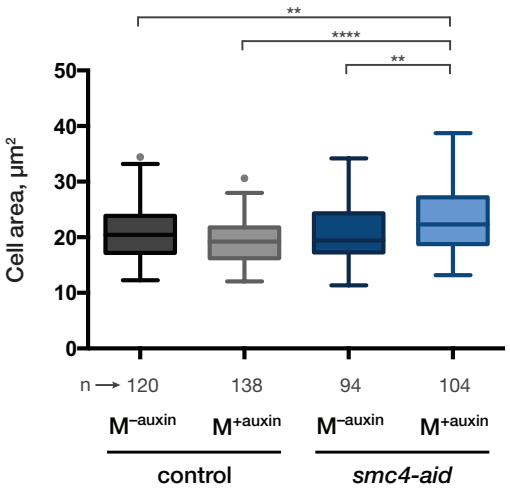

Figure 5.7 Mother cell area, box plot. Box-and-whisker plots of the distributions of mother cells areas in metaphase arrested control and *smc4-aid* strains, with or without auxin. The boxes span the 25-75 percentiles (the IQR) of the data, centred on the median; the whiskers extend to 1.5 x IQR either side of the upper and lower quartiles, while dots denote outliers thus defined. Only the auxin-treated *smc4-aid* strain has a mean significantly different from the others ($p < 0.01$). The number of cells measured for each condition is denoted by *n*. *Strains: RT174 (control), RT178 (smc4-aid)*.

5.1.3 Conclusion

These results extend to intact yeast cells, the validity of previous findings that used rDNA FISH on spread chromosome preparations in conjunction with temperature sensitive alleles to show the condensin dependence of a characteristic loop-like organisation of rDNA in metaphase (Freeman et al., 2000; Lavoie et al., 2004). In addition, the quantification of rDNA volume in metaphase-arrested control and *smc4-aid* cells described here shows that the loss of rDNA loop organisation on condensin depletion is associated with an increase in volume, suggesting that the metaphase loop is a condensed chromatin state. As a technical point, I note that this phenotypic effect is specific to the auxin-treated *smc4-aid* sample; therefore auxin has no artifactual effects on the control strain, nor the *aid* tag on Smc4 in the absence of auxin. Furthermore, statistical analysis uncovered a partial correlation between cell volume and rDNA volume, and although no causal direction can be directly inferred, there are a number of possible explanations for the correlation. One possibility is that when decondensed, rDNA or

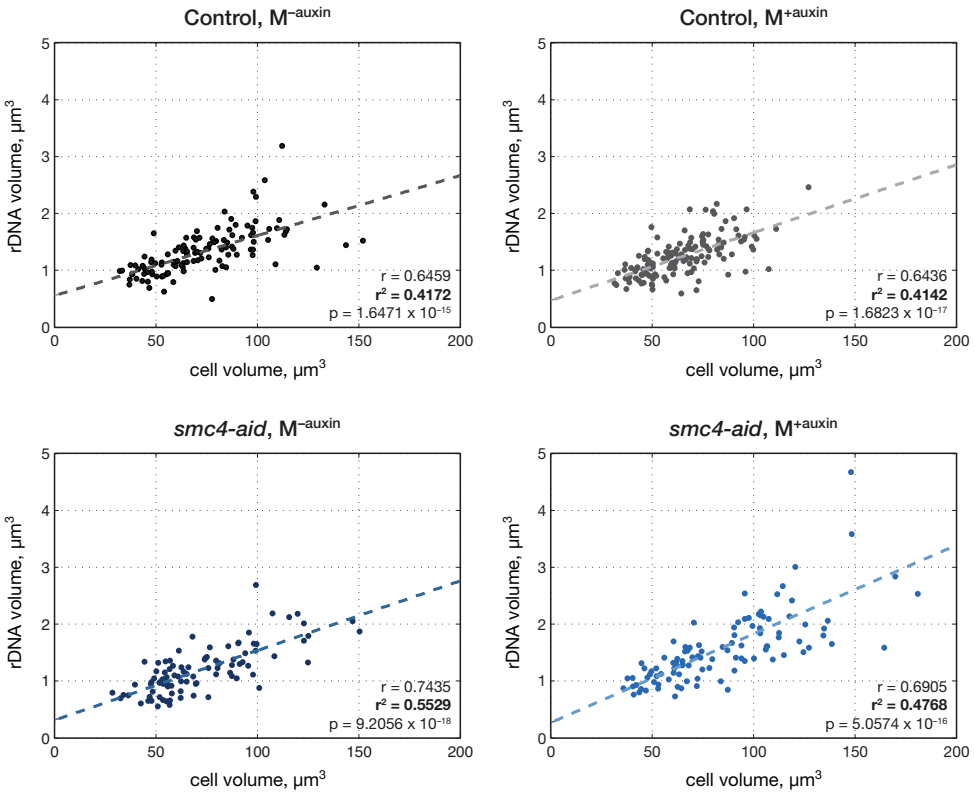

Figure 5.8 Correlation between cell and rDNA volume. Correlation coefficients between cell and rDNA volumes for control or *smc4-aid* strains, in the presence or absence of auxin. The bottom right corner of each plot shows the linear Pearson correlation coefficient r, the coefficient of determination r^2 and the p-value p, which denotes the probability of getting a correlation as large as the observed value by random chance, when the true correlation is zero.

chromatin more generally, could directly exert an outward force on the nuclear envelope resulting in enlarged nuclei, as has been measured for enzymatically-swelled or condensin-depleted chromatin in human cells (Mazumder et al., 2008; George et al., 2014); alternatively, continued transcription from uncondensed rDNA might allow unabated protein synthesis and cell growth in mitosis. On the other hand, condensin depletion might cause cell enlargement by altering transcription globally as has been proposed in the case of cohesin disruption (Sofueva et al., 2013), creating a larger volume for the rDNA to expand into.

5.2 G2/M analysis of chromosome condensation

To analyse the condensation status of chromatin in the G2 and M cell cycle phases, I introduced ectopic P_{GAL1}-*SWE1* into control and *smc4-aid* strains expressing fluorescent-tagged Net1 or histone H2B. This allowed the examination of rDNA (Net1-mCitrine) or total histone-wrapped DNA (Htb2-mCitrine) volumes in galactose inducible G2 or nocodazole inducible metaphase arrests (Figure 5.9).

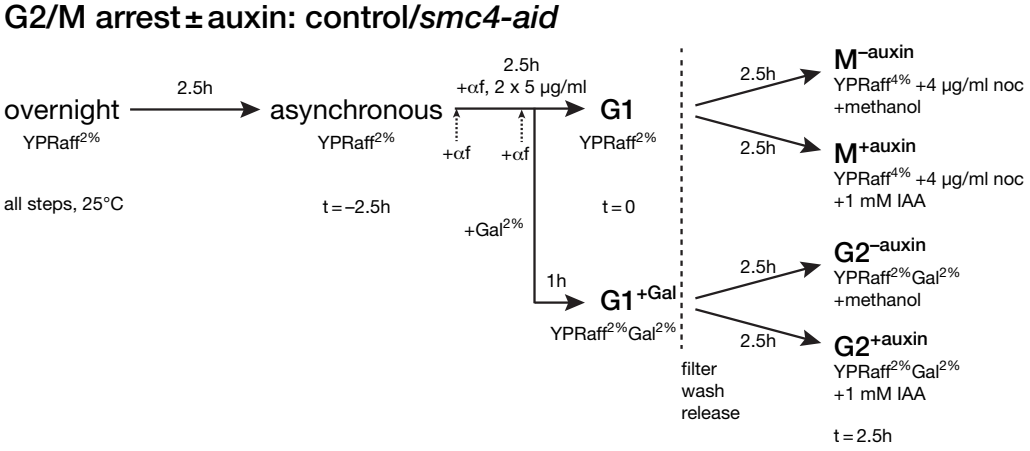

Figure 5.9 G2/M rDNA/chromatin volumes, experimental scheme. Asynchronous cultures of *aid* control and *smc4-aid* strains expressing Net1-mCitrine or Htb2-mCitrine grown in rich YPRaff medium were synchronised in G1 by addition of α factor and released into a galactose-induced G2 arrest or a nocodazole-induced metaphase arrest, in the presence or absence of IAA/auxin. *Strains: RT180, RT184, RT192, RT196*.

5.2.1 rDNA Volume

NET1-mCitrine P_{GAL1}-*SWE1* cells were grown overnight in YPRaffinose, synchronised in G1 by addition of α factor, and released into a G2 or metaphase arrest in

the presence of 1 mM IAA/auxin or methanol as control (experimental scheme, Figure 5.9). Samples were harvested at pre-synchronisation, G1, G2$^{\pm auxin}$ and M$^{\pm auxin}$ time points for quantification of rDNA volumes. Flow cytometry and immunoblotting were performed in parallel as controls to verify cell cycle arrests, and Smc4 depletion, respectively. Flow cytometry (Figure 5.10) showed the expected enrichment of 1C DNA peaks in G1, and 2C peaks in G2/M. Cell cycle progression between G1 and G2/M was unperturbed by condensin depletion. Immunoblotting (Figure 5.11) showed the expected degradation of Smc4-3Pk-miniAID in auxin-treated G2 and M *smc4-aid* samples relative to mock treatment, as well as the G2-specific galactose-induced expression of Swe1-3Pk.

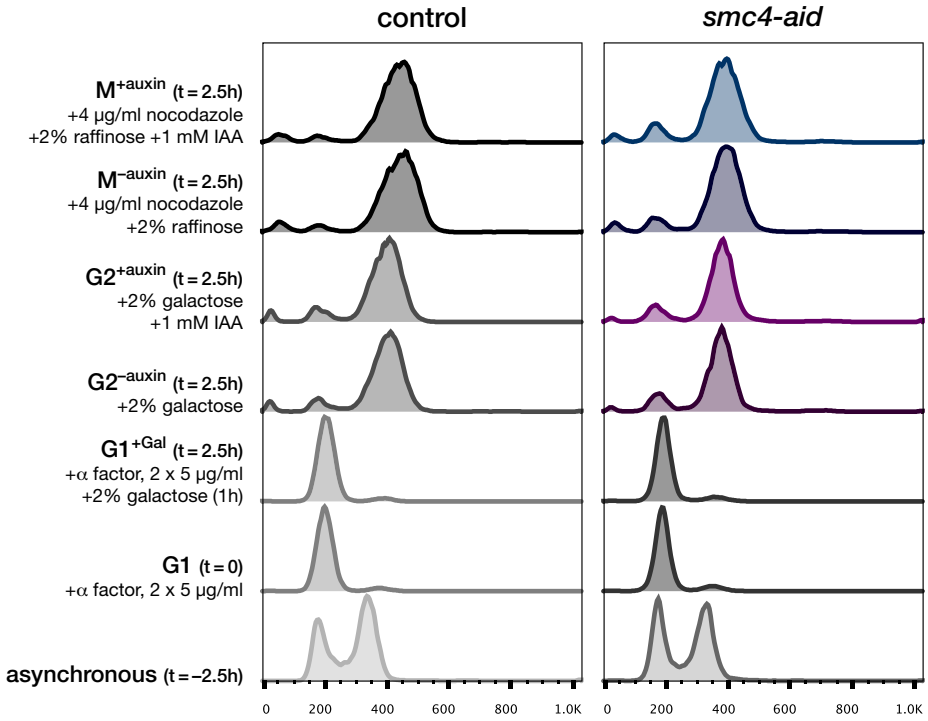

Figure 5.10 G2/M rDNA volume, flow cytometry. DNA content of asynchronous, G1 ± Gal, G2 ± auxin and M ± auxin samples was analysed by flow cytometry (Section 2.6), showing the expected enrichment of 1C peaks in G1 and 2C peaks in G2 and M. Cell cycle progression between G1 and G2/M was not hindered by condensin depletion. *Strains: RT180 (control), RT184 (smc4-aid)*.

For rDNA volume quantification, 15 x 0.25 µm images of mock– or auxin–treated *smc4-aid* samples were acquired and processed as in Section 5.1.1. As previously described (Freeman et al., 2000; Lavoie et al., 2004), metaphase rDNA was organised into loops, whereas G2 rDNA had a cluster-like appearance (Figure 5.12). In both these cell cycle phases, condensin depletion disrupted normal rDNA organisation, an effect that was qualitatively easier to discern in metaphase cells.

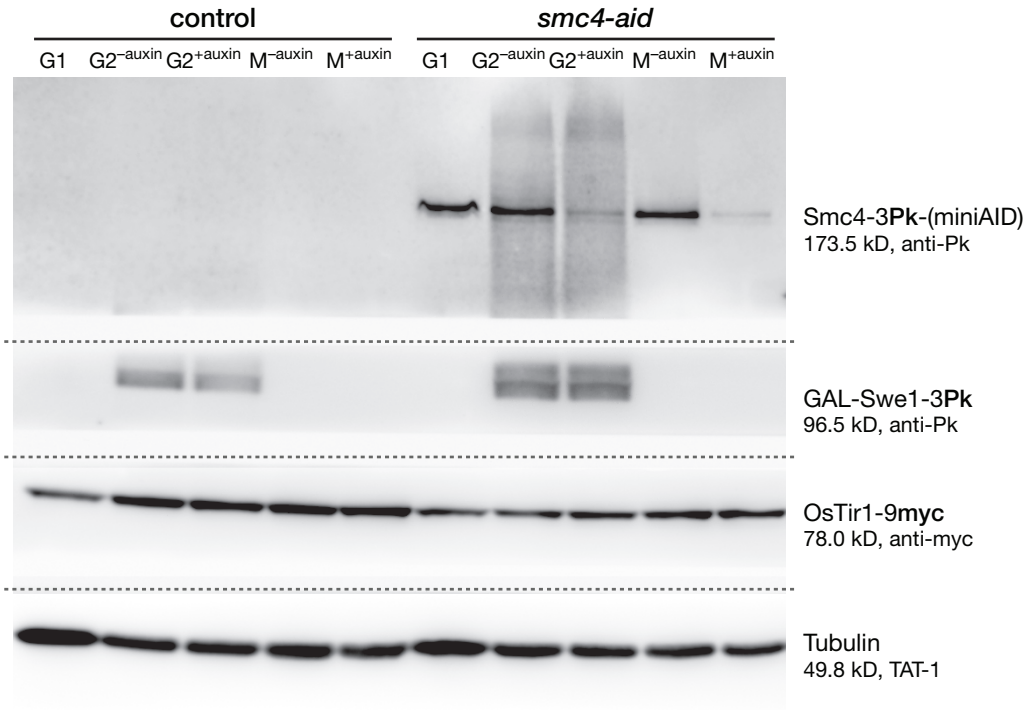

Figure 5.11 G2/M rDNA volume, immunoblotting. Immunoblots of whole cell protein extracts (Section 2.7.1) of G1, G2 ± auxin and M ± auxin samples were probed for Smc4-3Pk-miniAID (mouse anti-Pk, 1:1000), GAL-Swe1-3Pk (mouse anti-Pk, 1:50000) and the loading controls Tir1-9myc (mouse anti-myc, 1:1000) and α-tubulin (mouse anti–α-tubulin TAT-1, 1:20000). Detection with HRP–anti-mouse secondary antibody (1:5000) showed the expected auxin-induced degradation of Smc4-3Pk-miniAID (*top row*), as well as expression of GAL-Swe1-3Pk in G2 (*second row from top*). Exposure varies between proteins but not between lanes for a single protein. *Strains: RT180 (control), RT184 (smc4-aid)*.

However, quantification revealed that in both G2 and M, the observed morphological disruption of rDNA upon condensin depletion was accompanied by an increase in measured rDNA volume, as shown by a statistically significant increase in sample mean relative to the corresponding control ($p < 0.01$; Figure 5.13). In addition, I note that there was no measurable change in rDNA compaction between G2 clusters and metaphase loops.

5.2.2 Histone Volume

Similar to the experimental setup in Section 5.2.1, *HTB2-mCitrine* P_{GAL1}*-SWE1* control and *smc4-aid* cells were grown overnight in YPRaffinose, synchronised in G1 by addition of α factor, and released into a G2 or metaphase arrest in the presence of 1 mM IAA/auxin or methanol as control (experimental scheme, Figure 5.9). Samples were harvested at pre-synchronisation, G1, $G2^{\pm auxin}$ and $M^{\pm auxin}$ time points for quantification of whole cell histone-wrapped DNA volumes. Flow cytometry and immunoblotting were performed in parallel as controls to verify cell cycle arrests, and Smc4 depletion, respectively. Flow cytometry (Figure 5.14) showed the expected enrichment of 1C DNA peaks in G1, and 2C peaks in G2/M. Cell cycle progression from G1 to G2/M was not hindered by condensin depletion. Immunoblotting (Figure 5.15) showed the expected degradation of Smc4-3Pk-miniAID in auxin-treated G2 and M *smc4-aid* samples relative to mock-treated samples, as well as the G2-specific galactose-induced expression of Swe1-3Pk.

For quantification of bulk chromosomal DNA volume, 33 x 0.125 µm images (total depth, 4 µm) of auxin-treated *aid* control and *smc4-aid* samples were acquired in 3D-structured illumination microscopy (SIM) mode and processed as in Section 5.1.1, but using Htb2-mCitrine labels instead of Net1-mCitrine. The images showed a relatively compact but morphologically distinct chromatin configuration of the control strain in G2 and M, with loops of chromatin (presumably rDNA) projecting out of the bulk of histone-demarcated DNA in metaphase (Figure 5.16). This organisation was disrupted on condensin depletion in the auxin-treated *smc4-aid* strain, where chromatin appeared somewhat puffier, although quantification did not show a statistically significant difference in volume ($p < 0.01$; Figure 5.17).

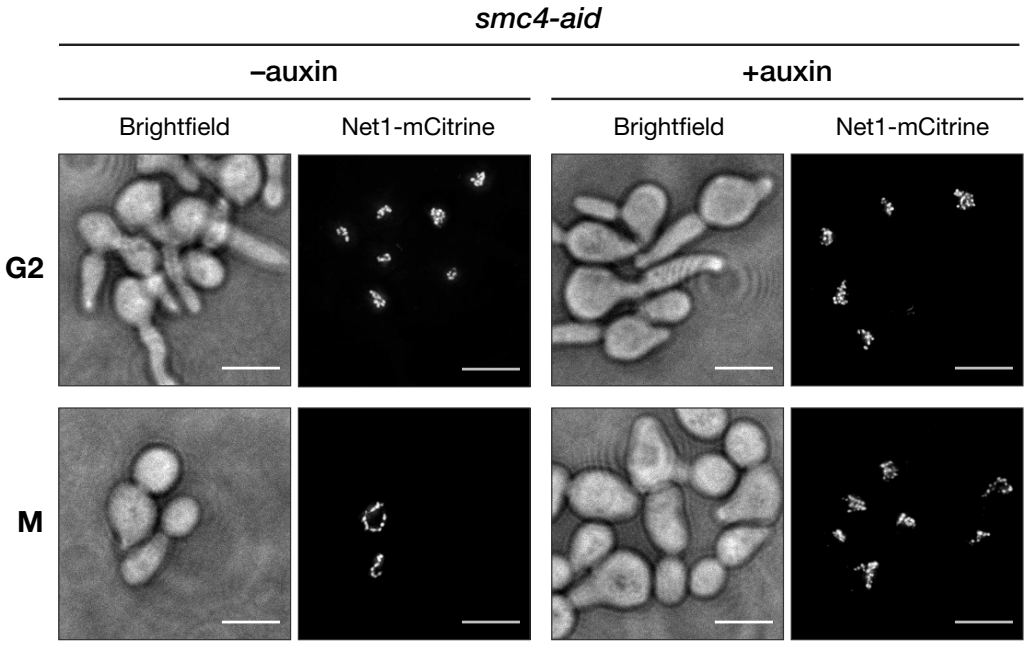

Figure 5.12 G2/M rDNA volume, representative images. Representative brightfield and fluorescent images of *smc4-aid NET1-mCitrine* cells in G2 or metaphase. Note the decompaction of rDNA in the auxin-treated samples (*right column*), accompanied by a loss of cluster-like organisation in G2, or loop-like organisation in metaphase. The fluorescent images are maximum intensity projections of 15 x 0.25 µm deconvolved images of 3.5 µm *z* depth. Scale bars represent 5 µm. *Strain: RT184*.

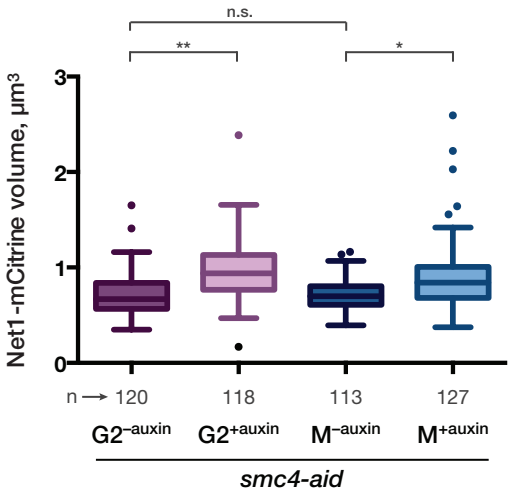

Figure 5.13 G2/M rDNA volume, box plot. Box-and-whisker plots of the distributions of rDNA volume in mock– or auxin–treated *smc4-aid* cells arrested in G2 or metaphase. The boxes span the 25-75 percentiles (the IQR) of the data, centred on the median; the whiskers extend to 1.5 x IQR either side of the upper and lower quartiles, while dots denote outliers. The number of cells measured for each condition is denoted by *n*. *Strain: RT184*.

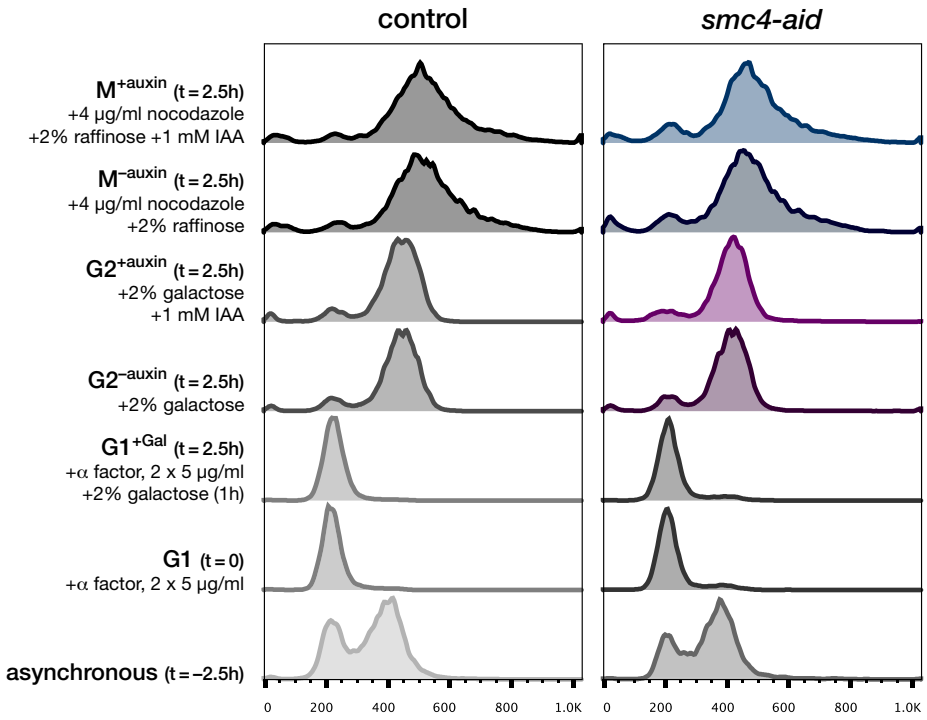

Figure 5.14 G2/M bulk chromatin volume, flow cytometry. DNA content of asynchronous, G1 ± Gal, G2 ± auxin and M ± auxin samples was analysed by flow cytometry (Section 2.6), showing the expected enrichment of 1C peaks in G1 and 2C peaks in G2 and M. Cell cycle progression between G1 and G2/M was not hindered by condensin depletion. *Strains: RT192 (control), RT196 (smc4-aid)*.

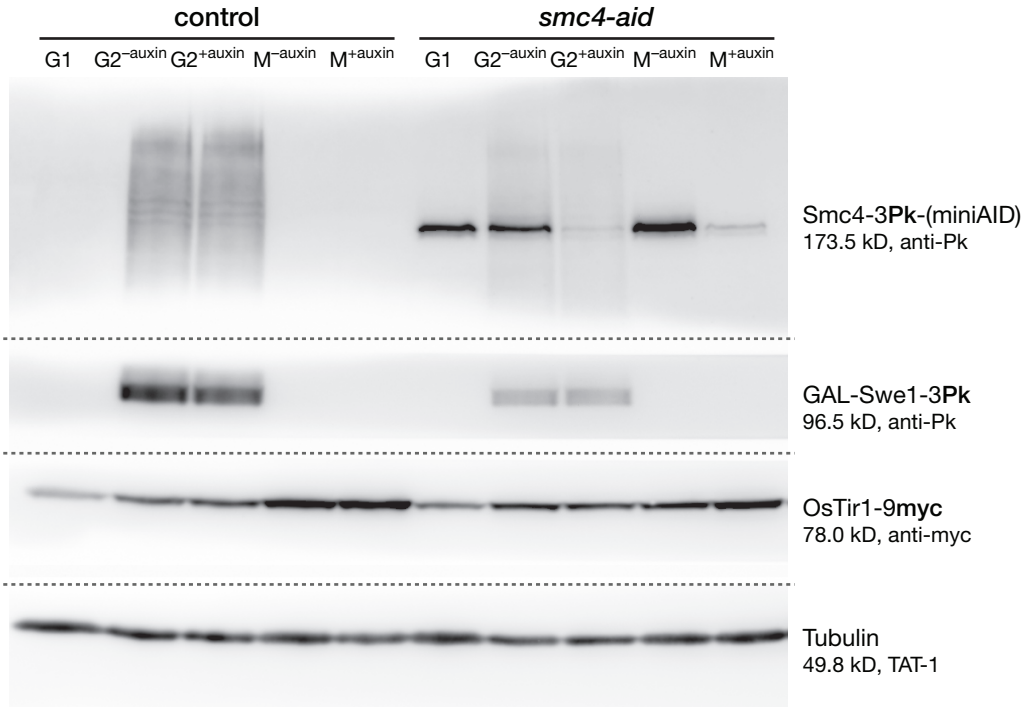

Figure 5.15 G2/M bulk chromatin volume, immunoblotting. Immunoblots of whole cell protein extracts (Section 2.7.1) of G1, G2 ± auxin and M ± auxin samples were probed for Smc4-3Pk-miniAID (mouse anti-Pk, 1:1000), GAL-Swe1-3Pk (mouse anti-Pk, 1:50000) and the loading controls Tir1-9myc (mouse anti-myc, 1:1000) and α-tubulin (mouse anti–α-tubulin TAT-1, 1:20000). Detection with HRP–anti-mouse secondary antibody (1:5000) showed the expected auxin-induced degradation of Smc4-3Pk-miniAID (*top row*), as well as expression of GAL-Swe1-3Pk in G2 (*second row from top*). Exposure varies between proteins but not between lanes for a single protein. *Strains: RT192 (control), RT196 (smc4-aid)*.

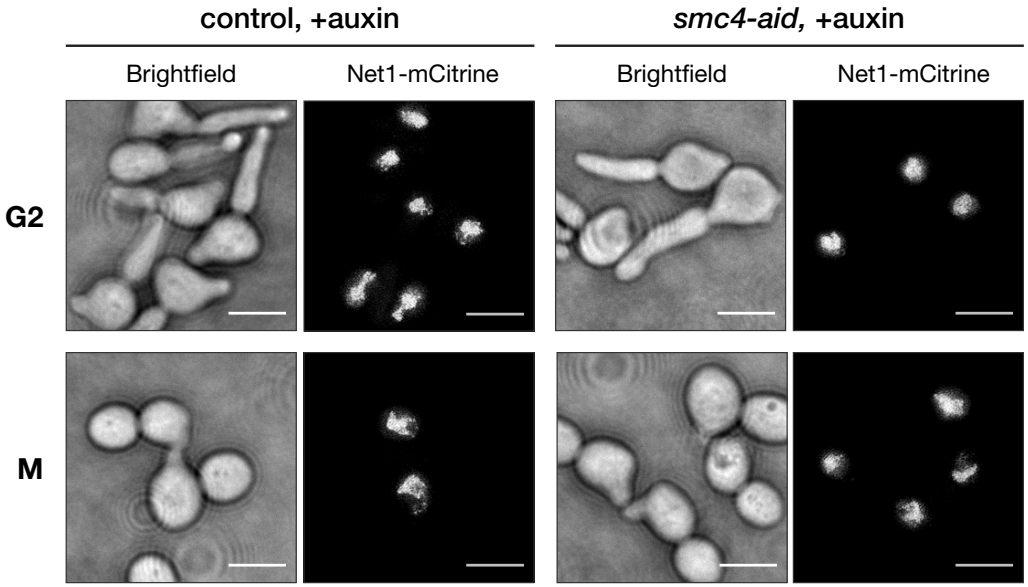

Figure 5.16 G2/M bulk chromatin volume, representative images. Representative brightfield and fluorescent images Htb2-mCitrine–expressing control and *smc4-aid* cells in G2 or metaphase. The fluorescent images are maximum intensity projections of 33 x 0.125 µm images of 4 µm *z* depth. Scale bars represent 5 µm. *Strains: RT192 (control), RT196 (smc4-aid)*.

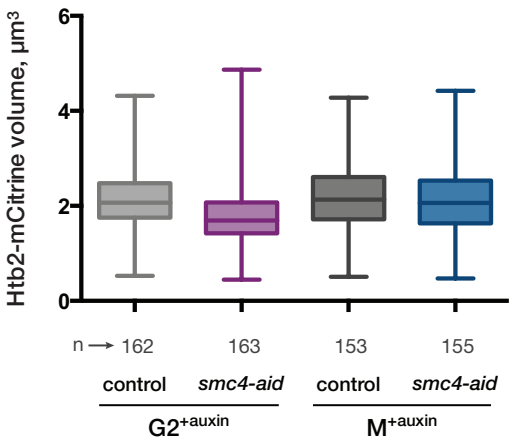

Figure 5.17 G2/M bulk chromatin volume, box plot. Box-and-whisker plots of the distributions of bulk chromatin volume in G2– and metaphase–arrested control and *smc4-aid* cells treated with auxin. The boxes span the 25-75 percentiles (the IQR) of the data, centred on the median; the whiskers extend to 1.5 x IQR either side of the upper and lower quartiles. The number of cells measured for each condition is denoted by *n*. *Strains: RT192 (control), RT196 (smc4-aid)*.

5.2.3 Conclusion

These results recapitulate previous interphase and metaphase characterisations of rDNA morphology from spread chromosome preparations (Freeman et al., 2000; Lavoie et al., 2000), and extend them to intact cells. In G2 and M, condensin depletion results in an increase in rDNA volume, suggesting that condensin might keep rDNA in a condensed state in both these cell cycle phases. In addition, the change in rDNA loop morphology from clusters in G2 to loops in metaphase is not accompanied by a reduction in volume and is therefore not a condensation reaction in the strictest sense but rather a reorganisation of chromatin, contrary to what has been assumed in previous reports. Although there is little detectable condensation between G2 and M in budding yeast, as measured by rDNA and histone volumes, condensin is required for maintaining the structural integrity of chromosomes in both interphase and mitosis. Indeed, more measurable condensation in yeast may well occur in anaphase, when the rDNA array has been reported to undergo hypercondensation (Sullivan et al., 2004). In an analogous situation, human chromosomes also reach their maximal compaction in anaphase (Mora-Bermúdez et al., 2007). As presented here, volume measurements of rDNA, which is a major condensin binding site in budding yeast, constitute a sensitive assay for the condensation effects of condensin depletion. The histone volume measurements are more difficult to interpret, but given their unprecedented resolution, the associated images show the first hints of visualisation of chromosome structure in budding yeast mitosis.

5.3 Cell cycle analysis of chromosome condensation

Since the rDNA volume measurements in Section 5.2.1 did not show any detectable condensation between G2 and metaphase, I further examined rDNA volume in various phases of the cell cycle, *viz.* late G1, S, G2, M and anaphase. As shown in the experimental scheme (Figure 5.18), asynchronous cultures of *NET1-mCitrine smc4-aid* strains growing in YPRaffinose were arrested in G1 by addition of α factor, and released into conditions that resulted in the following cell cycle arrests:

- Late G1 (P_{GAL1}-*SIC1*) – galactose-induced overexpression of a stabilised form of the S-phase Cdk1 inhibitor Sic1 (T5G, T33A, S76A) blocks the G1/S transition (Verma et al., 1997).

- S phase (hydroxyurea) – hydroxyurea halts DNA replication by preventing the expansion of nucleotide pools and arrests cells in early S phase (Slater, 1973; Koç et al., 2004).
- G2 (P_{GAL1}-*SWE1*) – galactose-induced overexpression of the Cdk1 inhibitor Swe1 arrests cells in G2 (Section 3.2; Booher et al., 1993).
- Metaphase (nocodazole): nocodazole induces the rapid disassembly of nuclear and cytoplasmic microtubules, activating the mitotic checkpoint, and resulting in a metaphase arrest (Li and Murray, 1991; Hoyt et al., 1991).
- Anaphase (P_{GAL1}-*BFA1*) – galactose-induced overexpression of Bfa1, a component of the mitotic exit network, prevents degradation of the mitotic cyclin Clb2, resulting in an anaphase arrest without blocking chromosome segregation (Li, 1999).

Once in the respective cell cycle arrests, cultures were treated with methanol as control, or with auxin to deplete Smc4-3Pk-miniAID. Samples were harvested at pre-synchronisation, G1, late $G1^{\pm auxin}$, $S^{\pm auxin}$, $G2^{\pm auxin}$, $M^{\pm auxin}$ and $Anaphase^{\pm auxin}$ time points for quantification of rDNA volumes. Flow cytometry and immunoblotting were performed in parallel as controls to verify cell cycle arrests, and Smc4 depletion, respectively. Flow cytometry (Figure 5.19) showed the expected enrichment of 1C DNA peaks in G1 (α factor), late G1 (P_{GAL1}-*SIC1*) and S phase (hydroxyurea), and 2C peaks in G2 (P_{GAL1}-*SWE1*), metaphase (nocodazole) and anaphase (P_{GAL1}-*BFA1*). Cell cycle release from α factor was not hindered by condensin depletion. Immunoblotting (Figure 5.20) showed the expected degradation, relative to mock treatment, of Smc4-3Pk-miniAID in auxin-treated *smc4-aid* samples from all cell cycle phases.

For rDNA volume quantification, 33 x 0.125 µm images of mock– or auxin–treated *smc4-aid* samples were acquired and processed as in Section 5.1.1. Metaphase rDNA was organised into loops, whereas interphase rDNA had a more diffuse cluster-like appearance, and anaphase rDNA was organised into lines (Figure 5.21). In all the cell cycle phases examined here, condensin depletion disrupted normal rDNA organisation, an effect that was qualitatively easiest to discern in metaphase cells. However, quantification revealed that throughout the cell cycle, the observed morphological disruption of rDNA upon condensin depletion was accompanied by an increase in measured rDNA volume, as shown by a statistically significant increase in sample mean relative to the corresponding control ($p < 0.01$; Figure 5.22). In addition, I note that the rDNA was most compact in G2 and metaphase, and least compact in an S phase arrest.

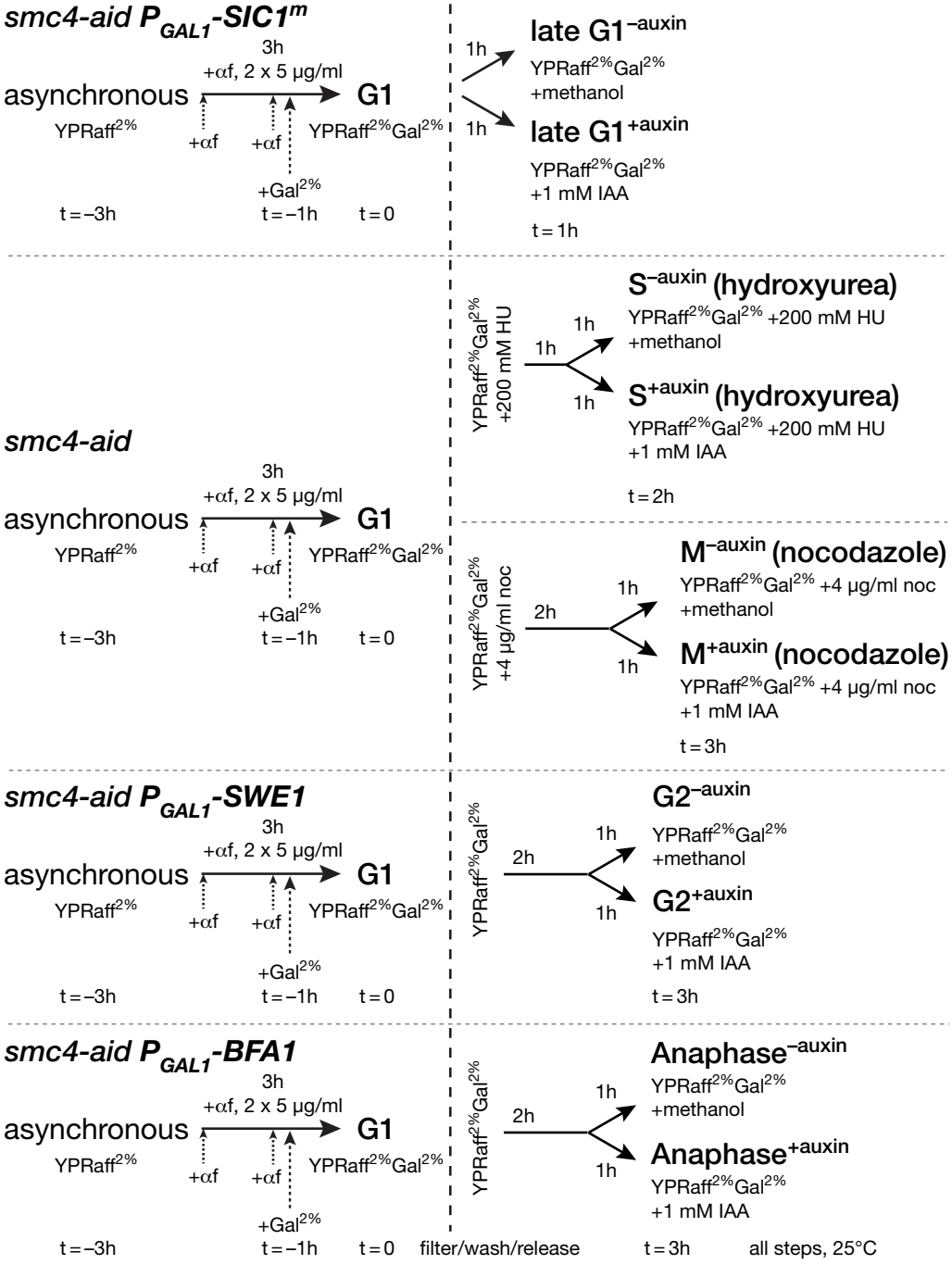

Figure 5.18 Cell cycle rDNA volumes, experimental scheme. Asynchronous cultures of *smc4-aid* strains expressing Net1-mCitrine grown in rich YPRaff medium were synchronised in G1 by addition of α factor and released into a late G1, S, G2, metaphase or anaphase arrest, in the presence or absence of IAA/auxin. Galactose was added to cultures 1 hour before release from G1 to induce expression from the P_{GAL1} promoter. *Strains: RT272, RT174, RT274, RT276.*

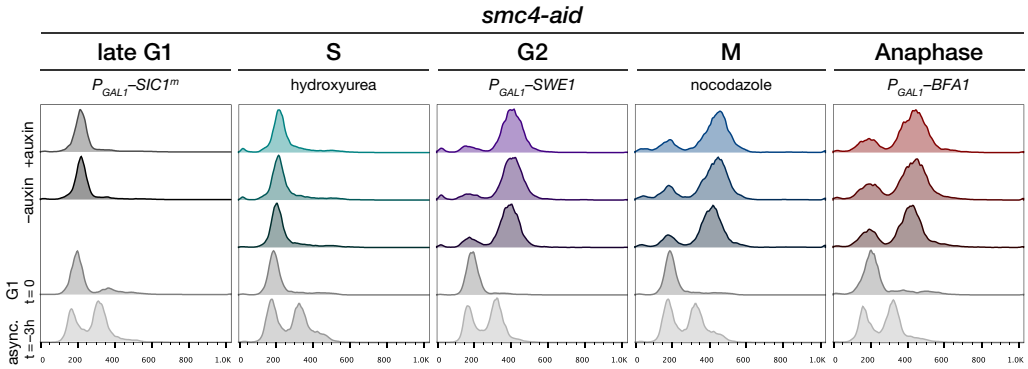

Figure 5.19 Cell cycle rDNA volume, flow cytometry. DNA content of asynchronous, G1 ± Gal, late G1 ± auxin, S ± auxin, G2 ± auxin, M ± auxin and anaphase ± auxin samples was analysed by flow cytometry (Section 2.6), showing the expected enrichment of 1C peaks in G1, late G1 and S phase, and 2C peaks in G2, M and anaphase. Cell cycle release from α factor was not hindered by condensin depletion. *Strains: RT272, RT174, RT274, RT276.*

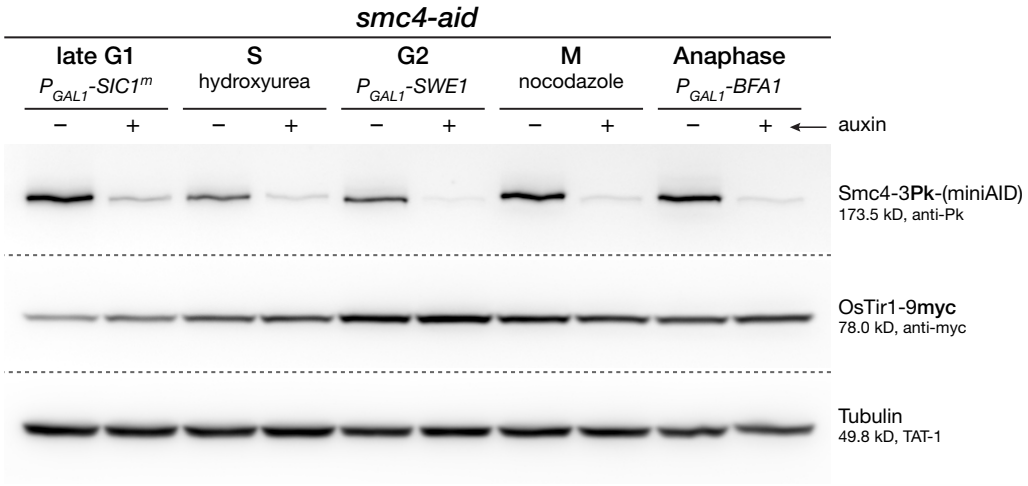

Figure 5.20 Cell cycle rDNA volume, immunoblotting. Immunoblots of whole cell protein extracts (Section 2.7.1) of late G1 ± auxin, S ± auxin, G2 ± auxin, M ± auxin and anaphase ± auxin samples were probed for Smc4-3Pk-miniAID (mouse anti-Pk, 1:1000), and the loading controls Tir1-9myc (mouse anti-myc, 1:1000) and α-tubulin (mouse anti–α-tubulin TAT-1, 1:20000). Detection with HRP–anti-mouse secondary antibody (1:5000) showed the expected auxin-induced degradation of Smc4-3Pk-miniAID (*top row*). Exposure varies between proteins but not among lanes for a single protein. *Strains: RT272, RT174, RT274, RT276.*

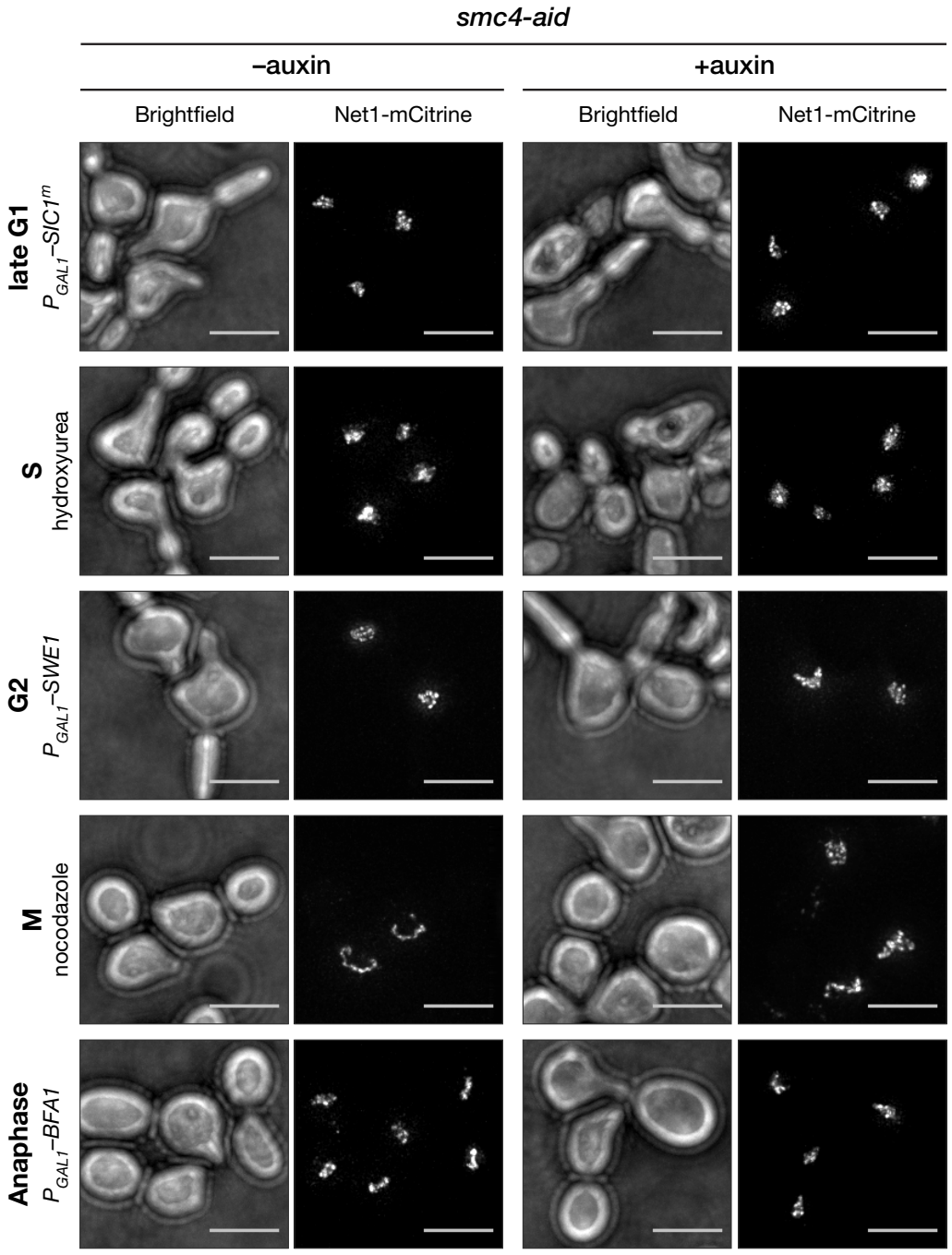

Figure 5.21 Cell cycle rDNA volume, representative images. Representative brightfield and fluorescent images of *smc4-aid NET1-mCitrine* cells in late G1, S phase, G2, metaphase and anaphase. Note the decompaction of rDNA in the auxin-treated samples (*right column*) in all cases. The fluorescent images are maximum intensity projections of 33 x 0.125 µm deconvolved images of 4 µm *z* depth. Scale bars represent 5 µm. *Strains: RT272, RT174, RT274, RT276.*

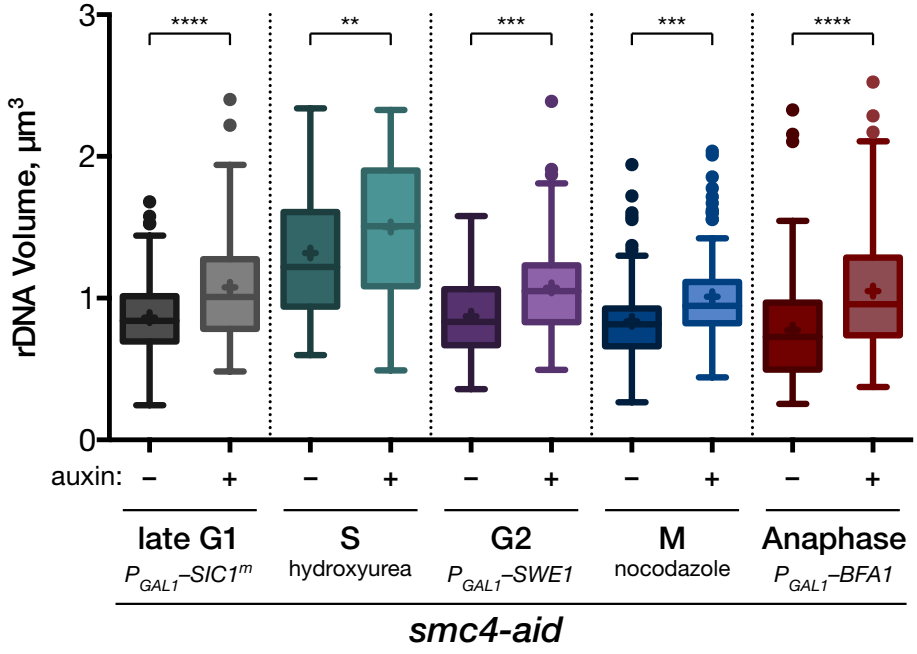

Figure 5.22 Cell cycle rDNA volume, box plot. Box-and-whisker plots of the distributions of rDNA volume in mock– or auxin–treated *smc4-aid* cells arrested in late G1, S phase, G2, metaphase and anaphase. The boxes span the 25-75 percentiles (the IQR) of the data, centred on the median; the whiskers extend to 1.5 x IQR either side of the upper and lower quartiles, while dots denote outliers. *Strains: RT272, RT174, RT274, RT276.*

5.3.1 Conclusion

These results recapitulate previous interphase and metaphase characterisations of rDNA morphology from spread chromosome preparations (Freeman et al., 2000; Lavoie et al., 2000), and extend them to intact cells. The fact that condensin could be depleted from chromatin in G1, S phase, G2, metaphase and anaphase arrests, and the consequent increase in rDNA volume, suggests that budding yeast chromosomes may be structurally similar throughout the cell cycle. In addition, condensin might function to constrain a tendency of the rDNA array to expand, offering a possible avenue of regulation of cell growth. Surprisingly, these rDNA volume measurements reveal that the rDNA array is more compact in metaphase than in anaphase, when Cdc14 plays a role in anaphase-specific rDNA compaction, in what is commonly assumed to be a hypercondensation reaction (Sullivan et al., 2004). However, it may still be the case that the rDNA is at its most compact in early anaphase, when structural rigidity would be required for withstanding forces generated by the elongating spindle, and at which time condensin has been reported to promote chromosome recoiling to remove residual sister chromatid cohesion (Renshaw et al., 2010).

6 Results IV: The Condensin ATPase Domains

The contribution of the condensin ATPase to its function has remained a largely unexplored area of study. While an analysis in chicken DT40 cells has outlined the chromatin binding properties of Smc2 ATPase mutants to some extent, their relation to condensation has been difficult to assess in this system (Hudson et al., 2008). ATPase mutants of the condensin SMC subunits have hitherto not been characterised in a genetically tractable eukaryote such as budding yeast. In this chapter, I discuss the generation of such structure-based point mutations, as well as their use to dissect the relation between the SMC catalytic cycle, the dynamic binding of condensin to chromatin, and chromosome condensation.

6.1 ATPase mutants of Smc2 and Smc4

A crystal structure of the archaeal SMC protein from *P. furiosus* has been used to identify point mutants deficient in particular aspects of the *Pf* SMC ATPase cycle (Lammens et al., 2004). I constructed a ClustalW multiple alignment (Figure 6.1; Larkin et al., 2007) of archaeal, bacterial and eukaryotic SMC proteins to identify the analogous amino acids in conserved nucleotide motifs of the budding yeast condensin SMC subunits; these are listed in Table 6.1, along with their predicted functional impairment. In addition, I modelled the structure of the yeast Smc2 and Smc4 head domains using Phyre2 (Figure 6.2; Kelley and Sternberg, 2009). The two highest confidence models (Pellegrino et al., 2012; Lammens et al., 2004) were superposed, and demonstrated conservation of ATPase domain organisation between *Pf* SMC and budding yeast Smc2 and Smc4. The indicated mutants of *SMC* and *SMC4* were cloned as described in Section 2.4.6, and integrated at ectopic loci in *smc2-aa* and *smc4-aid* backgrounds, respectively.

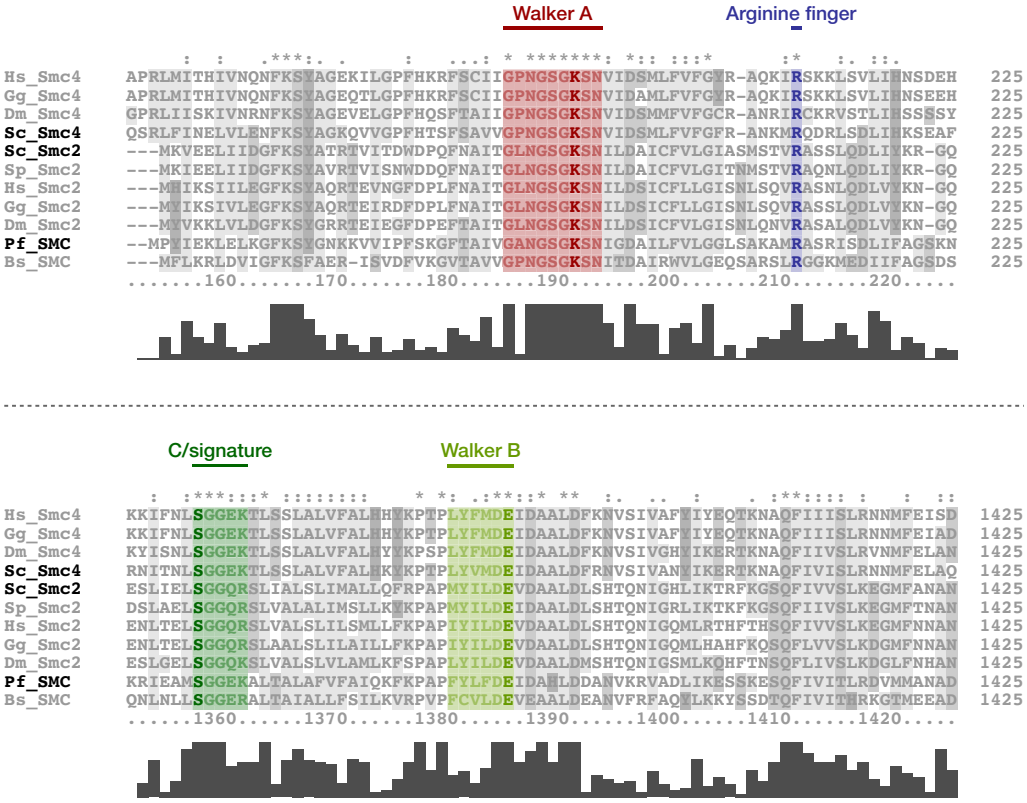

Figure 6.1 Multiple alignment of SMC proteins. Archaeal and eukaryotic condensin SMC proteins were aligned using ClustalW (Larkin et al., 2007). 75 amino acid long N- and C-terminal fragments of the proteins, containing the Walker A & arginine finger, and signature & Walker B motifs respectively, are shown. Residues mutated within these motifs are indicated in bold lettering. Bar graphs below sequences denote the extent of sequence identity. *Hs – H. sapiens; Gg – G. gallus; Dm – D. melanogaster; Sc – S. cerevisiae; Sp – S. pombe; Pf – P. furiosus; Bs – B. subtilis*.

Table 6.1 ATPase mutants of Smc2 and Smc4

Motif	Function disrupted	Amino acid substitution		
		***Pf*SMC**	**Smc2**	**Smc4**
Walker A	ATP binding	K39A	K38A	K191A
Arginine finger	DNA-stimulated ATPase activity	R59A	R58A	R210A/K*
C/signature	ATP-induced head dimerisation	S1070R	S1085R	S1324R
Walker B	ATP hydrolysis	E1098Q	E1113Q	E1352Q/D*

*R210K and E1352D are potentially subtler mutations than R210A and E1352Q.

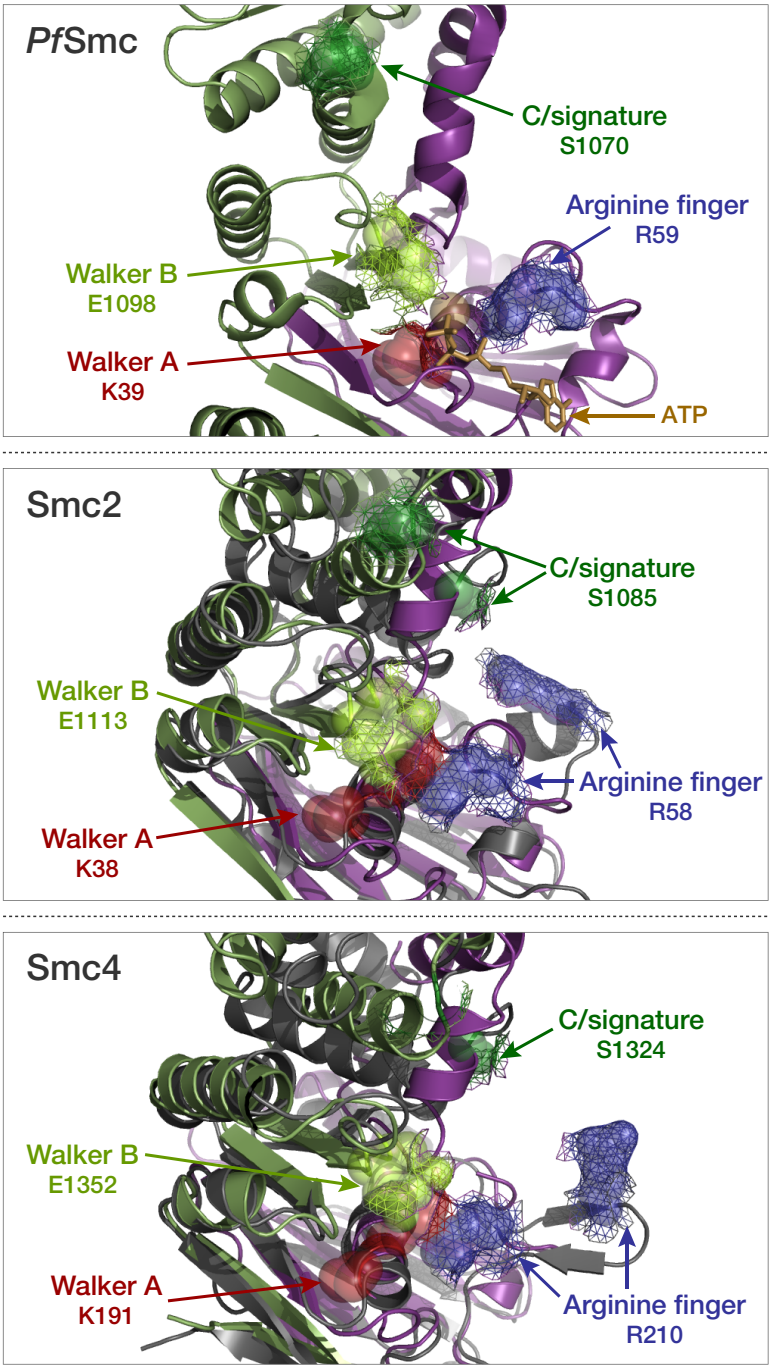

Figure 6.2 Structure of the SMC ATPase domain. *Top panel*: crystal structure of the *P. furiosus* ATPase domain, showing N- and C-terminal parts of the SMC head in purple and dark green, respectively, along with the ATP in yellow, at 20 Å zoom (PDB: 1XEX; Lammens et al., 2004). *Middle and bottom panels*: structure of budding yeast Smc2 and Smc4 ATPase domains, as predicted by Phyre2 (Kelley and Sternberg, 2009). The two highest confidence models, full-length SMC-like RecN (PDB: 4AD8; Pellegrino et al., 2012, shown in grey) and N- and C- terminal parts of the *Pf*SMC head (PDB: 1XEX; Lammens et al., 2004, chains shown in purple and dark green) are shown in superposition. The two models are in generally good agreement with the *Pf*SMC ATPase; the two possible conformations of the arginine finger may indicate its conformational change on ATP binding.

6.1.1 SMC ATPase mutant expression

Wild type or ATPase mutants of 3HA-tagged *SMC2* were integrated at the ectopic *URA3* locus in an *smc2-aa* background, and expressed in addition to *SMC2* tagged with FRB at its genomic locus. Clones were picked for expression as close as possible to endogenous levels of similarly tagged Smc2 (Figure 6.3).

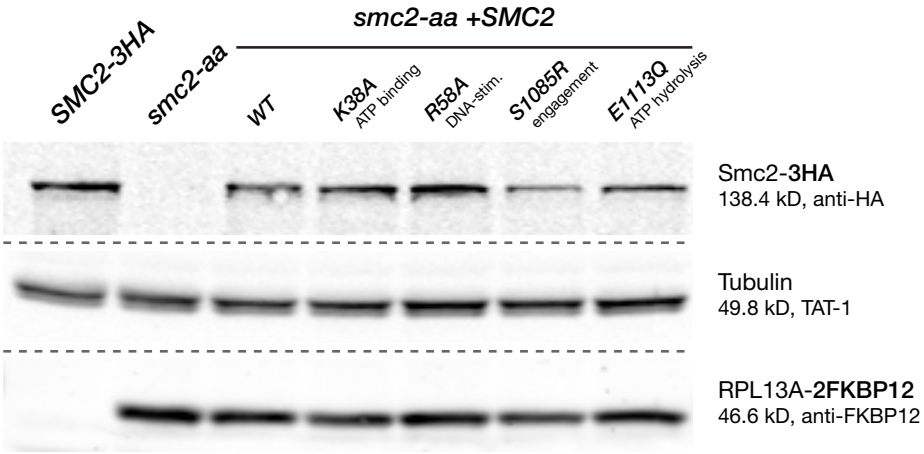

Figure 6.3 Smc2 mutant expression. Immunoblots of whole cell protein extracts (Section 2.7.1) of control strains *SMC2-3HA* and *smc2-aa*, as well as *smc2-aa* integrating the various *SMC2* mutants, were probed for wild type/mutant Smc2-3HA (mouse anti-HA, 1:10000), and loading controls α-tubulin (mouse anti–α-tubulin TAT-1, 1:10000) and FKBP12 (rabbit anti-FKBP12, 1:1000). Fluorescent detection was performed with IRDye800–anti-mouse and IRDye700–anti-rabbit antibodies (1:20000). Exposure varies between proteins but not between lanes for a single protein. *Strains, left to right: CSL3660, SH110, RT29, RT31, RT33, RT35, RT37*.

Similarly, wild type or ATPase mutants of 3HA-tagged *SMC4* were integrated at the ectopic *TRP1* locus in an *smc4-aid* background, and expressed in addition to *SMC4* tagged with 3Pk-miniAID at its genomic locus. Clones were picked for expression as close as possible to endogenous levels of identically tagged Smc4 (Figure 6.4).

6.1.2 Rescue of conditional inviability

To test the viability of ATPase mutants of *SMC2*, strains expressing them in an *smc2-aa* background were grown for two days at 25°C on solid rich YPD medium in the absence or presence of rapamycin, along with wild type, *aa* background and *smc2-aa* strains as controls (Figure 6.5). Under these conditions (which were earlier shown to lead to *smc2-aa* inviability in Figure 4.2), only the rescue

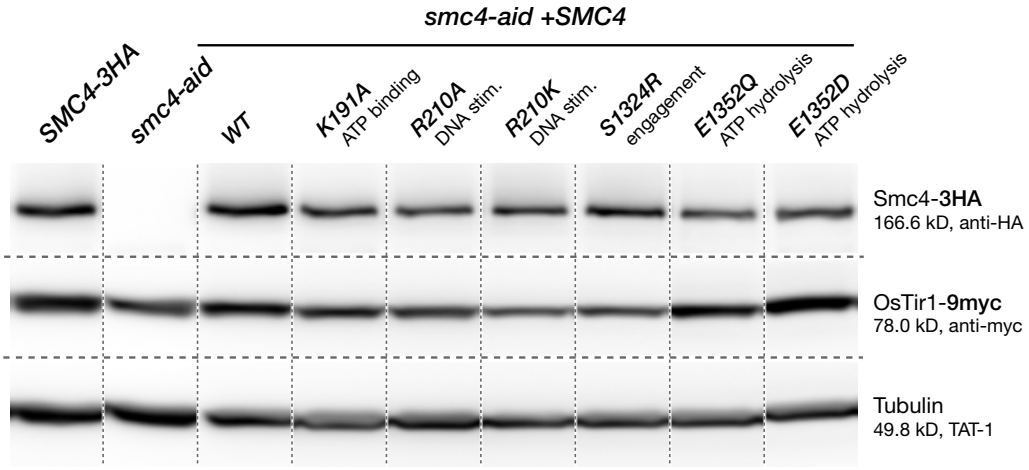

Figure 6.4 Smc4 mutant expression. Immunoblots of whole cell protein extracts (Section 2.7.1) of control strains *SMC4-3HA* and *smc4-aid*, as well as *smc4-aid* integrating the various *SMC4* mutants, were probed for wild type/mutant Smc4-3HA (mouse anti-HA, 1:5000), and loading controls Tir1-9myc (mouse anti-myc, 1:1000) and α-tubulin (mouse anti–α-tubulin TAT-1, 1:10000). Chemiluminiscent detection was performed with HRP–anti-mouse antibody (1:5000). Vertical lanes were spliced from a single image to remove duplicate lanes; exposure varies between proteins but not between lanes for a single protein. *Strains, left to right: RT159, RT149, RT242, RT244, RT246, RT248, RT250a, RT252, RT254*.

by wild type *SMC2* was effective, indicating that all the tested ATPase mutants of *SMC2* were inviable.

I similarly tested the viability of ATPase mutants of *SMC4* in an *smc4-aid* background by growth for two days at 25°C on YPD plates containing methanol as control or 1 mM auxin (Figure 6.6). Under these conditions (which were earlier shown to lead to *smc4-aid* inviability in Figure 4.4), only wild type *SMC4* and the arginine finger mutants $SMC4^{R210A}$ & $SMC4^{R210K}$ were viable, although $SMC4^{R210A}$ exhibited a slow growth phenotype.

6.2 Smc2 ATPase activity is dispensable for association with Brn1

In order to determine whether the ATPase activity of condensin was required for complex formation, I tested whether ATPase mutants of Smc2 could immunoprecipitate a different condensin subunit (the kleisin Brn1) from nuclease-treated extracts of metaphase-arrested cells. *BRN1* was tagged with a 3Pk epitope tag in control strains, as well as *smc2-aa* strains expressing an additional copy of wild type or mutant *SMC2-3HA*. Smc2-3HA was immunoprecipitated from whole cell

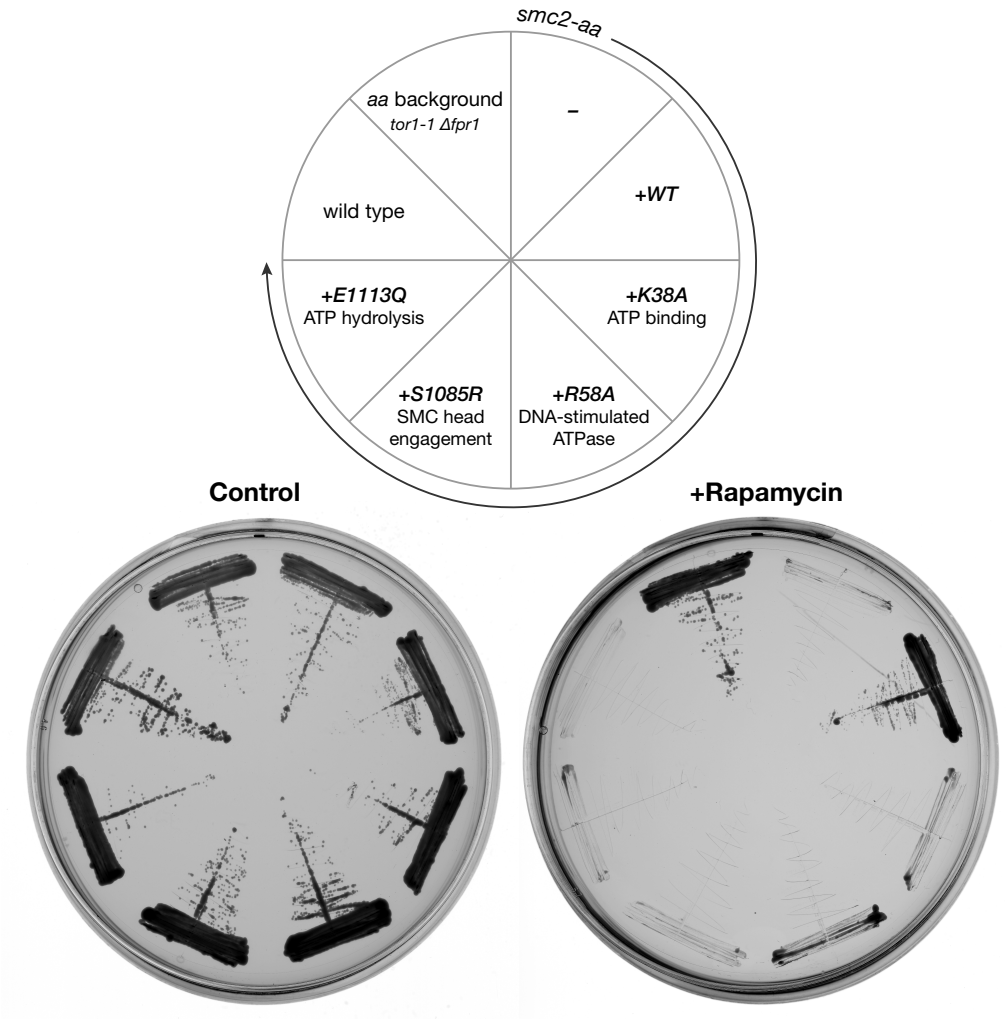

Figure 6.5 Viability of *SMC2* ATPase mutants. The indicated strains were grown for two days at 25°C on solid rich YPD medium containing either DMSO as control (*left*) or 1 µg/ml rapamycin (*right*). As rapamycin is toxic to wild type cells, all anchor-away strains use a *tor1-1 Δfpr1* background, which confers rapamycin resistance. Under these conditions, only the wild type *SMC2* rescued the rapamycin-induced inviability of *smc2-aa*. *Strains, clockwise from wild type: K700, CSL3793, SH110, RT29, RT31, RT33, RT35, RT37*.

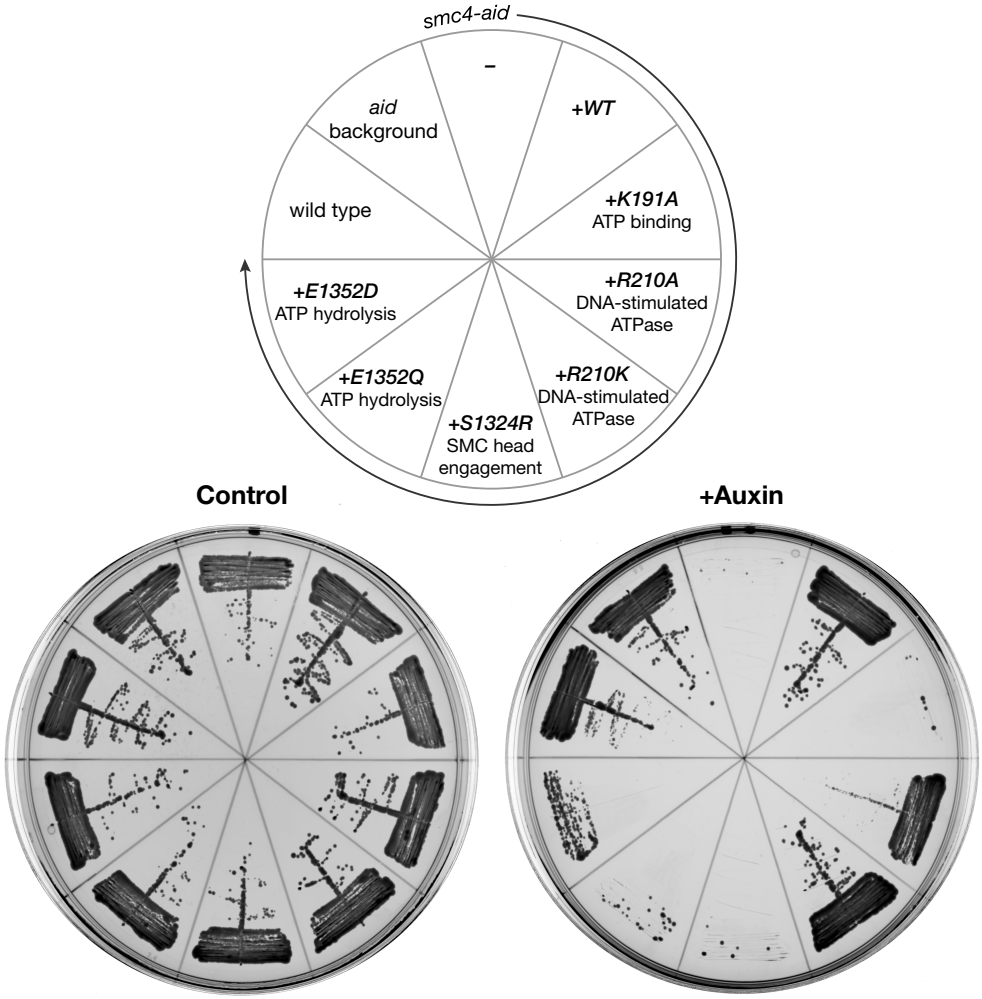

Figure 6.6 Viability of *SMC4* ATPase mutants. The indicated strains were grown for two days at 25°C on solid rich YPD medium containing either methanol as control (*left*) or 1 mM IAA/auxin (*right*). Under these conditions, wild type *SMC4*, as well as the arginine finger mutants $SMC4^{R210A}$ and $SMC4^{R210K}$, were effective in conferring viability on *smc4-aid*. *Strains, clockwise from wild type: K699, CSL4267, RT149, RT242, RT244, RT246, RT248, RT250a, RT252, RT254*.

extracts using an agarose-immobilised rat anti-HA affinity matrix, and eluted by boiling in SDS-PAGE sample buffer. The whole cell extract (W), the eluted immunoprecipitated fraction (IP) and flow-through of proteins not bound to the matrix (FT) were resolved by SDS-PAGE and immunoblotted. The membrane was probed for Smc2-3HA (mouse anti-HA, 1:10000), Brn1-3Pk (mouse anti-Pk, 1:5000) and the loading control α-tubulin (mouse anti–α-tubulin, 1:10000). Fluorescent detection with IRDye800–anti-mouse showed that all the ATPase mutants of Smc2 could immunoprecipitate Brn1-3Pk. Since the extracts were treated with benzonase, a potent nuclease, it is likely that the immunoprecipitated Brn1-3Pk reflected a direct association with Smc2, rather than a non-specific pull-down of chromatin-associated material. I therefore concluded that the ATPase activity of Smc2 was not required for its association with Brn1 (Figure 6.7).

6.3 Altered DNA-binding properties of Smc4 ATPase mutants

I examined the chromatin binding properties of Smc4 ATPase mutants by two complementary approaches: immunoblotting of fractionated chromatin and immunofluorescence microscopy of semi-spread preparations of chromosomes. Asynchronous cultures of *smc4-aid* cells expressing an additional copy of wild type or mutant *SMC4* tagged with 3HA were arrested in G1 by addition of α factor or in metaphase by treatment with nocodazole, in the presence of auxin, along with positive and negative controls (experimental scheme, Figure 6.8).

6.3.1 Co-pelleting with chromatin

To segregate chromatin-associated proteins from those not bound to chromatin, the G1– and metaphase–arrested cells were lysed after digestion of the cell wall and centrifuged through a sucrose cushion in the presence of the non-ionic detergent Triton X-100 (Section 2.8; Liang and Stillman, 1997). This effectively separated the whole cell extract (W) into a Triton-insoluble chromatin pellet (P) enriched in DNA-bound proteins, and a supernatant fraction (S) containing soluble proteins. The fractions were resolved by SDS-PAGE and following immunoblotting, probed for epitope-tagged Smc4 (Figure 6.9). As pelleting controls, soluble α-tubulin and chromatin-associated Hmo1 demonstrated that the chromatin fractionation was effective. While there were some indications that Smc4 ATP-

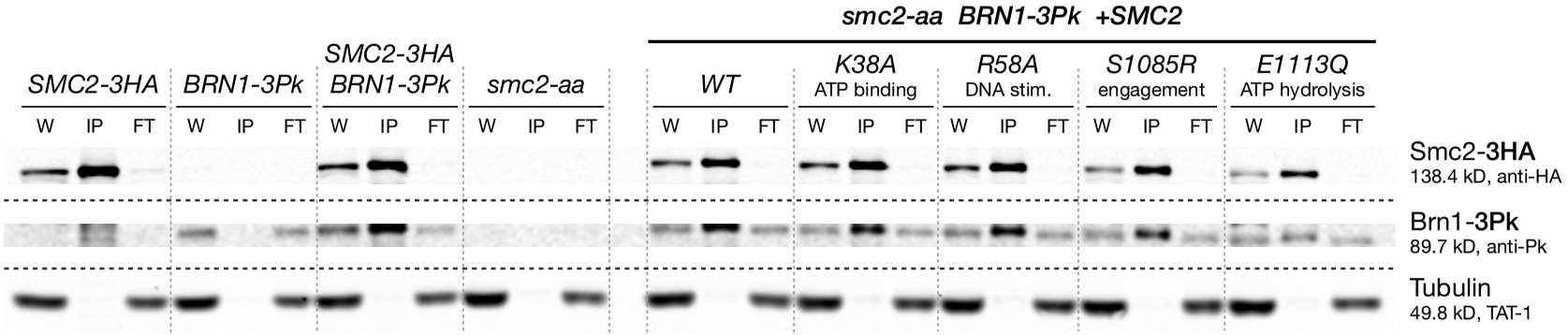

Figure 6.7 Smc2 ATPase activity is dispensable for interaction with Brn1. Smc2-3HA was immunoprecipitated from whole cell extracts (W) of the indicated strains using an agarose-coupled rat anti-HA antibody, and eluted by boiling in SDS-PAGE sample buffer. IP: immunoprecipitated fraction, FT: flow-through fraction. The immunoblot was probed for Smc2-3HA (mouse anti-HA, 1:10000), Brn1-3Pk (mouse anti-Pk, 1:5000) and the loading control α-tubulin (mouse anti–α-tubulin TAT-1, 1:10000). Fluorescent detection with IRDye800–anti-mouse antibody (1:20000) showed that all the ATPase mutants of Smc2 could immunoprecipitate Brn1-3Pk, indicating that Smc2 ATPase activity is not required for its interaction with Brn1. *Strains, left to right: RT49, RT63, RT65, SH110, RT67, RT69, RT71, RT73, RT75*.

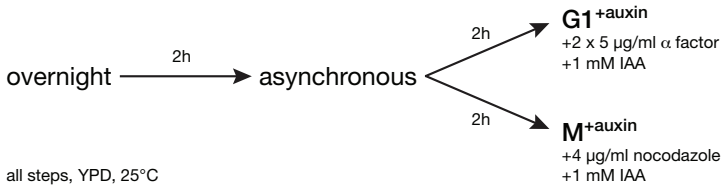

Figure 6.8 Smc4 ATPase mutant DNA binding assays, experimental scheme. Asynchronous cells were arrested in G1 by addition of 2 x 5 µg/ml α factor, or in metaphase by addition of 4 µg/ml nocodazole, in the presence of 1 mM IAA/auxin. *Strains: RT159, RT149, RT242, RT244, RT246, RT248, RT250a, RT252, RT254*.

ase mutants pelleted less efficiently with chromatin than the wild type, these results were difficult to interpret, given the somewhat variable expression of the mutants in whole cell extracts. Instead, the microscopic approach described in Section 6.3.2 below proved more conclusive.

6.3.2 Immunofluorescence microscopy

To further characterise the chromatin binding properties of the Smc4 ATPase mutants, I examined semi-spread preparations of chromosomes for Smc4 binding by indirect immunofluorescence (Section 2.9). Briefly, metaphase-arrested fixed cells were spheroplasted and lysed on multi-well glass slides with the detergent Lipsol. After washing away cellular debris, the adherent DNA was stained with DAPI, and bound Smc4-3HA visualised with anti-HA antibody, in conjunction with an Alexa594-conjugated secondary antibody. The chromosome spreads were imaged in structured illumination mode on an API OMX microscope using 592 nm and 405 nm laser excitation. Of all the Smc4 ATPase mutants, the Walker A mutant Smc4^{K191A}, predicted to be defective in ATP binding, showed the least colocalisation with chromatin (Figure 6.10). Maximum intensity projections were used for quantification since the chromosome spreads were unlikely to preserve much three-dimensional information. Wild type or mutant Smc4-3HA/Alexa594 staining intensity was measured as the absolute signal intensity in the 592 nm channel, using circles of 4.5 µm diameter drawn with the aid of DAPI-stained masses in the 405 nm channel. Because the ATPase mutants of Smc4 showed somewhat variable expression (Figure 6.11), I normalised the absolute staining intensity measured on chromosome spreads against whole cell expression of wild type or mutant Smc4 determined by Western blotting. As expected from the images of chromosome spreads, the quantification showed only the ATP binding mutant Smc4^{K191A} to be significantly impaired in chromatin as-

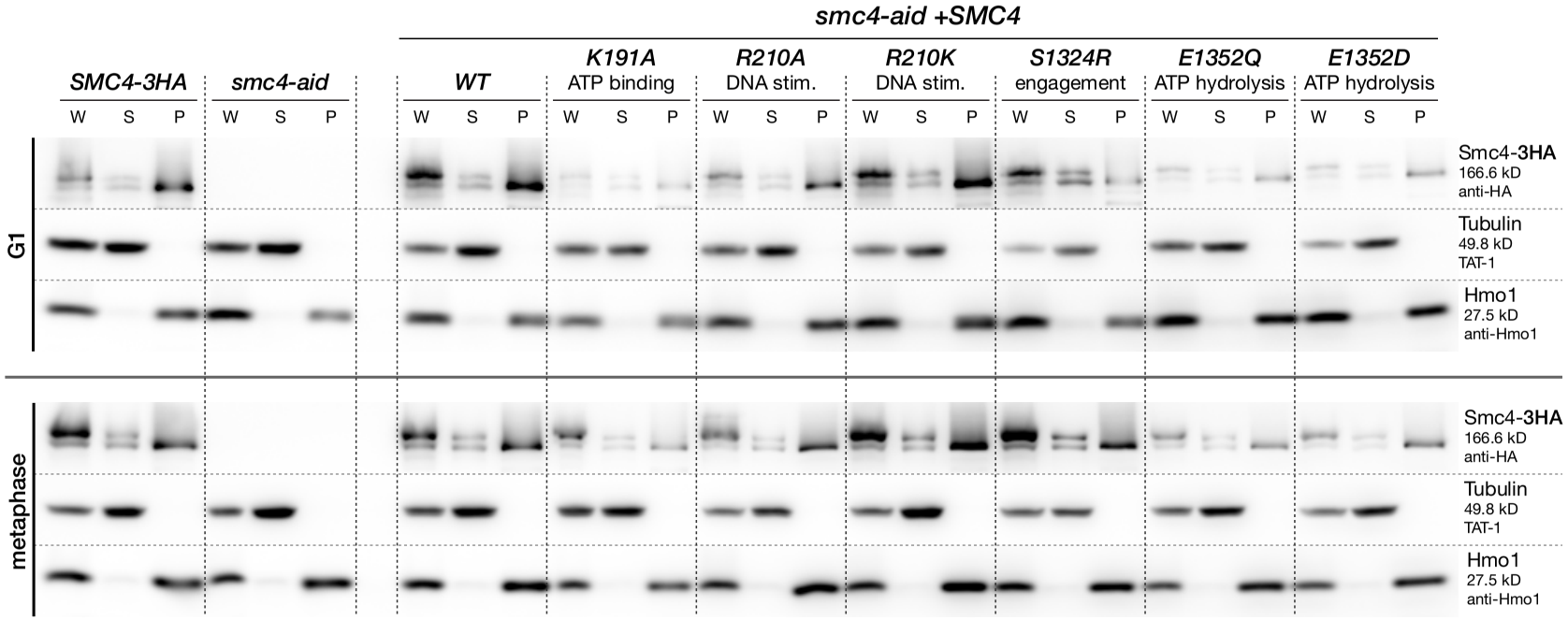

Figure 6.9 Smc4 ATPase mutants, copelleting with chromatin. Whole cell extracts (W) of the indicated strains were centrifuged through a sucrose cushion to separate the soluble fraction (S) from a chromatin-associated pellet of Triton-insoluble proteins (P). Wild type and R210A/K Smc4 efficiently co-pelleted with chromatin; other ATPase mutants showed somewhat altered chromatin association, but these results were difficult to interpret, given their variable expression levels in whole cell extracts. *Strains, left to right: RT159, RT149, RT242, RT244, RT246, RT248, RT250a, RT252, RT254*.

sociation (Figure 6.12). These results showed that ATP binding, but not SMC head engagement or ATP hydrolysis were required for the stable association of condensin with chromatin.

6.4 Contribution of the condensin ATPase to chromosome condensation

6.4.1 Smc2 ATPase mutants: chromatin volume

To determine whether Smc2 ATPase activity was required for chromosome condensation, I quantified DAPI-stained chromatin volumes (Section 2.11.2) in metaphase arrested *smc2-aa* cells expressing an additional copy of wild type or ATPase mutant *SMC2*. Asynchronous cultures of the *MAT*α cells were synchronised in G1 by addition of **a** factor and released into a nocodazole-induced metaphase arrest, in the presence of rapamycin (experimental scheme, Figure 6.13). Cells were fixed under mild conditions (3.6% formaldehyde, 10 minutes, room temperature), permeabilised and stained with DAPI. 33 slices x 0.125 µm (total depth, 4 µm) were acquired on an API OMX microscope in structured illumination mode (Figure 6.14). Although decompaction in the absence of condensin was not readily apparent from the images, quantification of chromatin volume revealed a statistically significant decompaction in the rapamycin-treated *smc2-aa* sample ($p < 0.05$; Figure 6.15). This condensation defect was rescued by expression of wild type Smc2 or the arginine finger mutant Smc2^{R58A}, but not Walker A (Smc2^{K38A}), C/signature motif (Smc2^{S1085R}) or Walker B (Smc2^{E1113Q}) mutants, showing that the ATPase activity of Smc2 was essential for chromosome condensation.

6.4.2 Smc4 ATPase mutants: rDNA volume

To determine whether Smc4 ATPase activity was required for chromosome condensation, I quantified rDNA volumes (Section 2.11.2) in metaphase-arrested *smc4-aid* cells expressing Net1-mCitrine, and an additional copy of wild type or ATPase mutant *SMC4*. Asynchronous cultures of the *MAT*a cells were synchronised in G1 by addition of α factor and released into a nocodazole-induced metaphase arrest, in the presence of 1 mM auxin/IAA (experimental scheme, Figure 6.16). Cells were subject to gentle fixation (3.6% formaldehyde, 10 minutes,

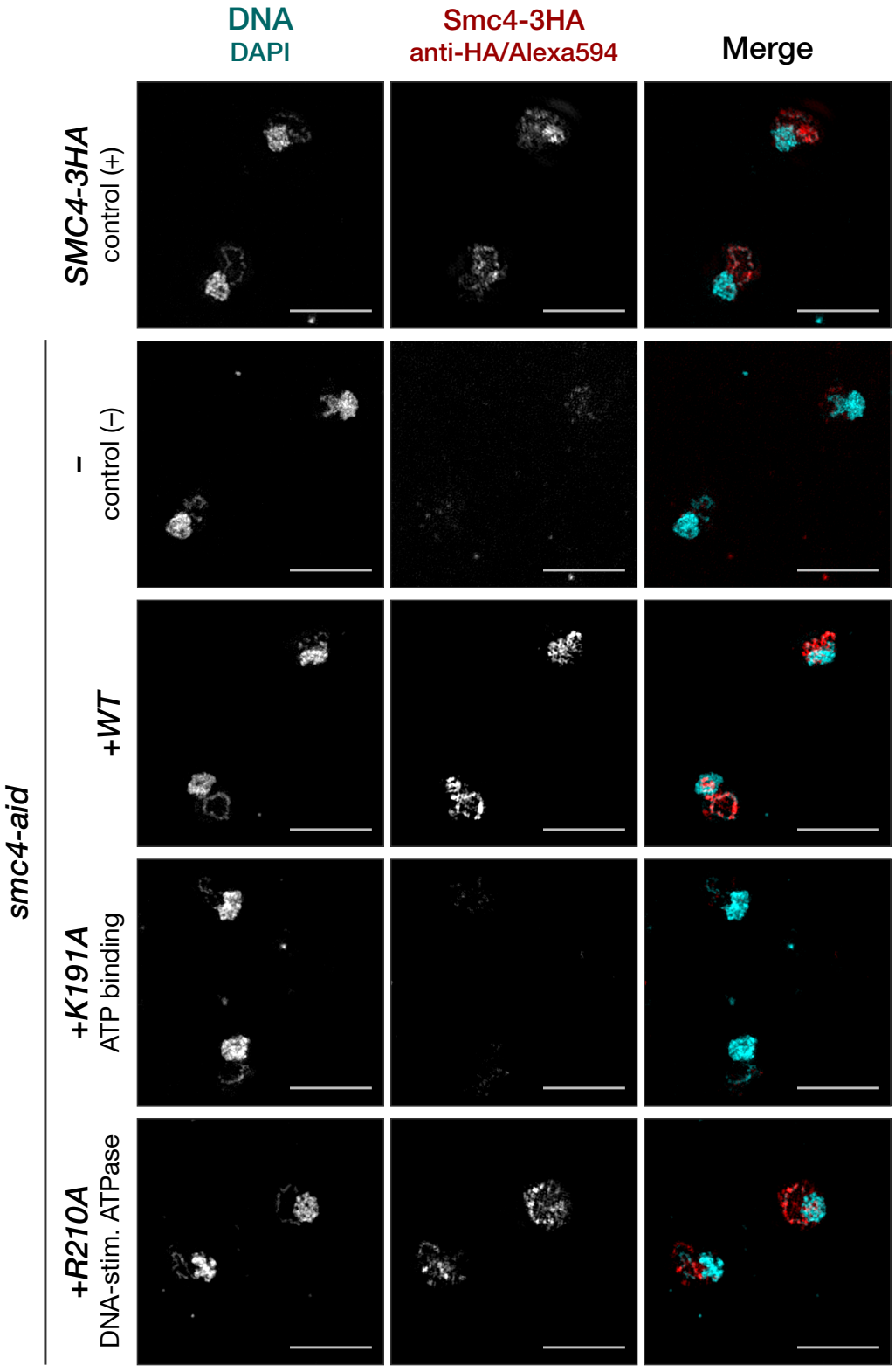

(a) Chromosome spreads, control, *smc4-aid*, *+WT*, *+K191A*, *+R210A*; *continued overleaf*.

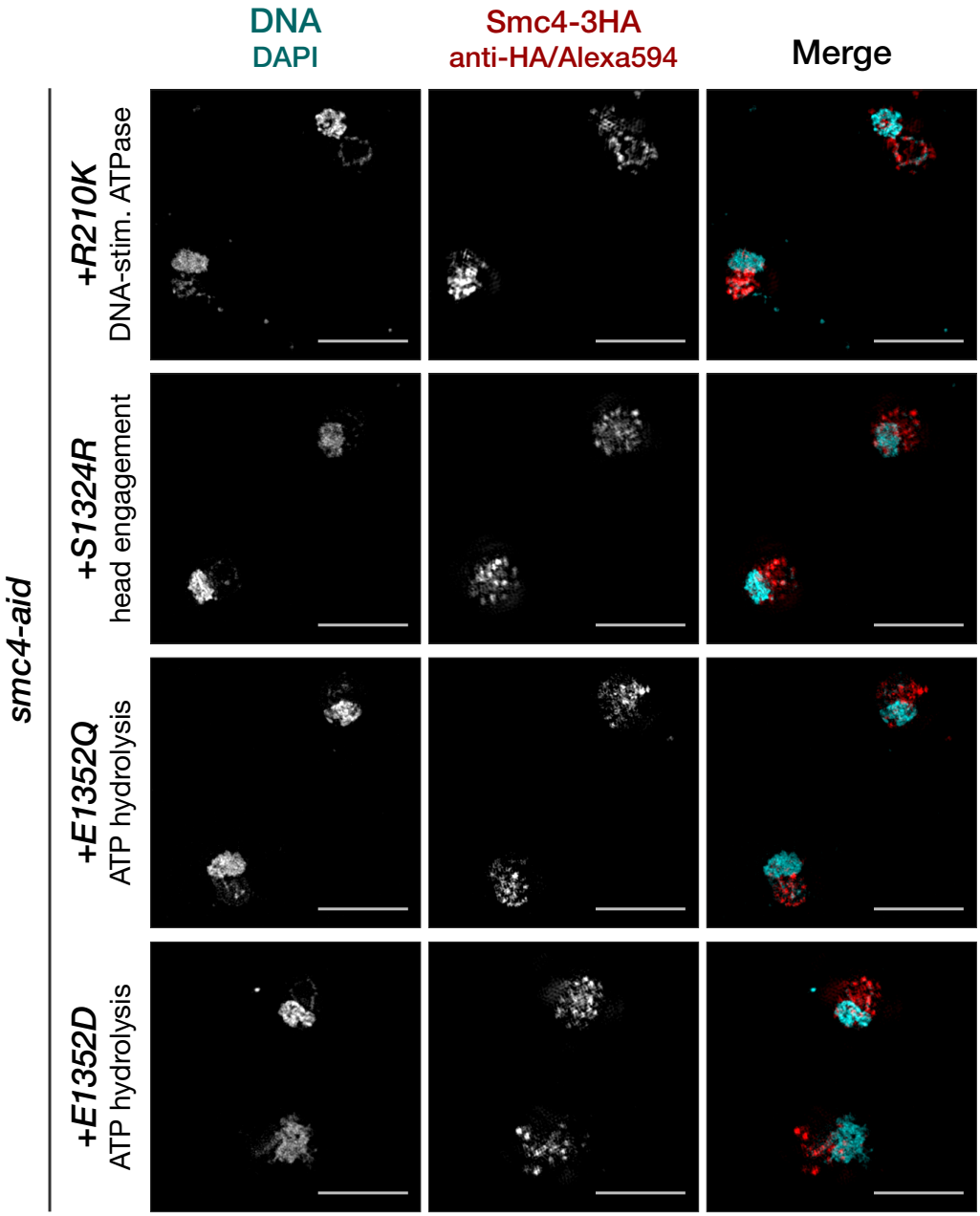

(b) Chromosome spreads, *+R210K*, *+S1324R*, *+E1352Q*, *+E1352D*.

Figure 6.10 Smc4 ATPase mutants, indirect immunofluorescence of chromosome spreads. Semi-spread preparations of metaphase chromosomes (Section 2.9) from the indicated strains were stained with rat anti-HA/Alexa594–anti-rat antibodies to detect Smc4-3HA, and the DNA-intercalating dye DAPI. The Walker A mutant Smc4^{K191A}, predicted to be defective in ATP binding, showed the least colocalisation with chromatin. Shown are maximum intensity projections of 17 x 0.125 µm images (total depth, 2 µm) acquired in structured illumination mode on an API OMX microscope. Scale bars represent 5 µm. *Strains, top to bottom: RT159, RT149, RT242, RT244, RT246, RT248, RT250a, RT252, RT254*.

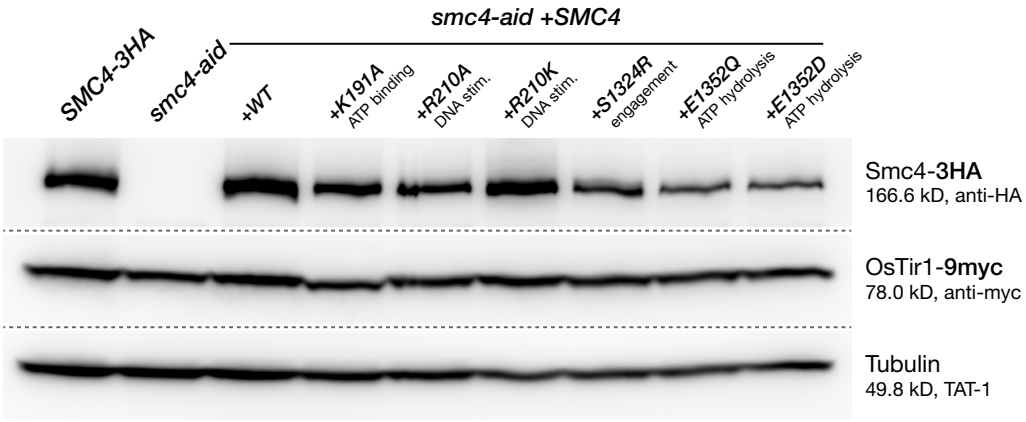

Figure 6.11 Smc4 ATPase mutants, western blotting. Expression of wild type or mutant Smc4 was examined in whole cell protein extracts (2.7.1) prepared in parallel with chromosome spreads. Immunoblots were probed for wild type/mutant Smc4-3HA (mouse anti-HA, 1:5000), and loading controls Tir1-9myc (mouse anti-myc, 1:1000) and α-tubulin (mouse anti–α-tubulin TAT-1, 1:10000). Chemiluminiscent detection was performed with HRP–anti-mouse antibody (1:5000). Exposure varies between proteins but not between lanes for a single protein. *Strains, left to right: RT159, RT149, RT242, RT244, RT246, RT248, RT250a, RT252, RT254*.

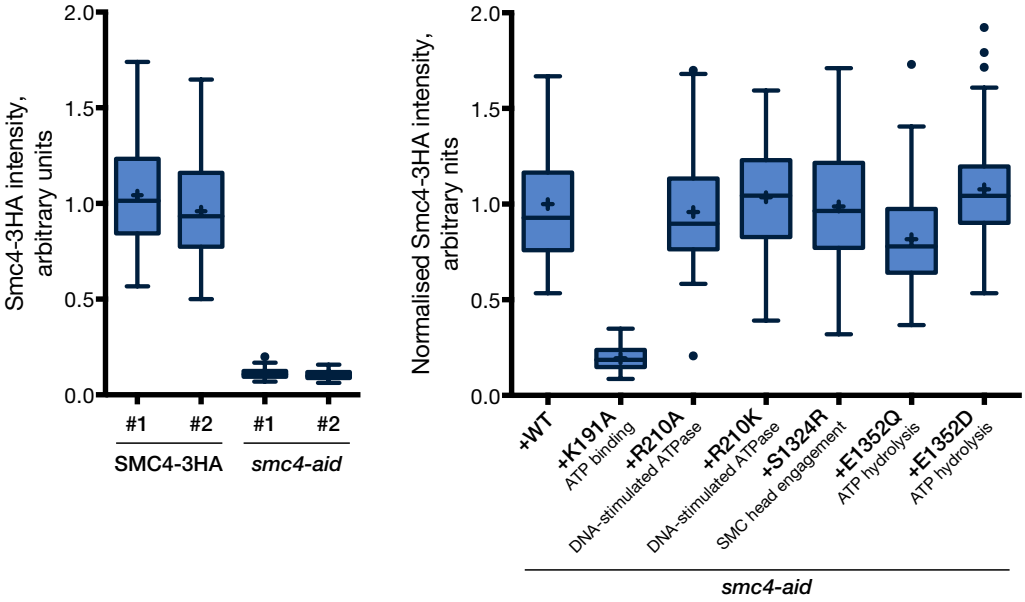

Figure 6.12 Smc4 ATPase mutants, quantification of chromosome speads. *Left*: Two technical replicates of the absolute Smc4-3HA staining intensity in positive (*SMC4-3HA*) and negative (*smc4-aid*) control strains showing the (low) extent of technical variation. *Right*: Smc4-3HA staining intensity in *smc4-aid* strains expressing wild type or mutant Smc4, normalised for expression in whole cell extracts. The ATP-binding mutant Smc4^{K191A}, which is expressed at normal levels in cell extracts, did not stably associate with chromatin. *Strains: RT159, RT149, RT242, RT244, RT246, RT248, RT250a, RT252, RT254*.

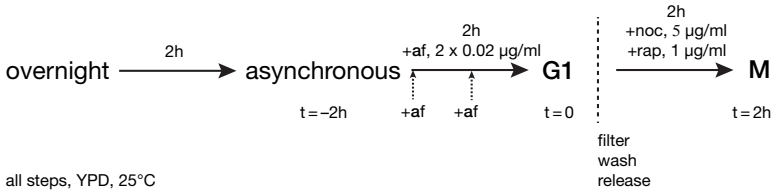

Figure 6.13 Chromosome condensation in Smc2 ATPase mutants, experimental scheme. Cultures were synchronised in G1 by addition of 2 x 0.02 µg/ml **a** factor, and released into a metaphase arrest by addition of 5 µg/ml nocodazole, in the presence of 1 µg/ml rapamycin. *Strains: RT65, SH110, RT67, RT69, RT71, RT73, RT75*.

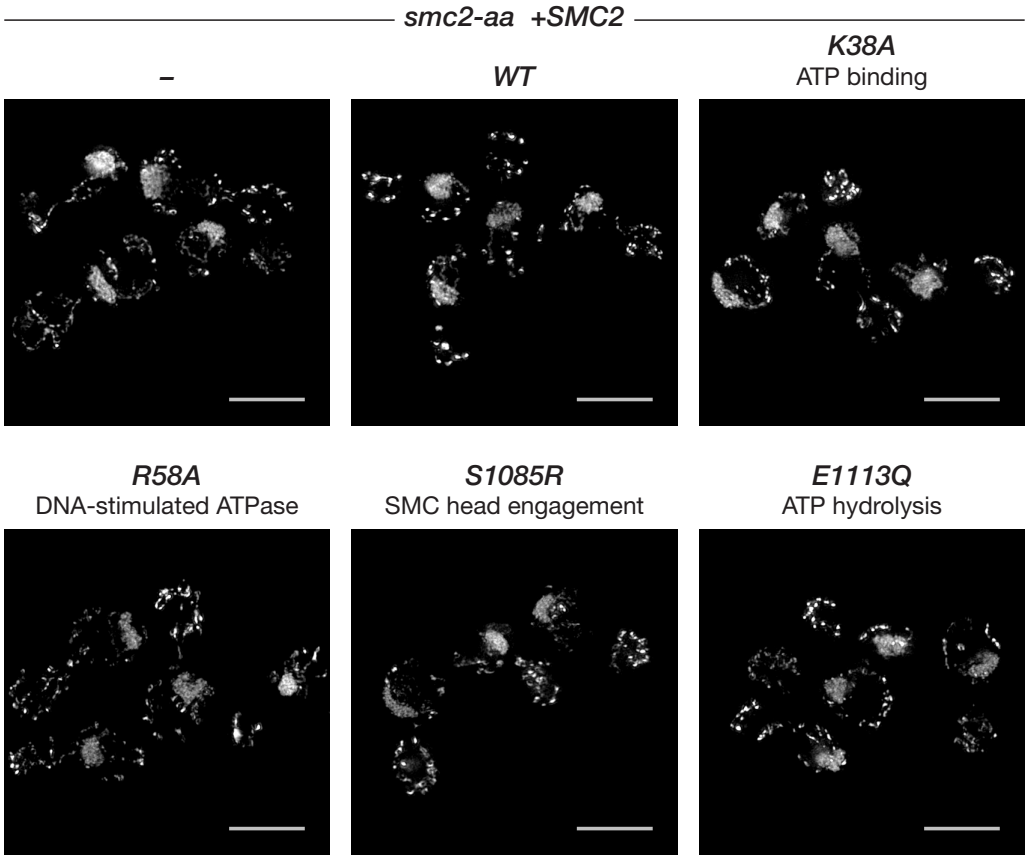

Figure 6.14 Chromosome condensation in Smc2 ATPase mutants, DAPI staining. Metaphase-arrested rapamycin-treated *smc2-aa* cells expressing wild type or ATPase mutants of *SMC2* stained with DAPI. Shown are maximum intensity projections of 33 x 0.125 µm (total depth, 4 µm) images acquired in structured illumination mode on an API OMX microscope. Scale bars represent 5 µm. *Strains, top left to bottom right: SH110, RT67, RT69, RT71, RT73, RT75*.

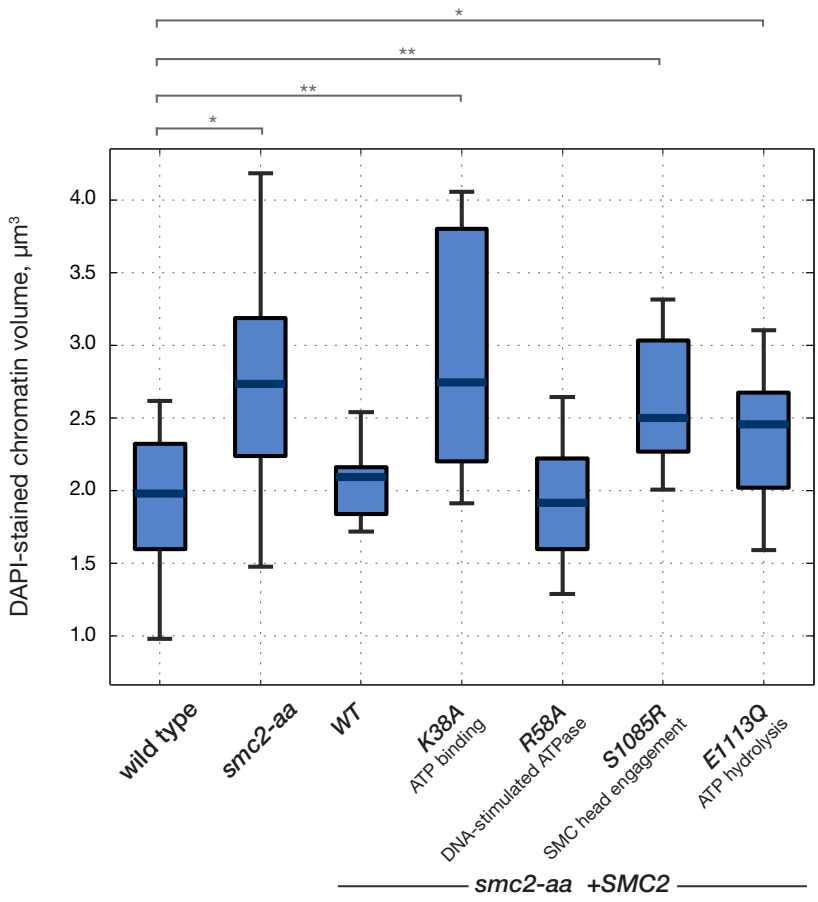

Figure 6.15 Chromosome condensation in Smc2 ATPase mutants, DNA volume. Box-and-whisker plots of the distributions of DAPI-stained chromatin volume in metaphase-arrested rapamycin-treated control and *smc2-aa* strains, ectopically expressing wild type or ATPase mutants of *SMC2*. The boxes span the 25-75 percentiles (the IQR) of the data, centred on the median; the whiskers extend to 1.5 x IQR either side of the upper and lower quartiles. Statistically significant differences in mean values are indicated by asterisks ($p < 0.05$). *Strains, left to right: RT65, SH110, RT67, RT69, RT71, RT73, RT75*.

room temperature) and 33 slices x 0.125 µm (total depth, 4 µm) were acquired on an API OMX microscope in conventional mode (Figure 6.17). As before, the *smc4-aid* strain showed a loss of loop-like organisation of the rDNA in metaphase, compared to the positive control. Quantification of rDNA volume revealed a statistically significant decompaction in the auxin-treated *smc4-aid* sample ($p < 0.01$; Figure 6.18). This condensation defect was completely rescued by expression of wild type Smc4 or the arginine finger mutant $Smc4^{R210K}$, partially by the arginine finger mutant $Smc4^{R210A}$, but not by Walker A ($Smc4^{K191A}$), C/signature motif ($Smc4^{S1324R}$) or Walker B ($Smc4^{E1352Q/D}$) mutants, showing that the ATPase activity of Smc4 was essential for rDNA condensation.

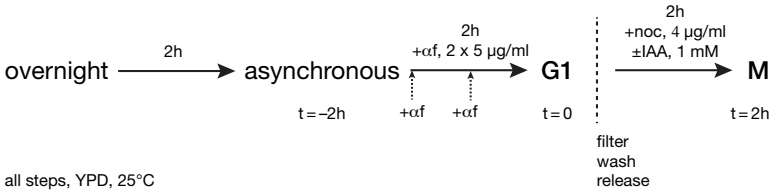

Figure 6.16 Chromosome condensation in Smc4 ATPase mutants, experimental scheme. Cultures were synchronised in G1 by addition of 2 x 5 µg/ml α factor, and released into a metaphase arrest by addition of 4 µg/ml nocodazole, in the presence of 1 mM IAA/auxin. *Strains: RT280, RT178, RT280, RT284, RT286, RT288, RT290, RT292, RT294*.

6.5 Conclusion

Taken together, the results described in this chapter show that the ATPase activity of condensin is crucial for its function. ATPase mutants of *SMC2* and *SMC4* predicted to be defective in ATP binding, SMC head engagement or ATP hydrolysis are inviable (Section 6.1.2). In the case of *SMC2* but not *SMC4*, mutations in a conserved arginine finger reaching into the nucleotide binding pocket, predicted to abolish the DNA-stimulated ATPase activity of the SMC catalytic domain, are inviable. The inviability of the SMC ATPase mutants is not due to altered levels of the ectopically expressed proteins (Section 6.1.1), or defects in their incorporation into complexes (Section 6.2). Instead, the SMC ATPase mutants exhibit altered DNA binding properties (Section 6.3), with the ATP binding mutant showing impairment of chromatin association. The chromatin binding properties of yeast Smc4 ATPase mutants characterised here are largely consistent with those of analogous chicken Smc2 point mutants, where ATP binding but not hydrolysis was reported to be essential for condensin localisation to chromosomes (Hudson et al., 2008). In addition, chromatin binding properties of condensin appear to

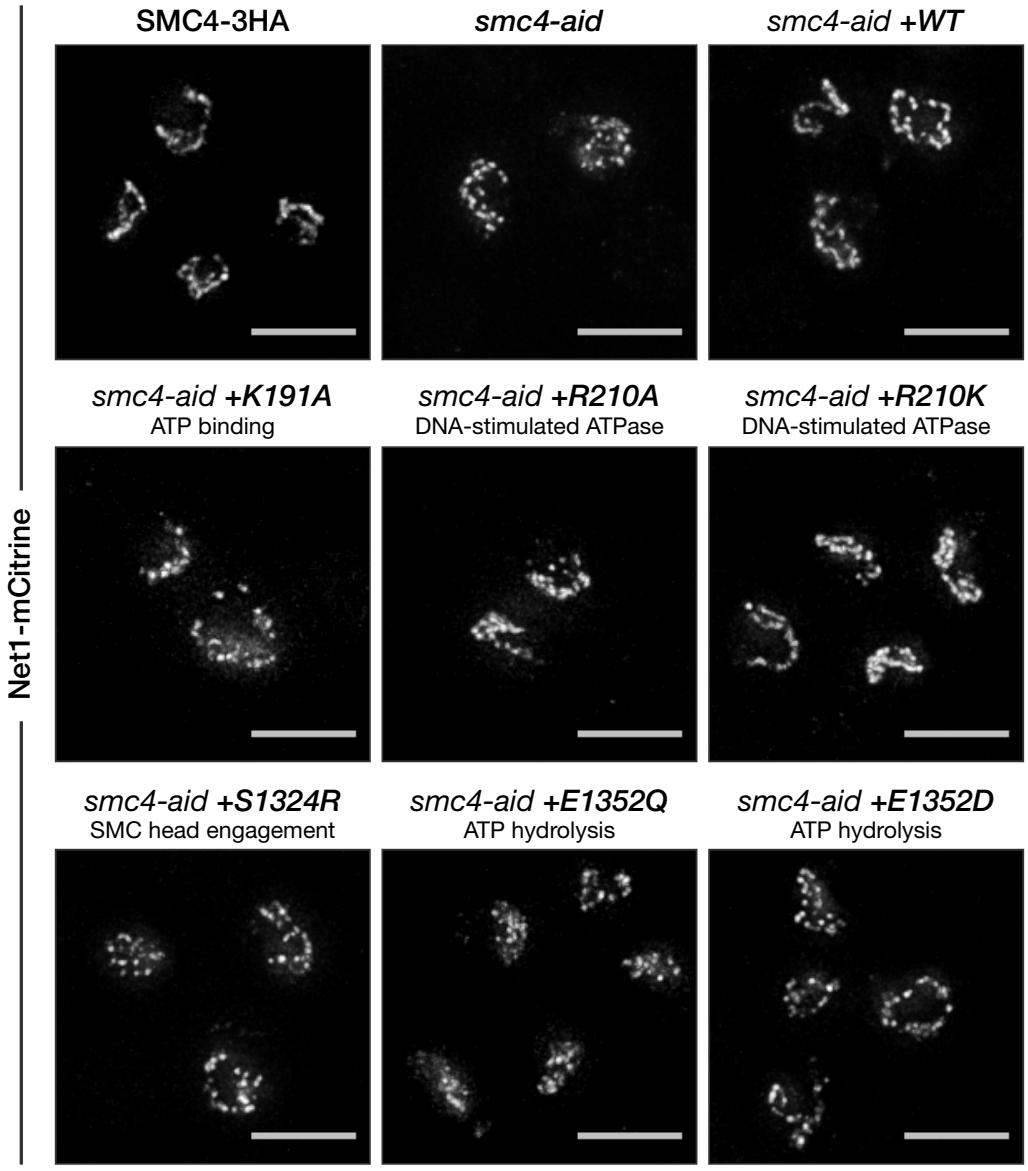

Figure 6.17 rDNA condensation in Smc4 ATPase mutants, Net1-mCitrine. Metaphase-arrested auxin-treated *smc4-aid* cells expressing wild type or ATPase mutants of *SMC4* and the rDNA label Net1-mCitrine. Shown are maximum intensity projections of 33 x 0.125 µm (total depth, 4 µm) images acquired in conventional mode on an API OMX microscope. Note the loss of metaphase rDNA loop organisation in the *smc4-aid* and ATPase mutant strains. Scale bars represent 5 µm. *Strains (top left to bottom right): RT280, RT178, RT280, RT284, RT286, RT288, RT290, RT292, RT294*.

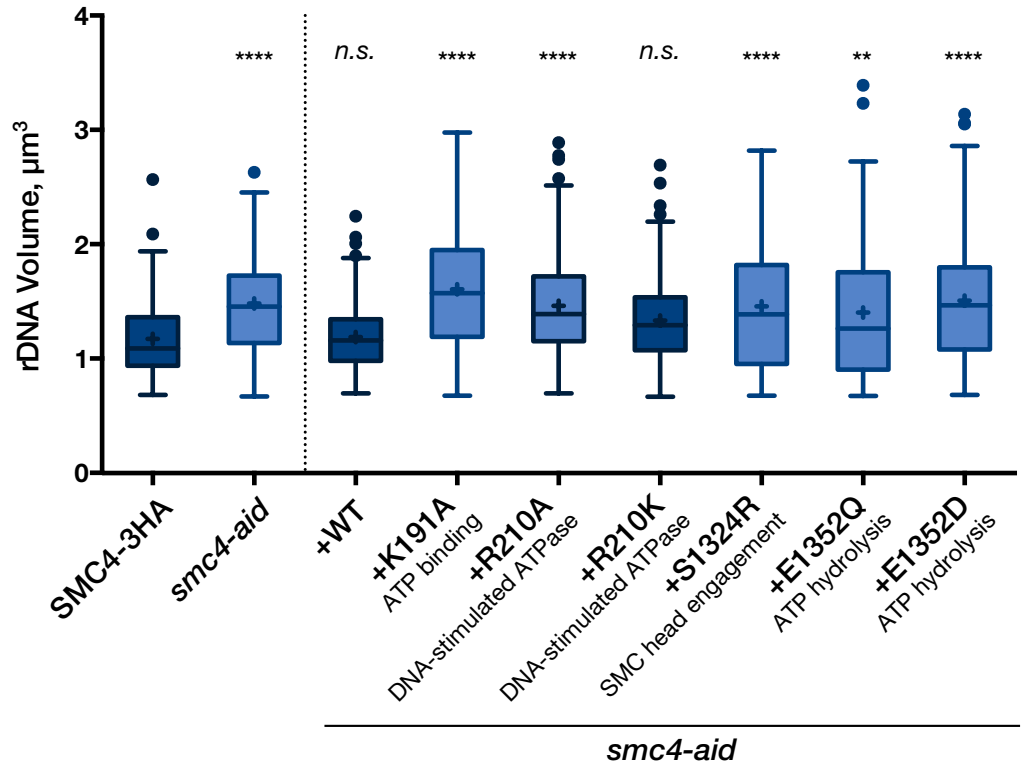

Figure 6.18 Condensation in Smc4 ATPase mutants, rDNA volume. Box-and-whisker plots of the distributions of Net1-mCitrine–demarcated rDNA volume in metaphase-arrested auxin-treated control and *smc4-aid* strains, ectopically expressing wild type or ATPase mutants of *SMC4* in addition to fluorescent-tagged *NET1*. The boxes span the 25-75 percentiles (the IQR) of the data, centred on the median; the whiskers extend to 1.5 x IQR either side of the upper and lower quartiles. Statistically significant differences in mean values are indicated by asterisks ($p < 0.01$); comparisons are to the positive control *SMC4-3HA*. *Strains (left to right): RT280, RT178, RT280, RT284, RT286, RT288, RT290, RT292, RT294*.

differ between G1 and metaphase, although the precise difference is difficult to assess by chromatin co-pelleting. Finally, mutations in the Smc2 and Smc4 ATPase domains compromise the formation of compact mitotic chromosomes (Section 6.4.1 and 6.4.2). Interestingly, the novel arginine finger mutant Smc2^{R58A} generated for the present work is inviable despite lacking a statistically significant condensation defect in metaphase, as assessed by DAPI-stained chromatin volume ($p < 0.05$). This suggests that the mutant may be compromised in later anaphase condensation of chromosomes or rDNA, with an attendant failure to provide structural rigidity to segregating chromosomes, or defective in chromosome resolution during segregation, investigations of which are of great interest for future experiments.

7 Discussion

The chromosomal condensin complex is now recognised as the major molecular effector of cellular chromosome condensation (Hirano et al., 1997; Freeman et al., 2000), and although details of the precise mechanism by which condensin promotes chromosome condensation remain to be worked out, the present work sheds some light on how the catalytic ATPase cycle at the SMC heads might be coupled to the mechanical cycle of condensin–chromatin interactions.

7.1 The condensin ATPase

The results described in Chapter 6 show that the ATPase activity of condensin is crucial for its function. In particular, ATP-binding, hydrolysis and SMC head engagement are essential for cell viability. Mutations of the conserved arginine finger reaching into the nucleotide binding pocket, interfering with DNA stimulation of ATPase activity, are lethal when introduced in Smc2 but not Smc4; in the latter case, arginine to alanine mutants show growth impairment compared to the wild type or to the subtler arginine to lysine mutants. Interestingly, the analogous arginine to alanine mutations of the cohesin Smc1 and Smc3 subunits are both viable, and have been shown to slow down, but not abolish, the DNA binding reaction (Lengronne et al., 2006). This suggests that careful regulation of the ATPase activity of condensin may be required for its proper function.

The chromatin binding defects observed in SMC ATPase mutants are consistent with a model in which ATP-induced conformational changes drive association of the complex with chromatin (Figure 7.1). In such a model, as has been proposed for *P. furiosus* Rad50 and SMC proteins, ATP binding to opposing Walker A and signature motifs enables SMC head engagement, while ATP hydrolysis allows their decoupling (Hopfner et al., 2000; Lammens et al., 2004). Thus ATP binding to SMC heads could ensure the closure of a ring-like configuration of condensin, the integrity of which has been shown to be necessary for its function, leading to stable association with chromatin (Section 6.3; Cuylen et al.,

2011; Hudson et al., 2008). On the other hand, ATP hydrolysis may move the SMC heads apart, allowing dissociation of the complex from chromatin. Indeed, this may require a transient loss of an SMC–kleisin interaction, as had been observed in *E. coli* MukBEF (Woo et al., 2009), to allow topological entry or exit of DNA from the condensin ring. Mutations that impair ATP hydrolysis could thus lock a subset of complexes in non-productive DNA linkages. Moreover, the fact that all aspects of condensin ATPase activity are required for chromosome condensation, along with the low intrinsic ATPase activity exhibited by SMC complexes, suggest that repeated cycles of such ATP-driven conformational changes may be necessary to compact chromatin (Section 6.4.1 & 6.4.2; Arumugam et al., 2006). Direct measurements of the chromatin binding dynamics of condensin ATPase mutants by approaches such as fluorescence recovery after photobleaching (FRAP), as well as analyses of the conformations of their SMC heads by fluorescence resonance energy transfer (FRET) or bimolecular fluorescence complementation (BiFC), are areas of great interest for forthcoming studies, and could provide *in vivo* confirmation for such a model of ATP-induced conformational changes driving chromosomal association of the condensin complex.

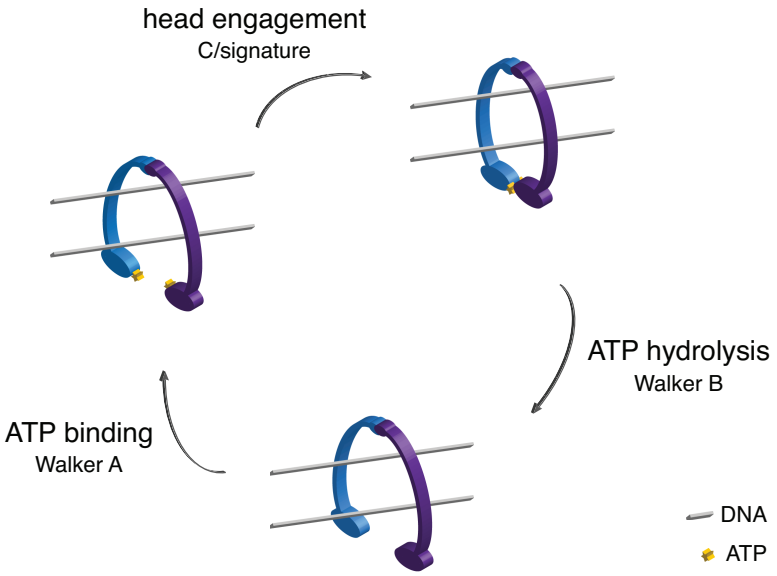

Figure 7.1 A model for condensin–chromatin association. Proposed model for condensin association with chromatin driven by ATP-induced conformational changes. ATP binding allows engagement of the SMC heads and stable association with chromatin. Conversely, ATP hydrolysis leads to SMC head disengagement, allowing dissociation of condensin from chromatin. For simplicity, only the SMC proteins are shown.

7.2 A model for mitotic chromosome condensation*

Condensin binds to specific sites along chromosomes, which likely involves the topological entrapment of chromatin. Such condensin–chromatin interactions could be translated into long-range chromosomal interactions that bring about condensation in two different ways. One scenario involves the sequential entrapment of two chromatin strands by a single condensin ring. A second is the dimerisation—or even multimerisation—of condensin complexes that have captured one strand of chromatin each (Figure 1.6). These two possibilities need not, of course, be mutually exclusive. In order to understand chromosome condensation, it is necessary to not only address the mechanism by which condensin associates with chromatin, but also to determine which pairs of DNA sequences along a chromosome condensin brings together, and how this pairing pattern changes as a function of cell cycle progression. Techniques such as chromosome conformation capture and its variants (Dekker et al., 2002) should be instructive in determining how condensin modulates intrachromosomal DNA interactions to drive mitotic chromosome condensation.

A model in which condensin promotes chromosome condensation by providing a meshwork of interactions between distant DNA sequences on the same chromosome is attractive for a number of reasons. Firstly, the biophysical properties of a mitotic vertebrate chromosome, as measured by mechanical micromanipulation studies, suggest that chromosomes are a composite network of DNA, crosslinked by protein interactions (Poirier and Marko, 2002). In contrast to popular models, no evidence for a contiguous protein scaffold has been found in native chromosomes. It should be emphasised that while a localised axis-like enrichment of condensin has been observed in fixed chromosome preparations (Maeshima and Laemmli, 2003; Hudson et al., 2008), the imaging of fluorescent-tagged condensin in live cells does not support the notion of such a scaffold (Hirota et al., 2004; Gerlich et al., 2006).

A scaffold would not be required if a broad network of condensin-mediated interactions between its binding sites compacts the chromosome. Recent structural studies of human mitotic chromosomes are also consistent with this mode of condensin action. Cryo-electron microscopy (cryo-EM) and x-ray scattering on close-to-native frozen chromosomes failed to find evidence for a hierarchical

*N.B. This section is based, in part, on the following self-authored review: Thadani R, Uhlmann F, Heeger S (2012), Condensin, chromatin crossbarring and chromosome condensation, *Curr Biol* **22**(23): R1012.

chromosome folding pattern of the kind portrayed in most molecular biology textbooks (Nishino et al., 2012). Instead of ordered structures, chromosomes appear to consist of a 'nucleosome melt', and it is arguable that a network of DNA interactions between condensin binding sites would be ideally suited to constrain the expansion of such a melt. Evidence from three dimensional imaging of lac operator arrays on metaphase chromosomes, in addition, shows that their folding pattern is irregular between cells and even between sister chromatids, as would be expected from a largely self-organising network of condensin binding site interactions (Strukov and Belmont, 2009). The modulation, by mitotic regulators, of the on– or off–rates of condensin at its binding sites, or of interactions between condensin complexes, could shift the compaction equilibrium from a loose packing in interphase towards a more condensed state in mitosis (Figure 7.2A). A prediction from this model is that interphase chromosome architecture might similarly be governed by condensin. Indeed, condensin appears to be required for constraining the expansion of rDNA in both interphase and mitosis, as its depletion leads to an increase in rDNA volume in several cell cycle phases (Section 5.3). Pictures of condensin in striking agreement with this model have been obtained by EM tomography of reconstituted *Xenopus* chromosomes (Figure 7.2B; König et al., 2007).

7.3 Future Work

More work is required to determine details of condensin action, and the exact nature of the interplay between its chromatin binding dynamics, and its various biochemical activities and posttranslational modifications. Investigations of the chromatin binding dynamics of condensin ATPase mutants, for instance by FRAP, could provide a link between the catalytic cycle of ATP binding and hydrolysis at the SMC heads on the one hand, and the mechanical cycle of condensin binding to and dissociating from chromatin on the other. These assays could be extended to condensin mutants defective in cell cycle modifications such as phosphodeficient Smc4, along with chromosome condensation measurements, to further link condensin dynamics and chromosome condensation to various cell cycle modifications such as CDK1 phosphorylation. An *in vitro* characterisation of the ATP binding and hydrolysis properties of the ATPase mutants of Smc2 and Smc4 is also of great interest, and could be attempted with SMC heads rather than holocomplexes in the first instance.

Future investigations towards uncovering mechanisms of chromosome condensation will, no doubt, lead to a better understanding of the fascinating problem of how cells store, retrieve and transmit information using DNA molecules several orders of magnitude longer than the spatial confines of a nucleus.

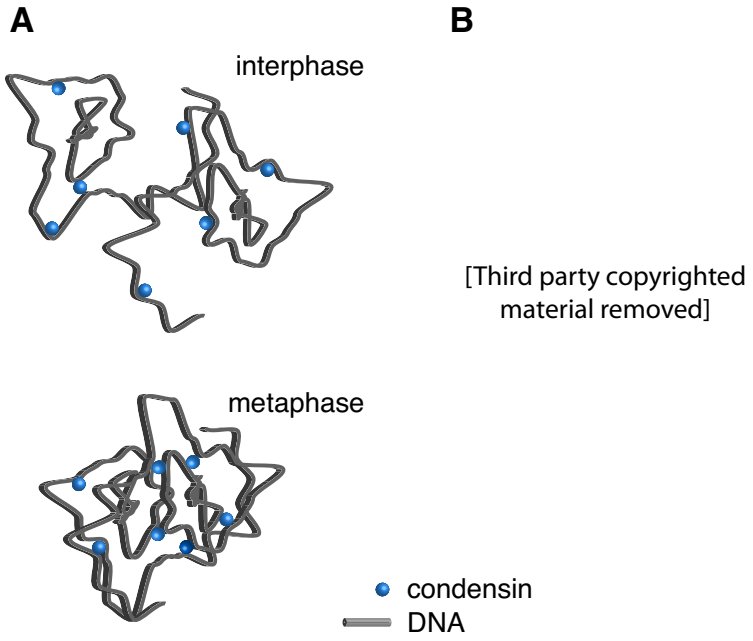

Figure 7.2 A model for condensin action. (A) *Left*: A meshwork of chromatin interactions bridged by condensin. In this model, condensin constrains the expansion of a 'nucleosome melt' by bridging distant DNA segments. The condensation reaction involves a change in the dynamic binding of condensin complexes to chromatin or each other. *Reproduced with permission from Thadani et al. (2012).* (B) *Right*: Reconstruction of the DNA path and condensin in reconstituted *Xenopus* chromosomes by EM tomography, showing condensin enriched at sites of chromatin intersections. *Figure from König et al. (2007) copyrighted by Springer removed.*

8 References

Abe, S., Nagasaka, K., Hirayama, Y., Kozuka-Hata, H., Oyama, M., Aoyagi, Y., Obuse, C. and Hirota, T. (2011). The initial phase of chromosome condensation requires Cdk1-mediated phosphorylation of the CAP-D3 subunit of condensin II. Genes Dev *25*, 863–74.

Arumugam, P., Gruber, S., Tanaka, K., Haering, C. H., Mechtler, K. and Nasmyth, K. (2003). ATP hydrolysis is required for cohesin's association with chromosomes. Curr Biol *13*, 1941–53.

Arumugam, P., Nishino, T., Haering, C. H., Gruber, S. and Nasmyth, K. (2006). Cohesin's ATPase activity is stimulated by the C-terminal Winged-Helix domain of its kleisin subunit. Curr Biol *16*, 1998–2008.

Bancaud, A., Huet, S., Daigle, N., Mozziconacci, J., Beaudouin, J. and Ellenberg, J. (2009). Molecular crowding affects diffusion and binding of nuclear proteins in heterochromatin and reveals the fractal organization of chromatin. EMBO J *28*, 3785–98.

Bazile, F., St-Pierre, J. and D'Amours, D. (2010). Three-step model for condensin activation during mitotic chromosome condensation. Cell Cycle *9*, 3243–55.

Belshaw, P. J., Ho, S. N., Crabtree, G. R. and Schreiber, S. L. (1996). Controlling protein association and subcellular localization with a synthetic ligand that induces heterodimerization of proteins. Proc Natl Acad Sci USA *93*, 4604–7.

Bhalla, N., Biggins, S. and Murray, A. W. (2002). Mutation of YCS4, a budding yeast condensin subunit, affects mitotic and nonmitotic chromosome behavior. Molecular biology of the cell *13*, 632–45.

Bhat, M. A., Philp, A. V., Glover, D. M. and Bellen, H. J. (1996). Chromatid segregation at anaphase requires the barren product, a novel chromosome-associated protein that interacts with Topoisomerase II. Cell *87*, 1103–14.

Biggins, S., Bhalla, N., Chang, A., Smith, D. L. and Murray, A. W. (2001). Genes involved in sister chromatid separation and segregation in the budding yeast Saccharomyces cerevisiae. Genetics *159*, 453–70.

Booher, R. N., Deshaies, R. J. and Kirschner, M. W. (1993). Properties of Saccharomyces cerevisiae wee1 and its differential regulation of p34CDC28 in response to G1 and G2 cyclins. EMBO J *12*, 3417–26.

Börner, G. V., Kleckner, N. and Hunter, N. (2004). Crossover/noncrossover differentiation, synaptonemal complex formation, and regulatory surveillance at the leptotene/zygotene transition of meiosis. Cell *117*, 29–45.

Boveri, T. (1888). Zellstudien II: die Befruchtung und Teilung des Eies von Ascaris megalocephala. Jena Z Naturw *22*, 685–882.

Britton, R. A., Lin, D. C. and Grossman, A. D. (1998). Characterization of a prokaryotic SMC protein involved in chromosome partitioning. Genes Dev *12*, 1254–9.

Chan, A. C.-H., Borts, R. H. and Hoffmann, E. (2009). Temperature-dependent modulation of chromosome segregation in msh4 mutants of budding yeast. PLoS ONE *4*, e7284.

Chan, K.-L., Roig, M. B., Hu, B., Beckouët, F., Metson, J. and Nasmyth, K. (2012). Cohesin's DNA exit gate is distinct from its entrance gate and is regulated by acetylation. Cell *150*, 961–74.

Chen, D., Toone, W. M., Mata, J., Lyne, R., Burns, G., Kivinen, K., Brazma, A., Jones, N. and Bähler, J. (2003). Global transcriptional responses of fission yeast to environmental stress. Molecular biology of the cell *14*, 214–29.

Chen, J., Zheng, X. F., Brown, E. J. and Schreiber, S. L. (1995). Identification of an 11-kDa FKBP12-rapamycin-binding domain within the 289-kDa FKBP12-rapamycin-associated protein and characterization of a critical serine residue. Proc Natl Acad Sci USA *92*, 4947–51.

Collette, K. S., Petty, E. L., Golenberg, N., Bembenek, J. N. and Csankovszki, G. (2011). Different roles for Aurora B in condensin targeting during mitosis and meiosis. Journal of cell science *124*, 3684–94.

Cui, Y., Petrushenko, Z. M. and Rybenkov, V. V. (2008). MukB acts as a macromolecular clamp in DNA condensation. Nat Struct Mol Biol *15*, 411–8.

Cuylen, S., Metz, J. and Haering, C. H. (2011). Condensin structures chromosomal DNA through topological links. Nature structural & molecular biology *18*, 894–901.

Cuylen, S., Metz, J., Hruby, A. and Haering, C. H. (2013). Entrapment of Chromosomes by Condensin Rings Prevents Their Breakage during Cytokinesis. Dev Cell *27*, 469–78.

D'Ambrosio, C., Kelly, G., Shirahige, K. and Uhlmann, F. (2008a). Condensin-dependent rDNA decatenation introduces a temporal pattern to chromosome segregation. Curr Biol *18*, 1084–9.

D'Ambrosio, C., Schmidt, C. K., Katou, Y., Kelly, G., Itoh, T., Shirahige, K. and Uhlmann, F. (2008b). Identification of cis-acting sites for condensin loading onto budding yeast chromosomes. Genes Dev *22*, 2215–27.

D'Amours, D., Stegmeier, F. and Amon, A. (2004). Cdc14 and condensin control the dissolution of cohesin-independent chromosome linkages at repeated DNA. Cell *117*, 455–69.

Dekker, J., Rippe, K., Dekker, M. and Kleckner, N. (2002). Capturing chromosome conformation. Science *295*, 1306–11.

Farkas, V., Kovarík, J., Kosinová, A. and Bauer, S. (1974). Autoradiographic study of mannan incorporation into the growing cell walls of Saccharomyces cerevisiae. J Bacteriol *117*, 265–9.

Felsenstein, J. (1981). Evolutionary trees from DNA sequences: a maximum likelihood approach. J Mol Evol *17*, 368–76.

Fennell-Fezzie, R., Gradia, S. D., Akey, D. and Berger, J. M. (2005). The MukF subunit of Escherichia coli condensin: architecture and functional relationship to kleisins. EMBO J *24*, 1921–30.

Fitch, I., Dahmann, C., Surana, U., Amon, A., Nasmyth, K., Goetsch, L., Byers, B. and Futcher, B. (1992). Characterization of four B-type cyclin genes of the budding yeast Saccharomyces cerevisiae. Mol Biol Cell *3*, 805–18.

Flemming, W. (1882). Zellsubstanz, Kern und Zelltheilung. FCW Vogel, Leipzig.

Freeman, L., Aragon-Alcaide, L. and Strunnikov, A. (2000). The condensin complex governs chromosome condensation and mitotic transmission of rDNA. J Cell Biol *149*, 811–24.

Fuentes-Perez, M. E., Gwynn, E. J., Dillingham, M. S. and Moreno-Herrero, F. (2012). Using DNA as a fiducial marker to study SMC complex interactions with the atomic force microscope. Biophys J *102*, 839–48.

Gasch, A. P., Spellman, P. T., Kao, C. M., Carmel-Harel, O., Eisen, M. B., Storz, G., Botstein, D. and Brown, P. O. (2000). Genomic expression programs in the response of yeast cells to environmental changes. Molecular biology of the cell *11*, 4241–57.

George, C. M., Bozler, J., Nguyen, H. Q. and Bosco, G. (2014). Condensins are Required for Maintenance of Nuclear Architecture. Cells *3*, 865–82.

Gerlich, D., Hirota, T., Koch, B., Peters, J.-M. and Ellenberg, J. (2006). Condensin I stabilizes chromosomes mechanically through a dynamic interaction in live cells. Curr Biol *16*, 333–44.

Giet, R. and Glover, D. M. (2001). Drosophila aurora B kinase is required for histone H3 phosphorylation and condensin recruitment during chromosome condensation and to organize the central spindle during cytokinesis. J Cell Biol *152*, 669–82.

Gietz, R. D. and Schiestl, R. H. (2007). High-efficiency yeast transformation using the LiAc/SS carrier DNA/PEG method. Nat Protoc *2*, 31–4.

Gosling, K. M., Makaroff, L. E., Theodoratos, A., Kim, Y.-H., Whittle, B., Rui, L., Wu, H., Hong, N. A., Kennedy, G. C., Fritz, J.-A., Yates, A. L., Goodnow, C. C. and Fahrer, A. M. (2007). A mutation in a chromosome condensin II subunit, kleisin beta, specifically disrupts T cell development. Proc Natl Acad Sci USA *104*, 12445–50.

Gould, K. L. and Nurse, P. (1989). Tyrosine phosphorylation of the fission yeast cdc2+ protein kinase regulates entry into mitosis. Nature *342*, 39–45.

Green, L. C., Kalitsis, P., Chang, T. M., Cipetic, M., Kim, J. H., Marshall, O., Turnbull, L., Whitchurch, C. B., Vagnarelli, P., Samejima, K., Earnshaw, W. C., Choo, K. H. A. and Hudson, D. F. (2012). Contrasting roles of condensin I and condensin II in mitotic chromosome formation. Journal of cell science *125*, 1591–604.

Griesbeck, O., Baird, G. S., Campbell, R. E., Zacharias, D. A. and Tsien, R. Y. (2001). Reducing the environmental sensitivity of yellow fluorescent protein. Mechanism and applications. The Journal of biological chemistry *276*, 29188–94.

Griese, J. J. and Hopfner, K.-P. (2011). Structure and DNA-binding activity of the Pyrococcus furiosus SMC protein hinge domain. Proteins *79*, 558–68.

Grote, A., Hiller, K., Scheer, M., Münch, R., Nörtemann, B., Hempel, D. C. and Jahn, D. (2005). JCat: a novel tool to adapt codon usage of a target gene to its potential expression host. Nucleic Acids Res *33*, W526–31.

Gruber, S. and Errington, J. (2009). Recruitment of condensin to replication origin regions by ParB/SpoOJ promotes chromosome segregation in B. subtilis. Cell *137*, 685–96.

Guacci, V., Koshland, D. and Strunnikov, A. (1997). A direct link between sister chromatid cohesion and chromosome condensation revealed through the analysis of MCD1 in S. cerevisiae. Cell *91*, 47–57.

Gustafsson, M. G. (2000). Surpassing the lateral resolution limit by a factor of two using structured illumination microscopy. J Microsc *198*, 82–7.

Gustafsson, M. G. L., Shao, L., Carlton, P. M., Wang, C. J. R., Golubovskaya, I. N., Cande, W. Z., Agard, D. A. and Sedat, J. W. (2008). Three-dimensional resolution doubling in wide-field fluorescence microscopy by structured illumination. Biophys J *94*, 4957–70.

Haering, C. H., Farcas, A.-M., Arumugam, P., Metson, J. and Nasmyth, K. (2008). The cohesin ring concatenates sister DNA molecules. Nature *454*, 297–301.

Haeusler, R. A., Pratt-Hyatt, M., Good, P. D., Gipson, T. A. and Engelke, D. R. (2008). Clustering of yeast tRNA genes is mediated by specific association of condensin with tRNA gene transcription complexes. Genes Dev *22*, 2204–14.

Hagstrom, K. A., Holmes, V. F., Cozzarelli, N. R. and Meyer, B. J. (2002). C. elegans condensin promotes mitotic chromosome architecture, centromere organization, and sister chromatid segregation during mitosis and meiosis. Genes Dev *16*, 729–42.

Hartl, T. A., Smith, H. F. and Bosco, G. (2008). Chromosome alignment and transvection are antagonized by condensin II. Science *322*, 1384–7.

Haruki, H., Nishikawa, J. and Laemmli, U. K. (2008). The anchor-away technique: rapid, conditional establishment of yeast mutant phenotypes. Mol Cell *31*, 925–32.

Hayama, R. and Marians, K. J. (2010). Physical and functional interaction between the condensin MukB and the decatenase topoisomerase IV in Escherichia coli. Proc Natl Acad Sci USA *107*, 18826–31.

Hegemann, B., Hutchins, J. R. A., Hudecz, O., Novatchkova, M., Rameseder, J., Sykora, M. M., Liu, S., Mazanek, M., Lénárt, P., Hériché, J.-K., Poser, I., Kraut, N., Hyman, A. A., Yaffe, M. B., Mechtler, K. and Peters, J.-M. (2011). Systematic phosphorylation analysis of human mitotic protein complexes. Sci Signal *4*, rs12.

Heitman, J., Movva, N. R. and Hall, M. N. (1991). Targets for cell cycle arrest by the immunosuppressant rapamycin in yeast. Science *253*, 905–9.

Hirano, M. and Hirano, T. (2006). Opening closed arms: long-distance activation of SMC ATPase by hinge-DNA interactions. Mol Cell *21*, 175–86.

Hirano, T. (2012). Condensins: universal organizers of chromosomes with diverse functions. Genes Dev *26*, 1659–1678.

Hirano, T., Kobayashi, R. and Hirano, M. (1997). Condensins, chromosome condensation protein complexes containing XCAP-C, XCAP-E and a Xenopus homolog of the Drosophila Barren protein. Cell *89*, 511–21.

Hirano, T. and Mitchison, T. J. (1994). A heterodimeric coiled-coil protein required for mitotic chromosome condensation in vitro. Cell *79*, 449–58.

Hirota, T., Gerlich, D., Koch, B., Ellenberg, J. and Peters, J.-M. (2004). Distinct functions of condensin I and II in mitotic chromosome assembly. Journal of cell science *117*, 6435–45.

Holland, A. J., Fachinetti, D., Han, J. S. and Cleveland, D. W. (2012). Inducible, reversible system for the rapid and complete degradation of proteins in mammalian cells. Proc Natl Acad Sci USA *109*, E3350–7.

Hopfner, K. P., Karcher, A., Shin, D. S., Craig, L., Arthur, L. M., Carney, J. P. and Tainer, J. A. (2000). Structural biology of Rad50 ATPase: ATP-driven conformational control in DNA double-strand break repair and the ABC-ATPase superfamily. Cell *101*, 789–800.

Hoyt, M. A., Totis, L. and Roberts, B. T. (1991). S. cerevisiae genes required for cell cycle arrest in response to loss of microtubule function. Cell *66*, 507–17.

Hu, B., Itoh, T., Mishra, A., Katoh, Y., Chan, K.-L., Upcher, W., Godlee, C., Roig, M. B., Shirahige, K. and Nasmyth, K. (2011). ATP hydrolysis is required for relocating cohesin from sites occupied by its Scc2/4 loading complex. Curr Biol *21*, 12–24.

Hudson, D. F., Ohta, S., Freisinger, T., Macisaac, F., Sennels, L., Alves, F., Lai, F., Kerr, A., Rappsilber, J. and Earnshaw, W. C. (2008). Molecular and genetic analysis of condensin function in vertebrate cells. Mol Biol Cell *19*, 3070–9.

Jans, J., Gladden, J. M., Ralston, E. J., Pickle, C. S., Michel, A. H., Pferdehirt, R. R., Eisen, M. B. and Meyer, B. J. (2009). A condensin-like dosage compensation complex acts at a distance to control expression throughout the genome. Genes Dev *23*, 602–18.

Johnson, R. T. and Rao, P. N. (1970). Mammalian cell fusion: induction of premature chromosome condensation in interphase nuclei. Nature *226*, 717–22.

Johzuka, K. and Horiuchi, T. (2009). The cis element and factors required for condensin recruitment to chromosomes. Mol Cell *34*, 26–35.

Johzuka, K., Terasawa, M., Ogawa, H., Ogawa, T. and Horiuchi, T. (2006). Condensin loaded onto the replication fork barrier site in the rRNA gene repeats during S phase in a FOB1-dependent fashion to prevent contraction of a long repetitive array in Saccharomyces cerevisiae. Mol Cell Biol *26*, 2226–36.

Jones, D. T., Taylor, W. R. and Thornton, J. M. (1992). The rapid generation of mutation data matrices from protein sequences. Comput Appl Biosci *8*, 275–82.

Kagami, Y., Nihira, K., Wada, S., Ono, M., Honda, M. and Yoshida, K. (2014). Mps1 phosphorylation of condensin II controls chromosome condensation at the onset of mitosis. J Cell Biol *205*, 781–90.

Kaitna, S., Pasierbek, P., Jantsch, M., Loidl, J. and Glotzer, M. (2002). The aurora B kinase AIR-2 regulates kinetochores during mitosis and is required for separation of homologous Chromosomes during meiosis. Curr Biol *12*, 798–812.

Kao, L., Wang, Y.-T., Chen, Y.-C., Tseng, S.-F., Jhang, J.-C., Chen, Y.-J. and Teng, S.-C. (2014). Global analysis of cdc14 dephosphorylation sites reveals essential regulatory role in mitosis and cytokinesis. Mol Cell Proteomics *13*, 594–605.

Kelley, L. A. and Sternberg, M. J. E. (2009). Protein structure prediction on the Web: a case study using the Phyre server. Nat Protoc *4*, 363–71.

Kim, H.-S., Vanoosthuyse, V., Fillingham, J., Roguev, A., Watt, S., Kislinger, T., Treyer, A., Carpenter, L. R., Bennett, C. S., Emili, A., Greenblatt, J. F., Hardwick, K. G., Krogan, N. J., Bähler, J. and Keogh, M.-C. (2009). An acetylated form of histone H2A.Z regulates chromosome architecture in Schizosaccharomyces pombe. Nature structural & molecular biology *16*, 1286–93.

Kimura, K., Hirano, M., Kobayashi, R. and Hirano, T. (1998). Phosphorylation and activation of 13S condensin by Cdc2 in vitro. Science *282*, 487–90.

Kimura, K. and Hirano, T. (1997). ATP-dependent positive supercoiling of DNA by 13S condensin: a biochemical implication for chromosome condensation. Cell *90*, 625–34.

Kimura, K. and Hirano, T. (2000). Dual roles of the 11S regulatory subcomplex in condensin functions. Proc Natl Acad Sci USA *97*, 11972–7.

Kimura, K., Rybenkov, V. V., Crisona, N. J., Hirano, T. and Cozzarelli, N. R. (1999). 13S condensin actively reconfigures DNA by introducing global positive writhe: implications for chromosome condensation. Cell *98*, 239–48.

Koç, A., Wheeler, L. J., Mathews, C. K. and Merrill, G. F. (2004). Hydroxyurea arrests DNA replication by a mechanism that preserves basal dNTP pools. J Biol Chem *279*, 223–30.

König, P., Braunfeld, M. B., Sedat, J. W. and Agard, D. A. (2007). The three-dimensional structure of in vitro reconstituted Xenopus laevis chromosomes by EM tomography. Chromosoma *116*, 349–72.

Ku, B., Lim, J.-H., Shin, H.-C., Shin, S.-Y. and Oh, B.-H. (2010). Crystal structure of the MukB hinge domain with coiled-coil stretches and its functional implications. Proteins *78*, 1483–90.

Kubota, T., Nishimura, K., Kanemaki, M. T. and Donaldson, A. D. (2013). The Elg1 replication factor C-like complex functions in PCNA unloading during DNA replication. Molecular Cell *50*, 273–80.

Lammens, A., Schele, A. and Hopfner, K.-P. (2004). Structural biochemistry of ATP-driven dimerization and DNA-stimulated activation of SMC ATPases. Curr Biol *14*, 1778–82.

Larkin, M. A., Blackshields, G., Brown, N. P., Chenna, R., McGettigan, P. A., McWilliam, H., Valentin, F., Wallace, I. M., Wilm, A., Lopez, R., Thompson, J. D., Gibson, T. J. and Higgins, D. G. (2007). Clustal W and Clustal X version 2.0. Bioinformatics *23*, 2947–8.

Lavoie, B. D., Hogan, E. and Koshland, D. (2002). In vivo dissection of the chromosome condensation machinery: reversibility of condensation distinguishes contributions of condensin and cohesin. J Cell Biol *156*, 805–15.

Lavoie, B. D., Hogan, E. and Koshland, D. (2004). In vivo requirements for rDNA chromosome condensation reveal two cell-cycle-regulated pathways for mitotic chromosome folding. Genes Dev *18*, 76–87.

Lavoie, B. D., Tuffo, K. M., Oh, S., Koshland, D. and Holm, C. (2000). Mitotic chromosome condensation requires Brn1p, the yeast homologue of Barren. Mol Biol Cell *11*, 1293–304.

Lénárt, P., Rabut, G., Daigle, N., Hand, A. R., Terasaki, M. and Ellenberg, J. (2003). Nuclear envelope breakdown in starfish oocytes proceeds by partial NPC disassembly followed by a rapidly spreading fenestration of nuclear membranes. J Cell Biol *160*, 1055–68.

Lengronne, A., McIntyre, J., Katou, Y., Kanoh, Y., Hopfner, K.-P., Shirahige, K. and Uhlmann, F. (2006). Establishment of sister chromatid cohesion at the S. cerevisiae replication fork. Mol Cell *23*, 787–99.

Letunic, I. and Bork, P. (2011). Interactive Tree Of Life v2: online annotation and display of phylogenetic trees made easy. Nucleic acids research *39*, W475–8.

Lew, D. J. and Reed, S. I. (1993). Morphogenesis in the yeast cell cycle: regulation by Cdc28 and cyclins. J Cell Biol *120*, 1305–20.

Lew, D. J. and Reed, S. I. (1995). A cell cycle checkpoint monitors cell morphogenesis in budding yeast. J Cell Biol *129*, 739–49.

Li, R. (1999). Bifurcation of the mitotic checkpoint pathway in budding yeast. Proc Natl Acad Sci USA *96*, 4989–94.

Li, R. and Murray, A. W. (1991). Feedback control of mitosis in budding yeast. Cell *66*, 519–31.

Li, Y., Stewart, N. K., Berger, A. J., Vos, S., Schoeffler, A. J., Berger, J. M., Chait, B. T. and Oakley, M. G. (2010). Escherichia coli condensin MukB stimulates topoisomerase IV activity by a direct physical interaction. Proc Natl Acad Sci USA *107*, 18832–7.

Liang, C. and Stillman, B. (1997). Persistent initiation of DNA replication and chromatin-bound MCM proteins during the cell cycle in cdc6 mutants. Genes Dev *11*, 3375–86.

Lipp, J. J., Hirota, T., Poser, I. and Peters, J.-M. (2007). Aurora B controls the association of condensin I but not condensin II with mitotic chromosomes. Journal of cell science *120*, 1245–55.

Liu, X. and Winey, M. (2012). The MPS1 family of protein kinases. Annu Rev Biochem *81*, 561–85.

Lohka, M. J. and Maller, J. L. (1985). Induction of nuclear envelope breakdown, chromosome condensation, and spindle formation in cell-free extracts. J Cell Biol *101*, 518–23.

MacCallum, D. E., Losada, A., Kobayashi, R. and Hirano, T. (2002). ISWI remodeling complexes in Xenopus egg extracts: identification as major chromosomal components that are regulated by INCENP-aurora B. Molecular biology of the cell *13*, 25–39.

Maddox, P. S., Portier, N., Desai, A. and Oegema, K. (2006). Molecular analysis of mitotic chromosome condensation using a quantitative time-resolved fluorescence microscopy assay. Proc Natl Acad Sci USA *103*, 15097–102.

Maeshima, K. and Laemmli, U. K. (2003). A two-step scaffolding model for mitotic chromosome assembly. Dev Cell *4*, 467–80.

Manukyan, A., Abraham, L., Dungrawala, H. and Schneider, B. L. (2011). Synchronization of yeast. Methods Mol Biol *761*, 173–200.

Mascarenhas, J., Soppa, J., Strunnikov, A. V. and Graumann, P. L. (2002). Cell cycle-dependent localization of two novel prokaryotic chromosome segregation and condensation proteins in Bacillus subtilis that interact with SMC protein. EMBO J *21*, 3108–18.

Matoba, K., Yamazoe, M., Mayanagi, K., Morikawa, K. and Hiraga, S. (2005). Comparison of MukB homodimer versus MukBEF complex molecular architectures by electron microscopy reveals a higher-order multimerization. Biochem Biophys Res Commun *333*, 694–702.

Mazumder, A., Roopa, T., Basu, A., Mahadevan, L. and Shivashankar, G. V. (2008). Dynamics of chromatin decondensation reveals the structural integrity of a mechanically prestressed nucleus. Biophys J *95*, 3028–35.

McElver, J. and Weber, S. (1992). FLAG N-terminal epitope overexpression of bacterial alkaline phosphatase and FLAG C-terminal epitope tagging by PCR one-step targeted integration. Yeast *8*, S627.

McIntyre, J., Muller, E. G. D., Weitzer, S., Snydsman, B. E., Davis, T. N. and Uhlmann, F. (2007). In vivo analysis of cohesin architecture using FRET in the budding yeast Saccharomyces cerevisiae. EMBO J *26*, 3783–93.

McMillan, J. N., Sia, R. A. and Lew, D. J. (1998). A morphogenesis checkpoint monitors the actin cytoskeleton in yeast. J Cell Biol *142*, 1487–99.

Mendenhall, M. D. and Hodge, A. E. (1998). Regulation of Cdc28 cyclin-dependent protein kinase activity during the cell cycle of the yeast Saccharomyces cerevisiae. Microbiol Mol Biol Rev *62*, 1191–243.

Minnen, A., Attaiech, L., Thon, M., Gruber, S. and Veening, J.-W. (2011). SMC is recruited to oriC by ParB and promotes chromosome segregation in Streptococcus pneumoniae. Mol Microbiol *81*, 676–88.

Mora-Bermúdez, F., Gerlich, D. and Ellenberg, J. (2007). Maximal chromosome compaction occurs by axial shortening in anaphase and depends on Aurora kinase. Nat Cell Biol *9*, 822–31.

Morawska, M. and Ulrich, H. D. (2013). An expanded tool kit for the auxin-inducible degron system in budding yeast. Yeast *30*, 341–51.

Morishita, J., Matsusaka, T., Goshima, G., Nakamura, T., Tatebe, H. and Yanagida, M. (2001). Bir1/Cut17 moving from chromosome to spindle upon the loss of cohesion is required for condensation, spindle elongation and repair. Genes Cells *6*, 743–63.

Mortimer, R. K. and Johnston, J. R. (1986). Genealogy of principal strains of the yeast genetic stock center. Genetics *113*, 35–43.

Nakazawa, N., Mehrotra, R., Ebe, M. and Yanagida, M. (2011). Condensin phosphorylated by the Aurora-B-like kinase Ark1 is continuously required until telophase in a mode distinct from Top2. Journal of cell science *124*, 1795–807.

Nakazawa, N., Nakamura, T., Kokubu, A., Ebe, M., Nagao, K. and Yanagida, M. (2008). Dissection of the essential steps for condensin accumulation at kinetochores and rDNAs during fission yeast mitosis. J Cell Biol *180*, 1115–31.

Neurohr, G., Naegeli, A., Titos, I., Theler, D., Greber, B., Díez, J., Gabaldón, T., Mendoza, M. and Barral, Y. (2011). A midzone-based ruler adjusts chromosome compaction to anaphase spindle length. Science *332*, 465–8.

Newport, J. and Spann, T. (1987). Disassembly of the nucleus in mitotic extracts: membrane vesicularization, lamin disassembly, and chromosome condensation are independent processes. Cell *48*, 219–30.

Niki, H., Jaffé, A., Imamura, R., Ogura, T. and Hiraga, S. (1991). The new gene mukB codes for a 177 kd protein with coiled-coil domains involved in chromosome partitioning of E. coli. EMBO J *10*, 183–93.

Nishimura, K., Fukagawa, T., Takisawa, H., Kakimoto, T. and Kanemaki, M. (2009). An auxin-based degron system for the rapid depletion of proteins in nonplant cells. Nat Methods *6*, 917–22.

Nishino, Y., Eltsov, M., Joti, Y., Ito, K., Takata, H., Takahashi, Y., Hihara, S., Frangakis, A. S., Imamoto, N., Ishikawa, T. and Maeshima, K. (2012). Human mitotic chromosomes consist predominantly of irregularly folded nucleosome fibres without a 30-nm chromatin structure. EMBO J *31*, 1644–53.

Nousiainen, M., Silljé, H. H. W., Sauer, G., Nigg, E. A. and Körner, R. (2006). Phosphoproteome analysis of the human mitotic spindle. Proc Natl Acad Sci USA *103*, 5391–6.

Nurse, P. and Thuriaux, P. (1980). Regulatory genes controlling mitosis in the fission yeast Schizosaccharomyces pombe. Genetics *96*, 627–37.

Nurse, P., Thuriaux, P. and Nasmyth, K. (1976). Genetic control of the cell division cycle in the fission yeast Schizosaccharomyces pombe. Mol Gen Genet *146*, 167–78.

Ohsumi, K., Yamazoe, M. and Hiraga, S. (2001). Different localization of SeqA-bound nascent DNA clusters and MukF-MukE-MukB complex in Escherichia coli cells. Mol Microbiol *40*, 835–45.

Ohta, S., Bukowski-Wills, J.-C., Sanchez-Pulido, L., de Lima Alves, F., Wood, L., Chen, Z. A., Platani, M., Fischer, L., Hudson, D. F., Ponting, C. P., Fukagawa, T., Earnshaw, W. C. and Rappsilber, J. (2010). The protein composition of mitotic chromosomes determined using multiclassifier combinatorial proteomics. Cell *142*, 810–21.

Oliveira, R. A., Heidmann, S. and Sunkel, C. E. (2007). Condensin I binds chromatin early in prophase and displays a highly dynamic association with Drosophila mitotic chromosomes. Chromosoma *116*, 259–74.

Onn, I., Aono, N., Hirano, M. and Hirano, T. (2007). Reconstitution and subunit geometry of human condensin complexes. EMBO J *26*, 1024–34.

Ono, T., Fang, Y., Spector, D. L. and Hirano, T. (2004). Spatial and temporal regulation of Condensins I and II in mitotic chromosome assembly in human cells. Molecular biology of the cell *15*, 3296–308.

Ono, T., Losada, A., Hirano, M., Myers, M. P., Neuwald, A. F. and Hirano, T. (2003). Differential contributions of condensin I and condensin II to mitotic chromosome architecture in vertebrate cells. Cell *115*, 109–21.

O'Reilly, N., Charbin, A., Lopez-Serra, L. and Uhlmann, F. (2012). Facile synthesis of budding yeast a-factor and its use to synchronize cells of □ mating type. Yeast *29*, 233–40.

Ouspenski, I. I., Cabello, O. A. and Brinkley, B. R. (2000). Chromosome condensation factor Brn1p is required for chromatid separation in mitosis. Molecular biology of the cell *11*, 1305–13.

Pagliuca, F. W., Collins, M. O., Lichawska, A., Zegerman, P., Choudhary, J. S. and Pines, J. (2011). Quantitative proteomics reveals the basis for the biochemical specificity of the cell-cycle machinery. Molecular Cell *43*, 406–17.

Pal, G., Paraz, M. T. Z. and Kellogg, D. R. (2008). Regulation of Mih1/Cdc25 by protein phosphatase 2A and casein kinase 1. J Cell Biol *180*, 931–45.

Paweletz, N. (2001). Walther Flemming: pioneer of mitosis research. Nat Rev Mol Cell Biol *2*, 72–5.

Pellegrino, S., Radzimanowski, J., de Sanctis, D., Erba, E. B., McSweeney, S. and Timmins, J. (2012). Structural and functional characterization of an SMC-like protein RecN: new insights into double-strand break repair. Structure *20*, 2076–89.

Pereira, G. and Schiebel, E. (2003). Separase regulates INCENP-Aurora B anaphase spindle function through Cdc14. Science *302*, 2120–4.

Petersen, J. and Hagan, I. M. (2003). S. pombe aurora kinase/survivin is required for chromosome condensation and the spindle checkpoint attachment response. Curr Biol *13*, 590–7.

Petes, T. D. (1979). Yeast ribosomal DNA genes are located on chromosome XII. Proc Natl Acad Sci USA *76*, 410–4.

Petrova, B., Dehler, S., Kruitwagen, T., Hériché, J.-K., Miura, K. and Haering, C. H. (2013). Quantitative analysis of chromosome condensation in fission yeast. Mol Cell Biol *33*, 984–98.

Petrushenko, Z. M., Cui, Y., She, W. and Rybenkov, V. V. (2010). Mechanics of DNA bridging by bacterial condensin MukBEF in vitro and in singulo. EMBO J *29*, 1126–35.

Petrushenko, Z. M., Lai, C.-H., Rai, R. and Rybenkov, V. V. (2006a). DNA reshaping by MukB. Right-handed knotting, left-handed supercoiling. The Journal of biological chemistry *281*, 4606–15.

Petrushenko, Z. M., Lai, C.-H. and Rybenkov, V. V. (2006b). Antagonistic interactions of kleisins and DNA with bacterial Condensin MukB. The Journal of biological chemistry *281*, 34208–17.

Petrushenko, Z. M., She, W. and Rybenkov, V. V. (2011). A new family of bacterial condensins. Mol Microbiol *81*, 881–96.

Piazza, I., Rutkowska, A., Ori, A., Walczak, M., Metz, J., Pelechano, V., Beck, M. and Haering, C. H. (2014). Association of condensin with chromosomes depends on DNA binding by its HEAT-repeat subunits. Nature structural & molecular biology *21*, 560–8.

Poirier, M. G. and Marko, J. F. (2002). Mitotic chromosomes are chromatin networks without a mechanically contiguous protein scaffold. Proc Natl Acad Sci USA *99*, 15393–7.

Queralt, E. and Uhlmann, F. (2008). Cdk-counteracting phosphatases unlock mitotic exit. Curr Opin Cell Biol *20*, 661–8.

Rancati, G. and Li, R. (2007). Polarized cell growth: double grip by CDK1. Curr Biol *17*, R600–3.

Renshaw, M. J., Ward, J. J., Kanemaki, M., Natsume, K., Nédélec, F. J. and Tanaka, T. U. (2010). Condensins promote chromosome recoiling during early anaphase to complete sister chromatid separation. Dev Cell *19*, 232–44.

Ribeiro, S. A., Gatlin, J. C., Dong, Y., Joglekar, A., Cameron, L., Hudson, D. F., Farr, C. J., McEwen, B. F., Salmon, E. D., Earnshaw, W. C. and Vagnarelli, P. (2009). Condensin regulates the stiffness of vertebrate centromeres. Molecular biology of the cell *20*, 2371–80.

Richardson, H., Lew, D. J., Henze, M., Sugimoto, K. and Reed, S. I. (1992). Cyclin-B homologs in Saccharomyces cerevisiae function in S phase and in G2. Genes Dev *6*, 2021–2034.

Ridler, T. W. and Calvard, S. (1978). Picture thresholding using an iterative selection method. IEEE Transactions on Systems, Man and Cybernetics *SMC-8*, 630–632.

Robinett, C. C., Straight, A., Li, G., Willhelm, C., Sudlow, G., Murray, A. and Belmont, A. S. (1996). In vivo localization of DNA sequences and visualization of large-scale chromatin organization using lac operator/repressor recognition. J Cell Biol *135*, 1685–700.

Saitoh, N., Goldberg, I. G., Wood, E. R. and Earnshaw, W. C. (1994). ScII: an abundant chromosome scaffold protein is a member of a family of putative ATPases with an unusual predicted tertiary structure. J Cell Biol *127*, 303–18.

Saka, Y., Sutani, T., Yamashita, Y., Saitoh, S., Takeuchi, M., Nakaseko, Y. and Yanagida, M. (1994). Fission yeast cut3 and cut14, members of a ubiquitous protein family, are required for chromosome condensation and segregation in mitosis. EMBO J *13*, 4938–52.

Schleiffer, A., Kaitna, S., Maurer-Stroh, S., Glotzer, M., Nasmyth, K. and Eisenhaber, F. (2003). Kleisins: a superfamily of bacterial and eukaryotic SMC protein partners. Molecular Cell *11*, 571–5.

Schmidt, C. K., Brookes, N. and Uhlmann, F. (2009). Conserved features of cohesin binding along fission yeast chromosomes. Genome Biol *10*, R52.

Schneider, C. A., Rasband, W. S. and Eliceiri, K. W. (2012). NIH Image to ImageJ: 25 years of image analysis. Nat Methods *9*, 671–5.

Seipold, S., Priller, F. C., Goldsmith, P., Harris, W. A., Baier, H. and Abdelilah-Seyfried, S. (2009). Non-SMC condensin I complex proteins control chromosome segregation and survival of proliferating cells in the zebrafish neural retina. BMC Dev Biol *9*, 40.

Sheff, M. A. and Thorn, K. S. (2004). Optimized cassettes for fluorescent protein tagging in Saccharomyces cerevisiae. Yeast *21*, 661–70.

Shintomi, K. and Hirano, T. (2011). The relative ratio of condensin I to II determines chromosome shapes. Genes Dev *25*, 1464–9.

Slater, M. L. (1973). Effect of reversible inhibition of deoxyribonucleic acid synthesis on the yeast cell cycle. J Bacteriol *113*, 263–70.

Sofueva, S., Yaffe, E., Chan, W.-C., Georgopoulou, D., Rudan, M. V., Mira-Bontenbal, H., Pollard, S. M., Schroth, G. P., Tanay, A. and Hadjur, S. (2013). Cohesin-mediated interactions organize chromosomal domain architecture. EMBO J *32*, 3119–29.

Soppa, J., Kobayashi, K., Noirot-Gros, M.-F., Oesterhelt, D., Ehrlich, S. D., Dervyn, E., Ogasawara, N. and Moriya, S. (2002). Discovery of two novel families of proteins that are proposed to interact with prokaryotic SMC proteins, and characterization of the Bacillus subtilis family members ScpA and ScpB. Mol Microbiol *45*, 59–71.

St-Pierre, J., Douziech, M., Bazile, F., Pascariu, M., Bonneil, E., Sauvé, V., Ratsima, H. and D'Amours, D. (2009). Polo kinase regulates mitotic chromosome condensation by hyperactivation of condensin DNA supercoiling activity. Mol Cell *34*, 416–26.

Stephens, A. D., Haase, J., Vicci, L., Taylor, R. M. and Bloom, K. (2011). Cohesin, condensin, and the intramolecular centromere loop together generate the mitotic chromatin spring. J Cell Biol *193*, 1167–80.

Straight, A. F., Shou, W., Dowd, G. J., Turck, C. W., Deshaies, R. J., Johnson, A. D. and Moazed, D. (1999). Net1, a Sir2-associated nucleolar protein required for rDNA silencing and nucleolar integrity. Cell *97*, 245–56.

Stray, J. E. and Lindsley, J. E. (2003). Biochemical analysis of the yeast condensin Smc2/4 complex: an ATPase that promotes knotting of circular DNA. J Biol Chem *278*, 26238–48.

Strick, T. R., Kawaguchi, T. and Hirano, T. (2004). Real-time detection of single-molecule DNA compaction by condensin I. Curr Biol *14*, 874–80.

Strukov, Y. G. and Belmont, A. S. (2009). Mitotic chromosome structure: reproducibility of folding and symmetry between sister chromatids. Biophys J *96*, 1617–28.

Strunnikov, A. V., Hogan, E. and Koshland, D. (1995). SMC2, a Saccharomyces cerevisiae gene essential for chromosome segregation and condensation, defines a subgroup within the SMC family. Genes Dev *9*, 587–99.

Sullivan, M., Higuchi, T., Katis, V. L. and Uhlmann, F. (2004). Cdc14 phosphatase induces rDNA condensation and resolves cohesin-independent cohesion during budding yeast anaphase. Cell *117*, 471–82.

Sullivan, N. L., Marquis, K. A. and Rudner, D. Z. (2009). Recruitment of SMC by ParB-parS organizes the origin region and promotes efficient chromosome segregation. Cell *137*, 697–707.

Surana, U., Robitsch, H., Price, C., Schuster, T., Fitch, I., Futcher, A. B. and Nasmyth, K. (1991). The role of CDC28 and cyclins during mitosis in the budding yeast S. cerevisiae. Cell *65*, 145–61.

Sutani, T., Yuasa, T., Tomonaga, T., Dohmae, N., Takio, K. and Yanagida, M. (1999). Fission yeast condensin complex: essential roles of non-SMC subunits for condensation and Cdc2 phosphorylation of Cut3/SMC4. Genes Dev *13*, 2271–83.

Tada, K., Susumu, H., Sakuno, T. and Watanabe, Y. (2011). Condensin association with histone H2A shapes mitotic chromosomes. Nature *474*, 477–83.

Takemoto, A., Kimura, K., Yanagisawa, J., Yokoyama, S. and Hanaoka, F. (2006). Negative regulation of condensin I by CK2-mediated phosphorylation. EMBO J *25*, 5339–48.

Takemoto, A., Maeshima, K., Ikehara, T., Yamaguchi, K., Murayama, A., Imamura, S., Imamoto, N., Yokoyama, S., Hirano, T., Watanabe, Y., Hanaoka, F., Yanagisawa, J. and Kimura, K. (2009). The chromosomal association of condensin II is regulated by a noncatalytic function of PP2A. Nature structural & molecular biology *16*, 1302–8.

Takemoto, A., Murayama, A., Katano, M., Urano, T., Furukawa, K., Yokoyama, S., Yanagisawa, J., Hanaoka, F. and Kimura, K. (2007). Analysis of the role of Aurora B on the chromosomal targeting of condensin I. Nucleic Acids Res *35*, 2403–12.

Thadani, R., Uhlmann, F. and Heeger, S. (2012). Condensin, chromatin crossbarring and chromosome condensation. Curr Biol *22*, R1012–21.

Uhlmann, F., Lottspeich, F. and Nasmyth, K. (1999). Sister-chromatid separation at anaphase onset is promoted by cleavage of the cohesin subunit Scc1. Nature *400*, 37–42.

Uhlmann, F. and Nasmyth, K. (1998). Cohesion between sister chromatids must be established during DNA replication. Curr Biol *8*, 1095–101.

van den Ent, F., Lockhart, A., Kendrick-Jones, J. and Löwe, J. (1999). Crystal structure of the N-terminal domain of MukB: a protein involved in chromosome partitioning. Structure *7*, 1181–7.

Vanoosthuyse, V., Legros, P., van der Sar, S. J. A., Yvert, G., Toda, K., Bihan, T. L., Watanabe, Y., Hardwick, K. and Bernard, P. (2014). CPF-associated phosphatase activity opposes condensin-mediated chromosome condensation. PLoS Genet *10*, e1004415.

Varela, E., Shimada, K., Laroche, T., Leroy, D. and Gasser, S. M. (2009). Lte1, Cdc14 and MEN-controlled Cdk inactivation in yeast coordinate rDNA decompaction with late telophase progression. EMBO J *28*, 1562–75.

Vas, A. C. J., Andrews, C. A., Matesky, K. K. and Clarke, D. J. (2007). In vivo analysis of chromosome condensation in Saccharomyces cerevisiae. Mol Biol Cell *18*, 557–68.

Verma, R., Annan, R. S., Huddleston, M. J., Carr, S. A., Reynard, G. and Deshaies, R. J. (1997). Phosphorylation of Sic1p by G1 Cdk required for its degradation and entry into S phase. Science *278*, 455–60.

Vjestica, A. and Oliferenko, S. (2012). Nuclear geometry: mitotic nucleus flares out when arrested. Curr Biol *22*, R489–91.

Wang, B.-D., Eyre, D., Basrai, M., Lichten, M. and Strunnikov, A. (2005). Condensin binding at distinct and specific chromosomal sites in the Saccharomyces cerevisiae genome. Mol Cell Biol *25*, 7216–25.

Watrin, E., Cubizolles, F., Osborne, H. B., Guellec, K. L. and Legagneux, V. (2003). Expression and functional dynamics of the XCAP-D2 condensin subunit in Xenopus laevis oocytes. The Journal of biological chemistry *278*, 25708–15.

Weitzer, S., Lehane, C. and Uhlmann, F. (2003). A model for ATP hydrolysis-dependent binding of cohesin to DNA. Curr Biol *13*, 1930–40.

Wilkins, B. J., Rall, N. A., Ostwal, Y., Kruitwagen, T., Hiragami-Hamada, K., Winkler, M., Barral, Y., Fischle, W. and Neumann, H. (2014). A cascade of histone modifications induces chromatin condensation in mitosis. Science *343*, 77–80.

Winey, M. and O'Toole, E. T. (2001). The spindle cycle in budding yeast. Nat Cell Biol *3*, E23–7.

Woo, J.-S., Lim, J.-H., Shin, H.-C., Suh, M.-K., Ku, B., Lee, K.-H., Joo, K., Robinson, H., Lee, J., Park, S.-Y., Ha, N.-C. and Oh, B.-H. (2009). Structural studies of a bacterial condensin complex reveal ATP-dependent disruption of intersubunit interactions. Cell *136*, 85–96.

Yamazoe, M., Onogi, T., Sunako, Y., Niki, H., Yamanaka, K., Ichimura, T. and Hiraga, S. (1999). Complex formation of MukB, MukE and MukF proteins involved in chromosome partitioning in Escherichia coli. EMBO J *18*, 5873–84.

Yeong, F. M., Hombauer, H., Wendt, K. S., Hirota, T., Mudrak, I., Mechtler, K., Loregger, T., Marchler-Bauer, A., Tanaka, K., Peters, J.-M. and Ogris, E. (2003). Identification of a subunit of a novel Kleisin-beta/SMC complex as a potential substrate of protein phosphatase 2A. Curr Biol *13*, 2058–64.

Yoshimura, S. H., Hizume, K., Murakami, A., Sutani, T., Takeyasu, K. and Yanagida, M. (2002). Condensin architecture and interaction with DNA: regulatory non-SMC subunits bind to the head of SMC heterodimer. Curr Biol *12*, 508–13.

Zacharias, D. A., Violin, J. D., Newton, A. C. and Tsien, R. Y. (2002). Partitioning of lipid-modified monomeric GFPs into membrane microdomains of live cells. Science *296*, 913–6.

Zhang, N., Kuznetsov, S. G., Sharan, S. K., Li, K., Rao, P. H. and Pati, D. (2008). A handcuff model for the cohesin complex. J Cell Biol *183*, 1019–31.

List of Strains

CSL3660	*MAT*α *ade2-1 can1-100 his3-11,15 leu2-3,112 trp1-1 GAL* [ϕ^+] *ura3-1::*P_{SMC2}*–SMC2-3HA–URA3*	94
CSL3793	*MAT*α *ade2-1 can1-100 his3-11,15 leu2-3,112 trp1-1 ura3-1 GAL* [ϕ^+] *tor1-1 Δfpr1::NAT RPL13A-2FKBP12–TRP1*	63, 96
CSL4267	*MAT*a *can1-100 his3-11,15 leu2-3,112 trp1-1 ura3-1 GAL* [ϕ^+] *ade2-1::OsTIR1-9myc–ADE2*	66, 97
K699	*MAT*a *ade2-1 can1-100 his3-11,15 leu2-3,112 trp1-1 ura3-1 GAL* [ϕ^+]	38, 39, 41, 54, 66, 97
K700	*MAT*α *ade2-1 can1-100 his3-11,15 leu2-3,112 trp1-1 ura3-1 GAL* [ϕ^+]	54, 63, 96
RT19	*MAT*α *ade2-1 can1-100 his3-11,15 leu2-3,112 trp1-1 ura3-1 GAL* [ϕ^+] *tor1-1 Δfpr1::NAT RPL13A-2FKBP12–TRP1 HTB2-YFP–SpHIS5*	37, 70
RT29	*MAT*α *ade2-1 can1-100 his3-11,15 leu2-3,112 trp1-1 GAL* [ϕ^+] *tor1-1 Δfpr1::NAT RPL13A-2FKBP12–TRP1 ura3-1::*P_{SMC2}*–SMC2-3HA–URA3*	94, 96
RT31	*MAT*α *ade2-1 can1-100 his3-11,15 leu2-3,112 trp1-1 GAL* [ϕ^+] *tor1-1 Δfpr1::NAT RPL13A-2FKBP12–TRP1 ura3-1::*P_{SMC2}*–SMC2*^{K38A}*-3HA–URA3*	94, 96
RT33	*MAT*α *ade2-1 can1-100 his3-11,15 leu2-3,112 trp1-1 GAL* [ϕ^+] *tor1-1 Δfpr1::NAT RPL13A-2FKBP12–TRP1 ura3-1::*P_{SMC2}*–SMC2*^{R58A}*-3HA–URA3*	94, 96
RT35	*MAT*α *ade2-1 can1-100 his3-11,15 leu2-3,112 trp1-1 GAL* [ϕ^+] *tor1-1 Δfpr1::NAT RPL13A-2FKBP12–TRP1 ura3-1::*P_{SMC2}*–SMC2*^{S1085R}*-3HA–URA3*	94, 96
RT37	*MAT*α *ade2-1 can1-100 his3-11,15 leu2-3,112 trp1-1 GAL* [ϕ^+] *tor1-1 Δfpr1::NAT RPL13A-2FKBP12–TRP1 ura3-1::*P_{SMC2}*–SMC2*^{E1113Q}*-3HA–URA3*	94, 96
RT49	*MAT*α *ade2-1 can1-100 his3-11,15 leu2-3,112 trp1-1 ura3-1 GAL* [ϕ^+] *tor1-1 Δfpr1::NAT RPL13A-2FKBP12–TRP1 SMC2-3HA–URA3*	37, 99

RT63	*MAT*α *ade2-1 can1-100 his3-11,15 leu2-3,112 trp1-1 ura3-1 GAL* [ϕ^+] *tor1-1 Δfpr1::NAT RPL13A-2FKBP12–TRP1 BRN1-3Pk–LEU2*	37, 99
RT65	*MAT*α *ade2-1 can1-100 his3-11,15 leu2-3,112 trp1-1 ura3-1 GAL* [ϕ^+] *tor1-1 Δfpr1::NAT RPL13A-2FKBP12–TRP1 SMC2-3HA–URA3 BRN1-3Pk–LEU2*	37, 99, 106, 107
RT67	*MAT*α *ade2-1 can1-100 his3-11,15 leu2-3,112 trp1-1 GAL* [ϕ^+] *tor1-1 Δfpr1::NAT RPL13A-2FKBP12–TRP1 ura3-1::*P_{SMC2}*–SMC2-3HA–URA3 BRN1-3Pk–LEU2*	99, 106, 107
RT69	*MAT*α *ade2-1 can1-100 his3-11,15 leu2-3,112 trp1-1 GAL* [ϕ^+] *tor1-1 Δfpr1::NAT RPL13A-2FKBP12–TRP1 ura3-1::*P_{SMC2}*–SMC2*^{K38A}*-3HA–URA3 BRN1-3Pk–LEU2*	99, 106, 107
RT71	*MAT*α *ade2-1 can1-100 his3-11,15 leu2-3,112 trp1-1 GAL* [ϕ^+] *tor1-1 Δfpr1::NAT RPL13A-2FKBP12–TRP1 ura3-1::*P_{SMC2}*–SMC2*^{R58A}*-3HA–URA3 BRN1-3Pk–LEU2*	99, 106, 107
RT73	*MAT*α *ade2-1 can1-100 his3-11,15 leu2-3,112 trp1-1 GAL* [ϕ^+] *tor1-1 Δfpr1::NAT RPL13A-2FKBP12–TRP1 ura3-1::*P_{SMC2}*–SMC2*^{S1085R}*-3HA–URA3 BRN1-3Pk–LEU2*	99, 106, 107
RT75	*MAT*α *ade2-1 can1-100 his3-11,15 leu2-3,112 trp1-1 GAL* [ϕ^+] *tor1-1 Δfpr1::NAT RPL13A-2FKBP12–TRP1 ura3-1::*P_{SMC2}*–SMC2*^{E1113Q}*-3HA–URA3 BRN1-3Pk–LEU2*	99, 106, 107
RT111	*MAT*a *ade2-1 can1-100 his3-11,15 trp1-1 ura3-1 GAL* [ϕ^+] *leu2-3,112::*P_{GAL1}*–SWE1-3Pk–LEU2*	54, 55
RT112	*MAT*α *ade2-1 can1-100 his3-11,15 trp1-1 ura3-1 GAL* [ϕ^+] *leu2-3,112::*P_{GAL1}*–SWE1-3Pk–LEU2*	54
RT145	*MAT*a *can1-100 his3-11,15 leu2-3,112 trp1-1 ura3-1 GAL* [ϕ^+] *ade2-1::OsTIR1-9myc–ADE2 SMC2-IAA17-9myc–KAN*	37, 66
RT146	*MAT*a *can1-100 his3-11,15 leu2-3,112 trp1-1 ura3-1 GAL* [ϕ^+] *ade2-1::OsTIR1-9myc–ADE2 SMC2-3Pk-miniAID–KAN*	37, 66, 67
RT148	*MAT*a *can1-100 his3-11,15 leu2-3,112 trp1-1 ura3-1 GAL* [ϕ^+] *ade2-1::OsTIR1-9myc–ADE2 SMC4-IAA17-9myc–KAN*	37, 66

RT149	*MAT*a *can1-100 his3-11,15 leu2-3,112 trp1-1 ura3-1 GAL* [ϕ^+] *ade2-1::OsTIR1-9myc–ADE2 SMC4-3Pk-miniAID–KAN*	37, 66, 67, 95, 97, 100, 101, 104, 105
RT155	*MAT*a *can1-100 his3-11,15 leu2-3,112 trp1-1 ura3-1 GAL* [ϕ^+] *ade2-1::OsTIR1-9myc–ADE2 SMC4-3Pk-miniAID–KAN BRN1-3HA–TRP1*	37, 67
RT159	*MAT*a *can1-100 his3-11,15 leu2-3,112 trp1-1 ura3-1 GAL* [ϕ^+] *ade2-1::OsTIR1-9myc–ADE2 SMC4-3HA–TRP1*	37, 95, 100, 101, 104, 105
RT161	*MAT*a *can1-100 his3-11,15 leu2-3,112 trp1-1 ura3-1 GAL* [ϕ^+] *ade2-1::OsTIR1-9myc–ADE2 SMC2-3Pk–TRP1*	37, 67
RT163	*MAT*a *can1-100 his3-11,15 leu2-3,112 trp1-1 ura3-1 GAL* [ϕ^+] *ade2-1::OsTIR1-9myc–ADE2 SMC4-3Pk–TRP1*	37, 67
RT174	*MAT*a *can1-100 his3-11,15 leu2-3,112 trp1-1 ura3-1 GAL* [ϕ^+] *ade2-1::OsTIR1-9myc–ADE2 NET1-mCitrine–SkHIS3*	37, 71, 73, 74, 86–89
RT178	*MAT*a *can1-100 his3-11,15 leu2-3,112 trp1-1 ura3-1 GAL* [ϕ^+] *ade2-1::OsTIR1-9myc–ADE2 SMC4-3Pk-miniAID–KAN NET1-mCitrine–SkHIS3*	37, 71, 73, 74, 108–110
RT180	*MAT*a *can1-100 his3-11,15 trp1-1 ura3-1 GAL* [ϕ^+] *ade2-1::OsTIR1-9myc–ADE2 NET1-mCitrine–SkHIS3 leu2-3,112::*P_{GAL1}*–SWE1-3Pk–LEU2*	37, 76–78
RT184	*MAT*a *can1-100 his3-11,15 trp1-1 ura3-1 GAL* [ϕ^+] *ade2-1::OsTIR1-9myc–ADE2 SMC4-3Pk-miniAID–KAN NET1-mCitrine–SkHIS3 leu2-3,112::*P_{GAL1}*–SWE1-3Pk–LEU2*	37, 76–78, 80
RT192	*MAT*a *can1-100 his3-11,15 trp1-1 ura3-1 GAL* [ϕ^+] *ade2-1::OsTIR1-9myc–ADE2 HTB2-mCitrine–SkHIS3 leu2-3,112::*P_{GAL1}*–SWE1-3Pk–LEU2*	37, 76, 81–83
RT196	*MAT*a *can1-100 his3-11,15 trp1-1 ura3-1 GAL* [ϕ^+] *ade2-1::OsTIR1-9myc–ADE2 SMC4-3Pk-miniAID–KAN HTB2-mCitrine–SkHIS3 leu2-3,112::*P_{GAL1}*–SWE1-3Pk–LEU2*	37, 76, 81–83
RT242	*MAT*a *can1-100 his3-11,15 leu2-3,112 ura3-1 GAL* [ϕ^+] *ade2-1::OsTIR1-9myc–ADE2 SMC4-3Pk-miniAID–KAN trp1-1::*P_{SMC4}*–SMC4-3HA–TRP1*	95, 97, 100, 101, 104, 105
RT244	*MAT*a *can1-100 his3-11,15 leu2-3,112 ura3-1 GAL* [ϕ^+] *ade2-1::OsTIR1-9myc–ADE2 SMC4-3Pk-miniAID–KAN trp1-1::*P_{SMC4}*–SMC4*^{K191A}*-3HA–TRP1*	95, 97, 100, 101, 104, 105

RT246	*MAT*a *can1-100 his3-11,15 leu2-3,112 ura3-1 GAL* [ϕ^+] *ade2-1::OsTIR1-9myc–ADE2 SMC4-3Pk-miniAID–KAN trp1-1::P_{SMC4}–SMC4^{R210A}-3HA–TRP1*	95, 97, 100, 101, 104, 105
RT248	*MAT*a *can1-100 his3-11,15 leu2-3,112 ura3-1 GAL* [ϕ^+] *ade2-1::OsTIR1-9myc–ADE2 SMC4-3Pk-miniAID–KAN trp1-1::P_{SMC4}–SMC4^{R210K}-3HA–TRP1*	95, 97, 100, 101, 104, 105
RT250a	*MAT*a *can1-100 his3-11,15 leu2-3,112 ura3-1 GAL* [ϕ^+] *ade2-1::OsTIR1-9myc–ADE2 SMC4-3Pk-miniAID–KAN trp1-1::P_{SMC4}–SMC4^{S1324R}-3HA–TRP1*	95, 97, 100, 101, 104, 105
RT252	*MAT*a *can1-100 his3-11,15 leu2-3,112 ura3-1 GAL* [ϕ^+] *ade2-1::OsTIR1-9myc–ADE2 SMC4-3Pk-miniAID–KAN trp1-1::P_{SMC4}–SMC4^{E1352Q}-3HA–TRP1*	95, 97, 100, 101, 104, 105
RT254	*MAT*a *can1-100 his3-11,15 leu2-3,112 ura3-1 GAL* [ϕ^+] *ade2-1::OsTIR1-9myc–ADE2 SMC4-3Pk-miniAID–KAN trp1-1::P_{SMC4}–SMC4^{E1352D}-3HA–TRP1*	95, 97, 100, 101, 104, 105
RT272	*MAT*a *can1-100 his3-11,15 leu2-3,112 ura3-1 GAL* [ϕ^+] *ade2-1::OsTIR1-9myc–ADE2 trp1-1::P_{GAL1}–SIC1^{m}–TRP1 NET1-mCitrine–SkHIS3*	86–89
RT274	*MAT*a *can1-100 his3-11,15 trp1-1 ura3-1 GAL* [ϕ^+] *ade2-1::OsTIR1-9myc–ADE2 leu2-3,112::P_{GAL1}–SWE1–LEU2 NET1-mCitrine–SkHIS3*	86–89
RT276	*MAT*a *can1-100 his3-11,15 trp1-1 ura3-1 GAL* [ϕ^+] *ade2-1::OsTIR1-9myc–ADE2 leu2-3,112::P_{GAL1}–BFA1–LEU2 NET1-mCitrine–SkHIS3*	86–89
RT280	*MAT*a *can1-100 his3-11,15 leu2-3,112 trp1-1 ura3-1 GAL* [ϕ^+] *ade2-1::OsTIR1-9myc–ADE2 SMC4-3HA–TRP1 NET1-mCitrine–SkHIS3*	108–110
RT280	*MAT*a *can1-100 his3-11,15 leu2-3,112 ura3-1 GAL* [ϕ^+] *ade2-1::OsTIR1-9myc–ADE2 SMC4-3Pk-miniAID–KAN trp1-1::P_{SMC4}–SMC4-3HA–TRP1 NET1-mCitrine–SkHIS3*	108–110
RT284	*MAT*a *can1-100 his3-11,15 leu2-3,112 ura3-1 GAL* [ϕ^+] *ade2-1::OsTIR1-9myc–ADE2 SMC4-3Pk-miniAID–KAN trp1-1::P_{SMC4}–SMC4^{K191A}-3HA–TRP1 NET1-mCitrine–SkHIS3*	108–110

RT286	*MAT*a *can1-100 his3-11,15 leu2-3,112 ura3-1 GAL* [ϕ^+] *ade2-1::OsTIR1-9myc–ADE2 SMC4-3Pk-miniAID–KAN trp1-1::P_{SMC4}–SMC4^{R210A}-3HA–TRP1 NET1-mCitrine–SkHIS3*	108–110
RT288	*MAT*a *can1-100 his3-11,15 leu2-3,112 ura3-1 GAL* [ϕ^+] *ade2-1::OsTIR1-9myc–ADE2 SMC4-3Pk-miniAID–KAN trp1-1::P_{SMC4}–SMC4^{R210K}-3HA–TRP1 NET1-mCitrine–SkHIS3*	108–110
RT290	*MAT*a *can1-100 his3-11,15 leu2-3,112 ura3-1 GAL* [ϕ^+] *ade2-1::OsTIR1-9myc–ADE2 SMC4-3Pk-miniAID–KAN trp1-1::P_{SMC4}–SMC4^{S1324R}-3HA–TRP1 NET1-mCitrine–SkHIS3*	108–110
RT292	*MAT*a *can1-100 his3-11,15 leu2-3,112 ura3-1 GAL* [ϕ^+] *ade2-1::OsTIR1-9myc–ADE2 SMC4-3Pk-miniAID–KAN trp1-1::P_{SMC4}–SMC4^{E1352Q}-3HA–TRP1 NET1-mCitrine–SkHIS3*	108–110
RT294	*MAT*a *can1-100 his3-11,15 leu2-3,112 ura3-1 GAL* [ϕ^+] *ade2-1::OsTIR1-9myc–ADE2 SMC4-3Pk-miniAID–KAN trp1-1::P_{SMC4}–SMC4^{E1352D}-3HA–TRP1 NET1-mCitrine–SkHIS3*	108–110
SH110	*MAT*α *ade2-1 can1-100 his3-11,15 leu2-3,112 trp1-1 ura3-1 GAL* [ϕ^+] *tor1-1 Δfpr1::NAT RPL13A-2FKBP12–TRP1 SMC2-FRB–KAN*	37, 63, 94, 96, 99, 106, 107
SH184	*MAT*α *ade2-1 can1-100 his3-11,15 leu2-3,112 trp1-1 ura3-1 GAL* [ϕ^+] *tor1-1 Δfpr1::NAT RPL13A-2FKBP12–TRP1 SMC4-FRB–KAN*	37, 63

All strains are isogenic with W303. Letter prefixes denote strain source: CSL – lab collection; K – Kim Nasmyth; RT – self-generated; SH – Sebastian Heeger.

List of Plasmids

pAG8734	pFA6a–linker–*Sp*HIS5 (Sheff and Thorn, 2004)	43
pCSL2	YIplac204	41
pCSL3	YIplac211	39
pCSL35	pUC19–3HA–*Kl*TRP1	37
pCSL42	pUC19–3HA–*Kl*URA3	37
pCSL43	pBS-SKII(-)–9myc	38
pCSL288	pFA6a–YFP–*Sp*HIS5	37
pCSL520	YIplac128–P_{GAL1}–3Pk	38
pCSL554	pUC19–3Pk–*Kl*TRP1	37
pCSL563	pUC19–3Pk–*Kl*LEU2	37
pCSL879	pFA6a–HIS3MX6	43
pES30578	pFA6a–FRB–kanMX6 (Haruki et al., 2008)	37
pMK43	pFA6a–IAA17–kanMX (Nishimura et al., 2009)	38, 39
pMK151	pFA6a–3miniAID–kanMX (Kubota et al., 2013)	39
pRT1	YIplac211–P_{SMC2}–SMC2-3HA	39, 41, 42
pRT2	YIplac211–P_{SMC2}–SMC2^{K38A}-3HA	43
pRT3	YIplac211–P_{SMC2}–SMC2^{R58A}-3HA	43
pRT5	YIplac211–P_{SMC2}–SMC2^{S1085R}-3HA	43
pRT6	YIplac211–P_{SMC2}–SMC2^{E1113Q}-3HA	43
pRT8	YIplac204–P_{SMC4}–SMC4-3HA	41, 42
pRT9	YIplac204–P_{SMC4}–SMC4^{K191A}-3HA	43
pRT10	YIplac204–P_{SMC4}–SMC4^{R210A}-3HA	43
pRT11	YIplac204–P_{SMC4}–SMC4^{R210K}-3HA	43
pRT12	YIplac204–P_{SMC4}–SMC4^{S1324R}-3HA	43
pRT13	YIplac204–P_{SMC4}–SMC4^{E1352Q}-3HA	43
pRT14	YIplac204–P_{SMC4}–SMC4^{E1352D}-3HA	43
pRT21	pFA6a–3Pk-miniAID–kanMX	37, 39
pRT22	pFA6a–yEmCitrine–*Sk*HIS3	37, 43
pRT40	pFA6a–IAA17-9myc–kanMX	37, 39
pRT41	YIplac128–P_{GAL1}–SWE1-3Pk	38

Letter prefixes denote plasmid source: pAG – Addgene; pCSL – lab collection; pES – Euroscarf; pMK – Masato Kanemaki; pRT – self-generated.

List of Oligonucleotides

co132	GGGTCTTCAGGACGAGATTTCAAGATGGTACCTCCGTAGTTA GTATAATGATCtccggttctgctgc	37
co133	TTGAAATATGATTACATTACAATATTTATTTGTCTTATGAAA ACTAACCAGAcctcgaggccagaag	37
co134	ATAGAACCAAAAGTACCACGATTAAAAACATAGATATCTTAA ACAGAACTATCtccggttctgctgc	37
co135	TAGCATGATATTACAATCAGCAAGTGCTCTTGAATTGATTAT TGTACTAGGAcctcgaggccagaag	37
co311	ATGACTTGATAGTGAATTATGAGGATCTAGCGACAACACAGG CAGCGTCAATCtccggttctgctgc	37
co312	GCGATAAAGGATTTCGTAAGCCCGAAGGCTTTAAGAAACTTT GCAGCACAGAcctcgaggccagaag	37
oRT1	AGAAGCCAAGTGGTGGATTTGCATCATTAATAAAAGATTTCA AGAAAAAAggtcgacggatccccggg	37
oRT2	TTTTTTTTACTAGCTTTCTGTGACGTGTATTCTACTGAGACT TTCTGGTAatcgatgaattcgagctcg	37
oRT4	TTGAAATATGATTACATTACAATATTTATTTGTCTTATGAAA ACTAACCAtgaattcgagctcgtttaaac	37
oRT6	TAGCATGATATTACAATCAGCAAGTGCTCTTGAATTGATTAT TGTACTAGtgaattcgagctcgtttaaac	37
oRT11	TCTCCGAAGGTACTAGGGCTGTTACCAAATACTCCTCCTCTA CTCAAGCCcggatccccgggttaattaa	37
oRT12	GCCACTAATAAAAAGAAAACATGACTAAATCACAATACCTAG TGAGTGACgaattcgagctcgtttaaac	37
oRT49	GGGTCTTCAGGACGAGATTTCAAGATGGTACCTCCGTAGTTA GTATAATGcggatccccgggttaattaa	37
oRT50	ATAGAACCAAAAGTACCACGATTAAAAACATAGATATCTTAA ACAGAACTcggatccccgggttaattaa	37
oRT56	GGGTCTTCAGGACGAGATTTCAAGATGGTACCTCCGTAGTTA GTATAATGCGTACGCTGCAGGTCGAC	37
oRT57	TTGAAATATGATTACATTACAATATTTATTTGTCTTATGAAA ACTAACCAATCGATGAATTCGAGCTCG	37
oRT58	ATAGAACCAAAAGTACCACGATTAAAAACATAGATATCTTAA ACAGAACTCGTACGCTGCAGGTCGAC	37

oRT59	TAGCATGATATTACAATCAGCAAGTGCTCTTGAATTGATTATTGTACTAGATCGATGAATTCGAGCTCG	37
oRT62	CGGGATCCGATGAGTTCTTTGGACGAGGAT	38
oRT63	TTACTGCAGTATAAAAAATTTTGGCTTAGG	38
oRT87	GCAGGTACCATGATGGGCAGTGTCGAG	38
oRT88	TAACCCGGGAGCTCTGCTCTTGCACTT	38
oRT89	CCCGGGTCTGGTTCTGGTAGTGGTGAACAAAAGTTG	38
oRT90	GGCAGATCTTTAGGATCCGTTCAAGTCTTC	38
oRT105	TGGGTCCGGTgctTCGAACATTTTGG	43
oRT106	TTTAGACCTGTAATAGCATTG	43
oRT107	GAGCACTGTGgctGCATCTAGCCTGCAAG	43
oRT108	ATTGATGCTATACCGAGC	43
oRT109	GATTGAATTGagaGGTGGGCAAAGG	43
oRT110	AAACTTTCCTTCCATATATTACC	43
oRT111	TATTTTGGATcaaGTTGATGCTGCTC	43
oRT112	TACATAGGCGCTGGTCGA	43
oRT113	TGGTTCAGGTgctTCAAATGTCATCGATTCCATGTTATTTGTATTTGGATTTAG	43
oRT114	TTGGGGCCTACCACGGCC	43
oRT115	GAACAAGATGgctCAGGACAGATTGTCG	43
oRT116	GCTCTAAATCCAAATACAAATAAC	43
oRT117	AACAAACCTTagaGGTGGTGAGAAAAC	43
oRT118	ATATTTCTCCAACTCTTTTTAGG	43
oRT119	TGTCATGGATcaaATAGATGCCG	43
oRT120	TAAAGGGGGGTTGGTTTATAC	43
oRT121	GATTACGCCAAGCTTGCATGCTTCTACCATCTCTAGAGGTGCTGT	39
oRT122	AAAGATAGAACCACCCCCGGGAGAACCACCCATTATACTAACTACGGA	39
oRT123	ATAATGGGTGGTTCTCCCGGGGGTGGTTCTATCTTTTACCCA	39
oRT124	AAAACGACGGCCAGTGAATTCTTACTGAGCAGCGTAATCTGG	39, 41
oRT125	GATTACGCCAAGCTTGCATGCGATTGAAAAGGCAATAATCCCATA	41
oRT126	AAAGATAGAACCACCCCCGGGAGAACCACCAGTTCTGTTTAAGATATC	41
oRT127	AGAACTGGTGGTTCTCCCGGGGGTGGTTCTATCTTTTACCCA	41
oRT136	cccattgttgggtttggactctatcccaaacccattgttgggtttggacGGTGCTGGTGCTGGTGCT	39
oRT137	tttgggatagagtccaaacccaacaatgggtttgggatagaaccagaaccGGCACCGTCGACCTGCAG	39
oRT138	AAGGCGCGCCAGATCTctATGTCTAAAGGTGAAGAATTATTCACTGGTGT	43

oRT143a	CAAGCTAAACAGATCTTTATTTGTACAATTCATCCATACCca aGGTAATACCAGcagca	43
oRT162	GAACAAGATGaaaCAGGACAGATTG	43
oRT163	TGTCATGGATgatATAGATGCCG	43
oRT176	TGAAGATCTGTTTAGCTTGC	39
oRT177	CTTGTACATCCTTAAGTCAATC	39

Letter prefixes denote oligonucleotide source: co – lab collection; oRT – self-generated.